

5-2014

## Image-Guided Proton Therapy for Online Dose-Evaluation and Adaptive Planning

Joey P. Cheung

Follow this and additional works at: [https://digitalcommons.library.tmc.edu/utgsbs\\_dissertations](https://digitalcommons.library.tmc.edu/utgsbs_dissertations)



Part of the [Oncology Commons](#), [Other Medicine and Health Sciences Commons](#), and the [Other Physics Commons](#)

---

### Recommended Citation

Cheung, Joey P., "Image-Guided Proton Therapy for Online Dose-Evaluation and Adaptive Planning" (2014). *The University of Texas MD Anderson Cancer Center UTHealth Graduate School of Biomedical Sciences Dissertations and Theses (Open Access)*. 439.  
[https://digitalcommons.library.tmc.edu/utgsbs\\_dissertations/439](https://digitalcommons.library.tmc.edu/utgsbs_dissertations/439)

This Dissertation (PhD) is brought to you for free and open access by the The University of Texas MD Anderson Cancer Center UTHealth Graduate School of Biomedical Sciences at DigitalCommons@TMC. It has been accepted for inclusion in The University of Texas MD Anderson Cancer Center UTHealth Graduate School of Biomedical Sciences Dissertations and Theses (Open Access) by an authorized administrator of DigitalCommons@TMC. For more information, please contact [digitalcommons@library.tmc.edu](mailto:digitalcommons@library.tmc.edu).

**IMAGE-GUIDED PROTON THERAPY FOR ONLINE DOSE-EVALUATION AND  
ADAPTIVE PLANNING**

by

Joey P. Cheung, B.A.

APPROVED:

---

Laurence E. Court, Ph.D.  
Supervisory Professor

---

Lei Dong, Ph.D.

---

Steven J. Frank, M.D.

---

Kenneth R. Hess, Ph.D.

---

Rajat J. Kudchadker, Ph.D.

---

X. Ronald Zhu, Ph.D.

---

APPROVED:

---

Dean, The University of Texas Health Science Center at Houston  
Graduate School of Biomedical Sciences

**IMAGE-GUIDED PROTON THERAPY FOR ONLINE DOSE-EVALUATION AND  
ADAPTIVE PLANNING**

A

DISSERTATION

Presented to the Faculty of  
The University of Texas  
Health Science Center at Houston  
and  
The University of Texas  
MD Anderson Cancer Center  
Graduate School of Biomedical Sciences

in Partial Fulfillment

of the Requirements

for the Degree of

DOCTOR OF PHILOSOPHY

by

Joey P. Cheung, B.A.  
Houston, Texas

May 2014

## **DEDICATION**

I would like to dedicate this work to my wife, Robin, to my mom and dad, and to my late grandma.

## ACKNOWLEDGEMENTS

I would like to thank my advisors Dr. Lei Dong and Dr. Laurence Court for all of their help and mentorship throughout my graduate career. Dr. Dong provided much advice and guidance to get this project started and going. His kind attention, thoughtful criticisms, and boundless encouragement inspired this work and my continued dedication to the field. He has instilled in me the sense to keep the big picture in mind and to look forward to needs in the future. Dr. Court admirably continued with this role after Dr. Dong's departure to become physics head of the new proton therapy center at Scripps Health. It has been a true delight working with Dr. Court as well as he has provided great insight to this project based on his experience. I truly appreciate his patience and attention to detail. Both advisors have been inspirational models for me to follow in my career and have provided not only great academic advice, but personal and professional advice as well.

I would also like to thank my committee members for all of their help during my candidacy: Dr. Rajat Kudchadker for chairing my candidacy exam committee, his willingness to allow me to shadow him during his clinical responsibilities, and especially for his professional mentorship and career advice; Dr. X Ronald Zhu for his kindness, advice, and in-depth discussion of proton physics; Dr. Steven Frank for his fervent encouragement and helpful clinical discussions; and Dr. Kenneth Hess for all of his helpful advice related to statistics and data analysis.

I also could not have done this without the help of other colleagues and friends along the way, including: the computational scientist group, Joy Zhang, Ryan Williamson, Jinzhong Yang, and Yongbin Zhang, for their help with troubleshooting issues and for software help; Matt Palmer, Mayank Amin, Rola Georges, and Jaques Bluett at the Proton

Therapy Center for their helpful proton related discussions and advice; Dr. Ed Jackson, Dr. Richard Wendt, Georgeanne Moore, Betsy Kindred, Gloria Mendoza, Lisa Watson, Sarah Welch, Deborah Mann, and Scharlene Wilson for all of their administrative help; Dr. Geoffrey Ibbott for his departmental support after Dr. Dong's departure; Kathryn Carnes at scientific publications for all of her helpful manuscript editing; all of my instructors and everyone at the GSBS including, but not limited to, Dr. Knutson, Brenda Gaughan, Dr. Mattox, Lily D'Agostino, Bunny Perez, Joy Lademora, and Eric Solberg, and Carol Helton.

I could not have gone through these years without the help and friendship of my former and current lab-mates: Peter Park, Adam Yock, Henry Yu, Luke Hunter, Ming Yang, Patty Chen, Josh Niedzielski, Ashley Rubinstein, Scott Ingram, Xenia Fave, and David Fried. My thanks goes also to all of my classmates in the medical physics program, but especially to Samuel Fahrenholtz, Landon Wootton, Lawrence Bronk, and Laura Rechner for their friendship and helpful discussion of my projects and career. I would also like to acknowledge my tutorial mentors Dr. Wayne Newhauser and Dr. Tinsu Pan for their early mentorship during my time at MD Anderson.

Last but not least, I would like to give a big thanks to my family: to my wife Robin for her endless love and support and for taking the journey with me which found us in a new city amongst new friends with many new and exciting experiences; to my parents for all of the sacrifices they made for me and my brother and for all of their inspiration and encouragement; to my brother, Daniel, for his motivation and for always being a helpful listener; to our dog Tinker, for her encouragement through her excitement, joy, and companionship; and to my late grandma for raising me since I was born and for teaching me how to be a good person - I miss you every day.

# **ABSTRACT**

## **IMAGE-GUIDED PROTON THERAPY FOR ONLINE DOSE-EVALUATION AND ADAPTIVE PLANNING**

Joey P. Cheung, B.A.

Supervisory Professor: Laurence E. Court, Ph.D.

The main advantage for using protons in radiotherapy is their finite range in patients, allowing for potential improved sparing of normal tissues. However, this comes at a cost of increased sensitivity to range uncertainties. Density changes along the beam path will affect the proton range and the resultant dose distribution, making it difficult to estimate the impact of visible anatomic changes to the patient dose distribution. In order to better understand the effect of anatomy change on proton dose, some form of treatment-time verification is required and methods to correct for observed changes would be beneficial. Therefore, this project aims to develop image-guidance techniques for proton therapy that incorporates proton range changes to allow for accurate treatment-time dose verification and corrective actions to ensure proper dose delivery.

A method for quick estimation of the treatment-time dose based on CT-imaging using prior dose information was developed and validated. This technique uses changes in calculated radiological pathlength on CT images to remap prior dose distributions on new anatomy or new setup position. We assessed the accuracy of this technique compared to full dose calculation and found the average passing rate of 3D gamma analysis (3% dose-

difference, 3-mm distance-to-agreement) were 96% and 89% for setup errors and severe anatomy changes, respectively. The average (maximum) of RMS deviation of the DVHs under the weekly anatomical change was 0.6% (2.7%) for all structures considered.

Using the quick dose estimation tool, we developed a method to position the patient based on dose information instead of simply using anatomic information. This would allow for dose-based optimization to be included in the patient setup process. We found a statistically significant improvement in target coverage and normal tissue sparing using our method when compared to anatomy-based setup.

Finally, we assessed a potential method to adapt spot scanning proton treatment plan beam parameters to account for anatomical changes. This range-adaptive method adjusts the proton beam directly to match the new range to anatomy in the treatment-time image. Using this technique, we were able to reduce normal tissue dose but ended up with increased target heterogeneity and reduced target coverage.



## TABLE OF CONTENTS

Acknowledgements .....	iv
Abstract .....	vi
List of Figures .....	xii
List of Tables .....	xv
Chapter 1: Background .....	1
1.1. Radiation therapy .....	1
1.1.1. Brief history of radiation therapy.....	1
1.1.2. Guiding principles of radiation therapy .....	1
1.2. Use of proton therapy for improved dose delivery .....	2
1.2.1. Brief history of proton therapy .....	2
1.2.2. Potential advantages of proton therapy.....	4
1.2.3. Proton interactions .....	4
1.2.4. Proton delivery techniques.....	7
1.2.5. Sources of uncertainty in proton therapy .....	9
1.2.6. Proton treatment planning and mitigating uncertainties .....	11
1.3. Evidence of variations of internal anatomy in radiation therapy over the course of treatment .....	13
1.4. Image-guided radiation therapy for accurate localization in conformal treatments.	17
1.5. Adaptive radiation therapy .....	18
1.6. Need for treatment time verification and adaptive planning for proton therapy.....	20
1.7. Proposed proton dose and range verification methods.....	23

1.8. Proton range calculation from CT imaging.....	24
1.9. Conceptual shift in utilizing IGRT for protons .....	26
Chapter 2: Hypothesis and Specific Aims .....	28
2.1. Goals for this project .....	28
2.2. Overall hypothesis.....	28
2.3. Specific Aims .....	29
Chapter 3: Specific Aim I - Development of CT-based fast proton range and dose verification tools .....	32
3.1. Introduction .....	32
3.1.1. Evaluation of setup and anatomical uncertainties for proton therapy.....	32
3.1.2. Using range deviations for dose approximation .....	34
3.2. Methods and Materials .....	35
3.2.1. Approximation under setup error or patient shift .....	39
3.2.2. Approximation under anatomical change .....	40
3.2.3. Validation for patient cases.....	41
3.3. Results .....	43
3.3.1. Dose distribution comparison and 3D gamma analysis.....	43
3.3.2. DVH comparisons.....	52
3.4. Discussion .....	56
3.5. Conclusion.....	59

Chapter 4: Specific Aim II - A dose-based alignment patient setup technique using pre-treatment CT images .....	60
4.1. Introduction .....	60
4.2. Methods and Materials .....	62
4.2.1. Patient data set .....	62
4.2.2. Anatomy-based alignment .....	65
4.2.3. Dose-based alignment.....	66
4.2.4. Statistical analysis.....	68
4.3. Results .....	69
4.4. Discussion .....	74
4.5. Conclusion.....	82
Chapter 5: Specific Aim III - A fast online range-adaptive technique to correct for range variations based on CT imaging .....	83
5.1. Introduction .....	83
5.2. Methods and Materials .....	85
5.2.1. Patient data set .....	85
5.2.2. Treatment Planning.....	85
5.2.3. Treatment-time image pre-processing .....	87
5.2.4. Range calculation in CT imaging .....	88
5.2.5. Adaptive algorithm .....	88
5.2.6. Adaptive Plan Evaluation .....	96
5.3. Results .....	97

5.4. Discussion .....	101
5.5. Conclusion.....	105
Chapter 6: Discussion and conclusion of dissertation .....	106
6.1. Testing of hypotheses.....	106
6.1.1. Overall hypothesis .....	106
6.1.2. Specific Aim I.....	106
6.1.3. Specific Aim II.....	108
6.1.4. Specific Aim III .....	109
6.2. Future work .....	110
Bibliography .....	112
Vita.....	130

## LIST OF FIGURES

Figure 1: Depth dose curves comparing the difference between a photon and a proton beam.	3
Figure 2: An example of a lung patient with shrinking tumor size due to response to treatment. ....	16
Figure 3: An example of a lung patient with shrinking tumor size due to response to treatment leading to cavitation of the tumor volume. ....	17
Figure 4: Flow chart of adaptive radiation therapy process.....	19
Figure 5: Patient statistics for new start and adaptive cases at the MD Anderson Cancer Center Proton Therapy Center (PTC) for select services in the years 2011-2013.....	22
Figure 6: Percentage of the total patients who received an adaptive intervention each year from 2011-2013 separated by treatment site.....	22
Figure 7: Example of the CT Number-to-SPR calibration curve used for a clinical CT scanner at the MD Anderson Proton Therapy Center .....	25
Figure 8: Example of dose variation due to anatomy change between photon and proton beam therapy.....	27
Figure 9: Example of the dose profile variation due to high density material.....	36
Figure 10: An example of estimating the range variation due to treatment day anatomy change using our radiological pathlength algorithm to calculate a range-equivalent isodose line.....	37
Figure 11: The dose distributions from the full dose recalculation from our treatment planning system (left) versus the range-compensated dose approximation (right) for the pelvic phantom with bone-like material inserted into the path of the beam. ....	37

Figure 12: An example of the resultant dose distributions for the lung case for dose approximation. ....	45
Figure 13: An example of the dose difference between different proton dose calculation methods. ....	46
Figure 14: A comparison of the dose calculation results in the presence of inter-fraction anatomical changes for the prostate case. ....	51
Figure 15: A comparison of the dose calculation results in the presence of inter-fraction anatomical changes for the head-and-neck case. ....	51
Figure 16: DVH comparisons between different dose calculation methods for a lung patient. ....	53
Figure 17: A mesh plot of the differences in DVH between the range-corrected approximation method and the full dose (TPS) calculation.....	54
Figure 18: Planned dose distribution and beam angles for patient 1 for Specific Aim 2 study. ....	64
Figure 19: Workflow diagram for the dose-based alignment method compared to the current IGRT workflow.....	68
Figure 20: Scatter plot and histogram of vector magnitude differences of the isocenter shifts comparing the dose-based alignments with the bony alignment and iGTV alignment. ....	71
Figure 21: Example DVHs for the dose-based alignment method versus the anatomical alignment method.....	72
Figure 22: An objective plot of the solution space of mean ipsilateral lung dose versus target $D_{99\%}$ for the dose-based alignment method. ....	73

Figure 23: Dose distributions for Patient 13 for the a) plan and the last weekly CT based on b) bony-alignment, and c) dose-alignment. ....	74
Figure 24: A graphical user interface for dose-based alignment with inputs for DVH-based objectives. ....	80
Figure 25: An example of the range-adaptation on a pelvic phantom. ....	90
Figure 26: Depth dose curves of all of the clinically available energies at our proton therapy center and the relative doses for all spots proximal to the given energies. ....	92
Figure 27: A graph showing the difference in the proton beam penumbra for a spot scanning system between (a) a uniform proton fluence and (b) an “edge-enhanced” proton fluence. ...	93
Figure 28: Image of the phantom and contours that were used for generation of the lateral size corrections lookup table. ....	94
Figure 29: Generation of lookup table for lateral size corrections. ....	95
Figure 30: The resultant correction factors for lateral size changes based on target coverage (target $V_{99\%} \geq 95\%$ ) and target hot spot (target $V_{110\%} < 5\%$ ) criteria. ....	95
Figure 31: Columnar scatter plots of the normal tissue DVH metric differences between the adaptive and non-adaptive plans for all 14 patients and for each of the six adaptive correction methods. ....	100
Figure 32: Columnar scatter plots for the ITV DVH metrics (top) and DVH metric differences between the adaptive and non-adaptive plans (bottom) for all 14 patients and for each of the six different adaptive correction methods. ....	101

## LIST OF TABLES

Table 1: Tumor regression rates in volume percentage per day as reported by various studies. .....	15
Table 2: The measured volume change of the target volumes of interest observed in the weekly CT images for the lung case in Specific Aim 1.....	44
Table 3: The result of the (3%, 3mm) 3D gamma analysis on both the ranged-corrected approximation and static dose approximation with respect to the full dose (TPS) calculation under position change and weekly CT simulations. ....	48
Table 4: The result of the (1%, 3mm) 3D gamma analysis on both the ranged-corrected approximation and static dose approximation with respect to the full dose (TPS) calculation under position change and weekly CT simulations. ....	49
Table 5: The result of the (3%, 4mm) 3D gamma analysis on both the ranged-corrected approximation and static dose approximation with respect to the full dose (TPS) calculation under position change and weekly CT simulations. ....	50
Table 6: The root mean square (RMS) deviations between the cumulative DVHs derived using a full dose (TPS) calculation and range-corrected dose approximation method under various simulations. ....	55
Table 7: Patient and tumor characteristics for Specific Aim 2. ....	64
Table 8: Target (ITV) coverage requirement and mean ipsilateral lung dose for patients assessed for dose-based alignment.....	70
Table 9: Tumor and treatment characteristics for Specific Aim 3 study. ....	86
Table 10: Target and normal tissue DVH metric comparisons for all of the adaptive techniques relative to the non-adaptive plans .....	99





## **CHAPTER 1: BACKGROUND**

### **1.1. Radiation therapy**

#### **1.1.1. Brief history of radiation therapy**

Radiation therapy has been a major form of curative or palliative cancer treatment for the past century. Very quickly after the discovery of x-rays by Wilhelm Röntgen in 1895,<sup>1</sup> physicians and scientists saw the promise of using ionizing radiation to treat cancer, with the earliest use of x-rays for cancer treatments dating as early as 1896, just one year after its discovery. Today, radiation therapy is one of several modern options for cancer treatment and is often the primary, if not complementary, treatment option for many treatment sites. Nearly two-thirds of all cancer patients receive radiation therapy at some point in their illness, with breast, prostate, and lung cancers making up more than half of all radiation treatments.<sup>2, 3</sup>

#### **1.1.2. Guiding principles of radiation therapy**

Ionizing radiation is effective in killing cancer cells by damaging DNA which leads to cell death. Tumor control is achieved by delivering enough radiation dose to the target, including suspected areas of microscopic or subclinical disease and pathways of known spread of disease including lymphatic drainage systems. However, radiation damage is not only limited to malignant tissues and any normal tissues within the irradiation volume will be subject to damage as well. Therefore, efforts made in the past century have largely been to increase the therapeutic ratio by reducing dose delivered to normal tissues while increasing dose as much as possible to the target tissues. In addition, a course of radiation therapy is often delivered over a period of several weeks (in many treatment fractions) in order to allow for damaged

normal tissue to heal and to improve tumor cell kill. Tumor cells are typically less efficient in repairing damage from ionizing radiation compared to normal tissues. Additionally, these gaps between treatment fractions allows for the tumor cells to reoxygenate and redistribute within their cell cycles, both of which will increase the sensitivity of tumor cell population to radiation damage.

The tolerated dose to normal tissues varies greatly depending on the organ-at-risk involved, which again varies depending on the treatment site. A large effort has been made recently to provide a comprehensive review of all current knowledge regarding radiation effects on normal tissue for many important organs involved in radiation therapy treatments and has been published in a special issue of the International Journal of Radiation Oncology\*Biology\*Physics.<sup>4</sup>

## **1.2. Use of proton therapy for improved dose delivery**

### **1.2.1. Brief history of proton therapy**

The use of protons for cancer therapy was first proposed by Robert R. Wilson in 1946.<sup>5</sup> In this seminal manuscript, Wilson outlines the properties of high energy proton beams and how they can be used to treat cancer patients. Figure 1 shows a comparison between the depth dose distributions for a proton beam and a photon beam. Traditional photon beams deposit most of their energy near the entrance of the beam within the patient, with an exponential decrease in dose with increasing depth. This results in a large amount of radiation dose being delivered to normal tissues both proximal and distal to the target. This is typically overcome by using many beams to surround the patient in order to spread out dose to normal tissues. Protons, on the other hand, deposit a low amount of entrance dose and deliver the majority of

their dose at the end of range, which is determined by the energy of the proton beam, and nearly zero dose beyond this range. This depth dose profile is called the Bragg peak, and potentially allows for improved sparing of normal tissues both proximal and distal to the target. In order to deliver a uniform dose to a larger volume of tissue, several Bragg peaks can be pieced together in order to create a spread-out Bragg peak (SOBP), as shown in Figure 1.

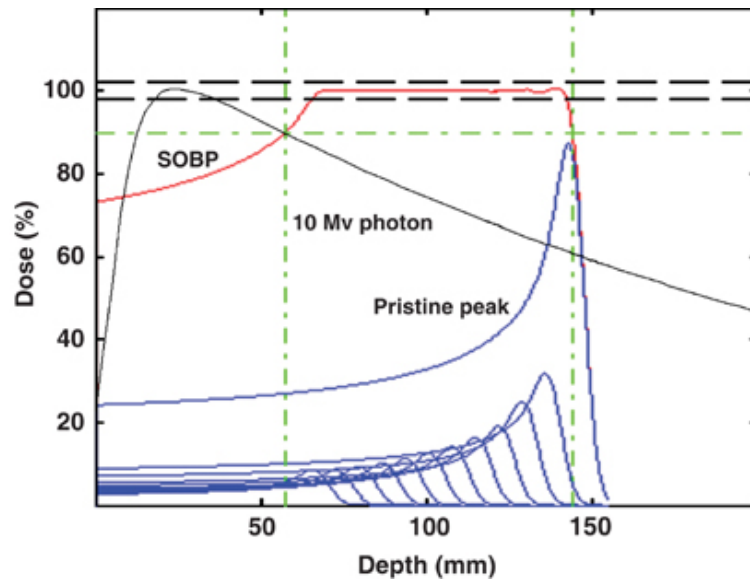


Figure 1: Depth dose curves comparing the difference between a photon and a proton beam. The 10MV photon beam is shown in black and the pristine Bragg peaks from proton beams are shown in blue. The resultant spread-out Bragg peak (SOBP) from the summation of pristine Bragg peaks is shown in red. Reprinted from *W. P. Levin, H. Kooy, J. S. Loeffler and T. F. DeLaney, "Proton beam therapy," Br. J. Cancer* **93**, 849-854 (2005) with permission from Macmillan Publishers Ltd on behalf of Cancer Research UK.<sup>6</sup>

While proton beams have been used to treat cancers for several decades now, only recently have large patient populations been able to get the treatment due to the opening of

several hospital-based proton treatment facilities.<sup>7-11</sup> As of the end of 2013, there are 40 proton therapy facilities in operation worldwide, with 13 facilities in the United States and many more being planned and under construction.<sup>12</sup> A total of over 100,000 patients have been treated with proton therapy since the first treatments in Berkeley, California in 1954.

### **1.2.2. Potential advantages of proton therapy**

Many planning studies have been published showing the improved dose distributions that can be obtained with proton beams compared to traditional photon beams.<sup>13-21</sup> The theoretical advantages stemming from the finite range of protons can also potentially improve treatment conformality with the use of fewer beams. Therefore, the integral (total) dose to the patient will be far lower with protons, which means an overall lower dose to normal tissues. In many cases, the delivery of radiation therapy to a specific disease site is limited by nearby critical structures. Therefore, if the dose conformality to the target can be improved, we can potentially increase the prescription dose delivered to the target in order to increase the probability of local control. Both of these factors can result in an improvement to enhance the therapeutic ratio in radiation therapy.

### **1.2.3. Proton interactions**

The dose delivery advantages of proton therapy stem from the fact that they are charged particles and interact with matter via Coulomb interactions. As a proton traverses through a medium, it loses energy through successive interactions with atoms in the medium until it loses all of its initial energy. Most of the energy loss of a proton comes from Coulomb interactions with atomic electrons. Small deflections of the proton beam that are caused by

Coulombic interactions with the atomic nucleus result in a lateral broadening of the beam due to angular deflection of the protons from their primary trajectory.

Most of the dose deposited by the beam is through the proton interactions with the outer-shell atomic electrons. This results in a very small loss of energy by the protons resulting in excitation or ionization of the electrons. The rate of energy loss per unit path length is defined to be the stopping power  $\left(\frac{dE}{dx}\right)$  and is dependent on the particle radiation of interest and properties of the medium that it traverses through. Due to the small loss of energy with each interaction for protons, the average path length of a monoenergetic proton beam can be very closely estimated using the continuous-slowing-down-approximation (CSDA). This approximation assumes that the rate of energy loss is equal to the total stopping power and that there is no lateral scattering of the beam. The CSDA range ( $R_{CSDA}$ ) can be calculated by integrating the reciprocal of the total stopping power with respect to energy:

$$R_{CSDA} = \int_0^{E_0} \left(\frac{dE}{dx}\right)^{-1} dE \quad (\text{Eq. 1})$$

where  $E_0$  is the initial kinetic energy of the protons.

The electronic or collisional proton stopping power of a charged particle in a material can be described using the Bethe formula:

$$-\frac{dE}{dx} = \frac{4\pi}{m_e c^2} \cdot \frac{nZ^2}{\beta^2} \cdot \left(\frac{e^2}{4\pi\epsilon_0}\right)^2 \cdot \left[ \ln\left(\frac{2m_e c^2 \beta^2}{I \cdot (1 - \beta^2)}\right) - \beta^2 \right] \quad (\text{Eq. 2})$$

where  $e$  and  $m_e$  are the charge and rest mass of the electron,  $c$  is the speed of light,  $\epsilon_0$  is the vacuum permittivity,  $\beta$  is the proton's velocity over the speed of light  $\beta = \left(\frac{v}{c}\right)$ ,  $n$  is the electron density of the material,  $Z$  is the atomic number of the material, and  $I$  is the mean

excitation potential of the material. Note that the stopping power is nearly proportional to the inverse square of the proton velocity. This relationship helps to intuitively describe the shape of the Bragg peak, since the protons will deposit much higher dose to the material when its velocity is very low near the end of its range. Calculated stopping powers and range tables for various materials using the Bethe formula can be found through the National Institute of Standards and Technology (NIST) PSTAR database.<sup>22</sup> In practice, these types of range-energy tables along with measured depth doses are used for practical purposes of dose calculation in proton therapy.

A beam of protons which is initially monoenergetic will end up with some distribution of energies due to statistical fluctuations in the process of losing energy. This results from the stochastic nature of the proton interactions causing a fluctuation in the number of interactions and the energy loss of each interaction. This results in a broadening of the Bragg peak in the depth direction, also called energy or range straggling.

The scatter of protons is due to elastic Coulomb interactions with target nuclei in the material. This results in many small angle deflections that serve to broaden the beam (also called multiple Coulomb scattering), causing a radial spread of the proton beam in the lateral direction. This can be described using Molière's theory of multiple scattering, but in practice we typically use Highland's Gaussian approximation:

$$\sqrt{\langle \theta^2 \rangle} = z \frac{14.1 \text{ MeV}}{pv} \sqrt{\frac{x}{X_0}} \left( 1 + \frac{1}{9} \log_{10} \frac{x}{X_0} \right) \quad (\text{Eq. 3})$$

where  $z$  is the charge of the particle,  $p$  and  $v$  are the momentum and velocity of the particle,  $x$  is the thickness of the material, and  $X_0$  is the radiation length of the material in which the particle energy is reduced by a factor of  $1/e$  due to radiation losses only. This approximation

works well for many practical applications and has been shown to agree to better than 5% for many materials compared to the full theory.<sup>23</sup>

Protons can also undergo non-elastic nuclear interactions with target nuclei, which can cause a reduction in the proton fluence with depth and also generate secondary particles that will deposit dose either locally or at a distance. These secondary particles include neutrons, protons, deuterons, alpha particles, and recoil nuclei. These particles in general contribute a very low dose compared to the primary proton dose. However, the higher relative biological effectiveness of these particles may be a concern. Much attention has especially been given to secondary neutron dose that is delivered to the patient, but contributions of secondary particles of other forms are generally more problematic for particles that are heavier than protons.

#### **1.2.4. Proton delivery techniques**

Currently, there are two main delivery methods for proton therapy, passive scattering proton therapy (PSPT) and active scanning or spot scanning proton therapy (SSPT). Both methods can be used to deliver proton therapy treatments to a 3-dimensional target volume, but each has its advantages and disadvantages.

PSPT uses scattering devices, physical range modulators, and physical apertures and compensators in order to shape the proton beam to deliver dose to the tumor. The scattering system typically uses double scatterers for large fields in order to spread the beam in the lateral direction and generate a uniform beam for patient treatment.<sup>24</sup> The beam is spread in the depth direction through the use of a range modulator wheel or a ridge filter which introduces material of variable thicknesses in the path of the beam to spread out the beam



ranges. This allows multiple Bragg peaks of differing energies to be added together to deliver a nearly uniform dose to the target in the depth direction, namely the SOBP as shown in Figure 1. The scattering and range modulation systems allow for the treatment of a volumetric target. In order to shape the beam to conform the dose laterally to the shape of the target, patient- and field-specific apertures are designed using the treatment planning system in order to block out the beam to minimize dose to surrounding normal tissues. To shape the beam to match the distal edge of the target volume, a range compensator is used to correct for the differences in range needed to reach the distal edge of the target. This delivery method can result in some drawbacks. Since a single SOBP is used for any given field, normal tissue proximal to the target volume may receive a high dose. Additionally, since patient-specific physical apertures and compensators need to be manufactured before treatment delivery, there is additional overhead needed for each new case as well as if any modifications need to be made during the course of treatment. Furthermore, the scattering system generates undesirable secondary neutrons which deposit additional background dose to the patient.

SSPT uses magnets to steer proton pencil beams of different energies and scan the pencil beam to deliver dose to the tumor.<sup>25</sup> This method essentially places Bragg peaks of different energies throughout the target volume at different depths. The magnetic steering allows for the dose to be spread in the lateral direction of the beam and is usually performed through the use of two sets of scanning magnets to scan the beam in orthogonal directions to each other. The energy can be changed either by the particle accelerator during the beam acceleration and extraction process (synchrotron), or through the use of energy absorbers along the beam transport system (cyclotron). Unlike PSPT, SSPT can conform the dose to both the distal and proximal boundaries of the target because there is no need to deliver only

a single SOBP width. Optimization techniques in the treatment planning process can be used to optimize spot positions and parameters to achieve the desired dose distribution. This can be performed using a single-field optimization (SFO) (also referred to as single field uniform dose or SFUD) technique in which each field is optimized individually to deliver the full prescribed dose to the target or using a multi-field optimization (MFO) (also referred to as intensity-modulated proton therapy or IMPT) technique in which spots from all fields are optimized simultaneously. The MFO technique can result in each field delivering a non-uniform dose distribution, but the total sum of all fields will yield the desired dose distribution as determined by the optimization parameters. MFO plans typically result in patched fields which are much more complex than an SFO plan on a field-by-field basis.

The increased ability for SSPT plans to modulate the proton beam and reduce the high dose delivered to normal tissues proximal to the target allows SSPT plans to be much more conformal and flexible than PSPT plans. It also minimizes neutron contamination due to the absence of high density physical scatterers and blocks in the path of the beam. However, potential problems exist because the dose is delivered with many different pencil beams instead of a broad beam like PSPT uses. This makes SSPT much more sensitive to uncertainties in the planning process and plan delivery as will be discussed in the next section.

### **1.2.5. Sources of uncertainty in proton therapy**

While one of the main advantages of protons is that they have a finite range and stop within the patient, this property also makes the delivery of proton therapy especially vulnerable to uncertainties. The distal falloff of a proton beam is very sharp, with the distal 90% to 10%

depth dose falloff being on the order of a few millimeters. Therefore, the proper localization and description of where this distal edge of the beam ends up within the patient is very important.

Many sources of uncertainty exist in radiation therapy including patient setup error and immobilization, patient internal motion and anatomic deformation, patient weight loss or gain, inconsistencies in target delineation, uncertainties in dose calculation algorithms, and limitations in the mechanics of beam delivery.<sup>26-28</sup> While all of these uncertainties exist in both photon and proton treatments, the impact of these on delivered dose to the patient may be more substantial for proton treatment.<sup>29-31</sup> All of the uncertainties listed can potentially affect the penetration range of the proton beam inside the patient and therefore affect the dose distribution that is delivered. An additional source of uncertainty for proton therapy is the added uncertainty in the conversion of computed tomography (CT) numbers to proton stopping power ratios (SPR). The SPR is needed in order to properly calculate proton range, and therefore proton dose, within the patient as will be described in Section 1.8. Since CT scans are the primary method for incorporating patient specific 3D geometry and organ information for planning and dose calculation, these CT number-to-SPR uncertainties can dramatically impact the planned versus actual delivered dose.<sup>32</sup>

Compared to PSPT, SSPT techniques tend to be more sensitive to uncertainties because of the method of delivery. While PSPT delivers a broad beam of protons that are physically spread out, SSPT delivery relies on the appropriate superposition of individual proton beamlets to deliver the correct dose to the target. Each of these individual beamlets is potentially subject to different degrees of uncertainties and any deviations from the original planning conditions can largely affect the shape of the dose distribution. This is especially

true for MFO plans since deviations from planning conditions can result in the “patched-fields” to deliver unintentionally overlapping or separated patches and result in heterogeneous total dose distributions. Because of these uncertainties, the evaluation of robustness of SSPT plans is important to ensure that the proper total dose is being delivered on a daily basis to the patient.

#### **1.2.6. Proton treatment planning and mitigating uncertainties**

While the general concepts in treatment planning for photons apply similarly to protons, there are several notable factors that need to be kept in mind that make proton therapy different from traditional photon therapy. These differences stem from the additional uncertainties that need to be taken into account. ICRU Report 78 presents a comprehensive outline of the principles of proton therapy and the considerations necessary for planning, treatment, and dosimetry.<sup>33</sup> The proton treatment planning process gets started in the same manner as photon treatment planning by setting up and acquiring a simulation CT scan of the patient, often referred to as the planning CT. Image segmentation is performed on these CT images to define the geometry of the patient and the relation of normal tissue structures to the treatment target of interest. In defining these structures, certain uncertainties need to be taken into account. The target volume is usually defined at several different levels as first described in ICRU Report 50.<sup>34</sup> The gross tumor volume (GTV) is tumor that can be clinically determined through palpation or imaging (anatomical or functional). This can include both the primary tumor and metastatic involvement. The clinical target volume (CTV) includes suspected microscopic and subclinical disease. This is usually determined based on experience and data based on the probability of clinical spread of the disease including the

disease pathological staging and likely pathways of spread. The internal target volume (ITV) includes the CTV and uncertainties associated with internal variation of the CTV including movement and possible deformation of the CTV. The planning target volume (PTV) is a geometric concept that is used purely for treatment planning and takes into account possible variations in the beam delivery including patient setup uncertainties and uncertainties and limitations in the beam delivery. Commonly, the CTV and PTV are derived from the substructures as a geometric expansion based on measured or estimated setup uncertainties.<sup>28</sup>

Once the target and normal tissue structures are delineated, the images and segmented structures can be used to plan the radiation treatment by defining beam parameters such as beam angles, beam weights, and field sizes. In defining the beam parameters, uncertainties in treatment planning need to be kept in mind. Typical strategies will place the proton beams in such a way to avoid aiming directly at normal structures such that the sharp distal dose gradient stops immediately or close to the surface of a critical structure due to the potential over-ranging of protons into the normal structure anatomy. Similarly, attempts to avoid using beams that stop in or near tissues of low density (such as lung tissue) should be made in order to reduce uncertainties of the proton range due to day-to-day variations that can occur over the course of treatment. However, the finite range of protons can sometimes allow the incident fields to be limited to a single side of the patient in order to spare normal tissue far away from the distal edge of the field. Unlike in photon therapy, the beams do not need to be distributed around the patient in order to maximally spare normal tissues. Consideration should also be made to use the shortest possible path to the tumor in order to reduce the integral dose to the normal tissues that lie proximal to the tumor volume.

A problem with the current standard treatment planning techniques described above is that they do not take into account potential morphological changes in the entire patient anatomy other than the target over the course of treatment. This includes changes in the size and shape of all organs in the body. This is especially important for proton therapy because of the sensitivity of the proton beam to materials all along the path of the beam. Therefore, it is not necessarily enough to simply include the setup and anatomical uncertainties only in relation to movement of the target volume in the creation of the PTV. Of course, it is not currently possible to accurately predict the changes that a given patient will undergo during treatment, which makes it difficult to include this uncertainty in the treatment planning process which inherently only looks at a single snapshot of the patient at the time of CT simulation. Therefore, direct methods to evaluate patient anatomical variations are needed.

### **1.3. Evidence of variations of internal anatomy in radiation therapy over the course of treatment**

Variations in patient setup and patient anatomy changes that can occur over the course of treatment can potentially compromise the treatment if not properly accounted or corrected for. Therefore, an accurate assessment and monitoring of patient changes throughout the duration of the therapy is an integral component if anatomical changes are expected or observed.

Traditionally, patients were set up using external markers (usually placed on the patient's skin or on the immobilization devices). While this method has been shown to provide good target coverage using older treatment techniques using larger treatment fields,<sup>35</sup> the use of external landmarks to align patients to the radiation fields does not necessarily

guarantee the correct alignment of internal anatomy for more conformal beam deliveries in which there is much less room for error. There may be large relative differences between the patient's external anatomy compared to internal anatomy between different treatment deliveries (inter-fraction) and even during a given delivery (intra-fraction) of radiation therapy. These relative differences can be in position, shape, and volume. Many studies have investigated the magnitude of tumor and normal tissue inter- and intra-fraction motion and changes during the course of radiation therapy for many different treatment sites.<sup>28, 36-40</sup> Langen and Jones<sup>36</sup> have written a comprehensive review of many scientific articles that quantify inter- and intra-fraction changes. Their review found, for example, that prostate motion was dominant in the anterior-posterior (AP) and superior-inferior (SI) directions due to variations in bladder and rectal filling with displacements as large as 20 mm. A similar study by Sonke et al.<sup>39</sup> showed that for non-small cell lung cancer (NSCLC) patients, the inter-fraction baseline variations are largest in the superior-inferior directions with an average systematic variation of 3.9 mm.

Morphological changes in tumor shape and volume have been well demonstrated as well. For example, Barker et al.<sup>37</sup> quantified the changes in volume and shape of targets and normal tissues in head and neck radiation therapy and found that the gross tumor volume (GTV), which included the primary tumor and involved lymph nodes, decreased progressively in volume at a median rate of  $0.2 \text{ cm}^3$  or 1.8% of the original volume per treatment day, with a median total relative loss of 69.5% by the end of treatment. Sonke et al.<sup>40</sup> compiled a comprehensive review of many studies that have reported tumor and lymph node regression rates based on volumetric changes during radiation therapy of lung cancer. Their findings are summarized in Table 1. These studies report regression rates of tumor

volume ranging from 0.6% to 2.4% per day. A key difference in tumor volume changes in the lung compared to many other treatment sites is that the reduction in soft tissue tumor typically gives way to lung tissues with low density. Figure 2 and Figure 3 show examples of lung tumor morphology changes that can occur in response to treatment for two cases from our institution. The tumor can shrink radially either isotropically or anisotropically (Figure 2), or can cavitate and develop abnormal textures that will affect the position and shape of the tumor (Figure 3).

Table 1: Tumor regression rates in volume percentage per day as reported by various studies.

Reprinted from *J.-J. Sonke and J. Belderbos, "Adaptive Radiotherapy for Lung Cancer,"*

*Semin. Radiat. Oncol.* **20**, 94-106 (2010) with permission from Elsevier.<sup>40</sup>

Study	No. Patients	Modality	Regression Rate (%/d)	Observations
Erridge 2003 Edinburgh-NKI/AvL	25	EPID	-0.9	Microscopic extensions mentioned
Kupelian 2005 M.D. Anderson	10	In room MV-CT	-1.2	Increased dose to PTV and lungs
Siker 2006 Wisconsin	25	MVCT	-2.4	Mixed group, radical, palliative and stereotactic RT
Bosmans 2008 Maastricht	23	FDG-PET/CT	-0.39	Lymph node regression only
McDermott 2006 NKI/AvL	1	EPID	-1.5	Increased dose to PTV and lungs
Underberg 2006 VUMC	40	4D-CT and conventional CT	-1.4	Volume. increase 1st and 2nd wk
Britton 2007 M.D. Anderson	8	In room KV-CT	-1.3	Volume increase 1st and 2nd wk
Woodford 2007 Ontario	17	In room MV-CT	-0.79	
Fox 2009 Johns Hopkins	22	MVCT	-1.2	Regression greater (-1.4%) in first 3 wk
Feng 2009 Michigan	14	Mid-RT FDG-PET/CT	-1.4	Planning study
Van Zwienen 2008 NKI/AvL	114	In room kV-CBCT	-0.6	Frequent anatomical changes occurred

All of these variations in target shape and size are important to monitor and may result in target underdosage or severe damage to normal tissues if not taken into account properly during treatment planning or treatment delivery. Additionally, many of the



described changes are not immediately apparent when observing a patient externally. While some quantitative measurements such as patient weight, body circumference, or the source-to-surface distance (SSD) indicator measurements can give hints to patient anatomy change, most of these metrics fail to detect morphological changes of internal anatomy.

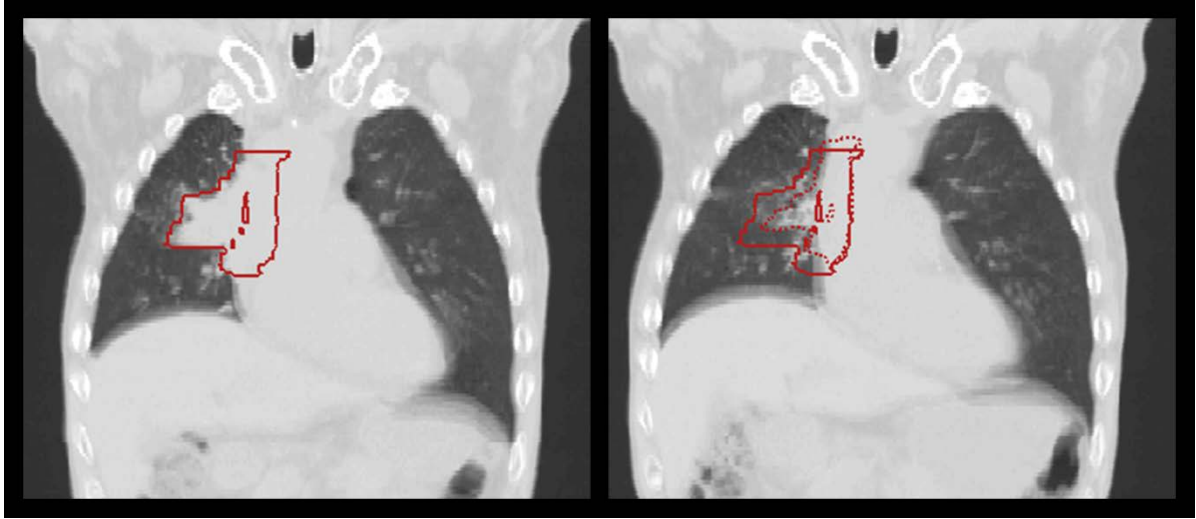


Figure 2: An example of a lung patient with shrinking tumor size due to response to treatment. On the left is the anatomy from a CT scan before treatment and on the right is the anatomy from a CT scan after 6 weeks of treatment. The GTV is displayed in red with the solid lines showing the original GTV and the dotted lines showing the new GTV on the 6<sup>th</sup> week of treatment.

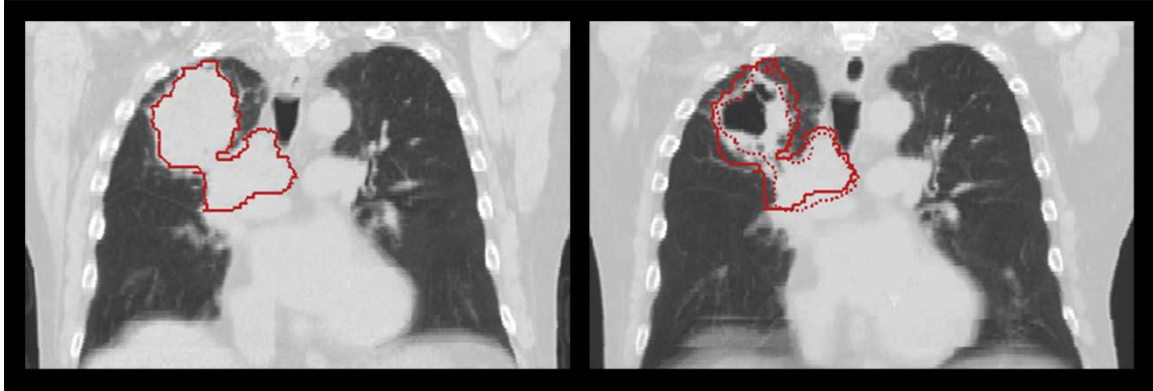


Figure 3: An example of a lung patient with shrinking tumor size due to response to treatment leading to cavitation of the tumor volume. On the left is the anatomy from a CT scan before treatment and on the right is the anatomy from a CT scan after 7 weeks of treatment. The GTV is displayed in red with the solid lines showing the original GTV and the dotted lines showing the new GTV on the 7<sup>th</sup> week of treatment.

#### **1.4. Image-guided radiation therapy for accurate localization in conformal treatments**

Image-guided radiation therapy (IGRT) using in-room imaging devices has allowed for the assessment and correction of observed anatomical changes over the course of radiation therapy.<sup>41-44</sup> This is performed by capturing images of the internal patient anatomy immediately before treatment delivery and localizing the target volume. These imaging and localization capabilities, in conjunction with patient immobilization devices, have been shown to improve dose delivery by reducing treatment margins and ensuring accurate target alignment.<sup>45-48</sup> Additionally, images from IGRT can be used to track changes of the patient anatomy over the course of the treatment, including tumor volume changes, normal tissue changes, and patient external contour changes. This information can then be used to evaluate

the progress of the treatment on the tumor as well as effects of radiation on normal tissues, and decisions can also be made on whether adjustments need to take place in order to accommodate large changes in patient anatomy that could affect the treatment.<sup>49-51</sup> This may lead to the need for an intervention in the middle of a course of treatment to alter the delivery of the therapy. This can be as simple as adjusting the position of the patient and re-creating the patient immobilization device, or can be as advanced as completely replanning the treatment to compensate for the changes. The effort to replan and implement the treatment during a course of radiation therapy is often called adaptive radiation therapy (ART) and has been a subject of much research in the past couple of decades.

### **1.5. Adaptive radiation therapy**

Adaptive radiation therapy was introduced as a way to incorporate patient-specific changes over the course of treatment to optimize treatment delivery in the face of anatomic changes.<sup>49</sup> Figure 4 shows a flow diagram of the adaptive treatment system process as described by Yan.<sup>52</sup> The information gathered for the feedback process can be any number of things including anatomical, biological, or possibly even tumor genetic variations due to treatment response. Ultimately, the modification will be made to the dose delivery system, so an estimation of the delivered treatment dose is an important step in the process as well such that a decision on the necessary changes can be made.

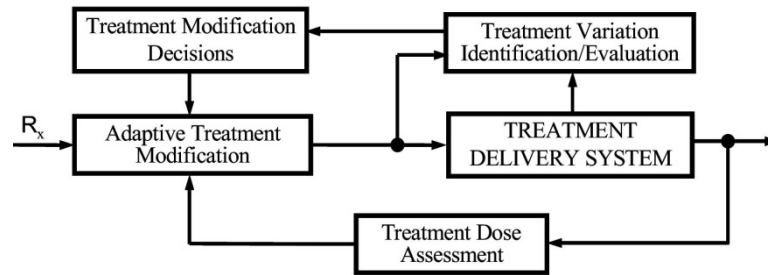


Figure 4: Flow chart of adaptive radiation therapy process. Reprinted from *D. Yan, "Adaptive Radiotherapy: Merging Principle Into Clinical Practice," Semin. Radiat. Oncol. 20, 79-83 (2010)* with permission from Elsevier.<sup>52</sup>

Since morphological and physiological changes are difficult to predict and can vary dramatically between different patients, these evaluations are inherently patient-specific and the acquisition of patient-specific information is one of the key aspects of adaptive radiation therapy. As noted, this can be anatomical or biological in nature, and should be evaluated frequently enough to be able to discover variations that may compromise the treatment as well as allow time for a response to take place. The utilization of imaging information from IGRT can be an excellent source of feedback information as it would serve the purpose of patient localization for setup purposes as well as assess anatomical changes that take place and can be used for treatment dose reconstruction.<sup>53</sup> While biological information of the treatment response would be immensely beneficial toward improving our ability to tailor dose prescriptions over time to meet the needs of specific patients and their response, the clinical application of biologic feedback is in its early stages. Most applications that are in practice today utilize anatomical information and are typically used to adjust the treatment plan in order to meet the original clinical goals.

The clinical implementation of adaptive radiation therapy, however, is a complex issue due to the large amount of resources needed to monitor treatment progress and to implement the treatment modifications. With current technology and systems in place, these modifications usually require a long sequence of events to execute, including time-intensive treatment replanning, quality assurance, and scheduling. This can be a burden for the workload of a radiation oncology clinic and efforts to reduce the time for any of these steps and to streamline the workflow are necessary before wide-ranging implementation can take place.

#### **1.6. Need for treatment time verification and adaptive planning for proton therapy**

As discussed earlier, a major problem with proton therapy is its sensitivity to range uncertainties.<sup>30, 31, 54-56</sup> This is especially the case if there are large anatomical changes that occur during treatment. For example, if the patient loses weight or the tumor shrinks, the proton beam will traverse through less tissue before reaching the target, resulting in the proton beam overshooting the target and overdosing distal normal tissues. Alternatively, if the patient gains weight or the tumor grows due to cancer progression, the beam may encounter a higher density of material, resulting in the proton beam undershooting the target and underdosing the tumor. Any change in tissue density along the path of the proton beam will affect the proton penetration range. Therefore, in proton therapy it is not only important for the target anatomy to be in the same position, but all surrounding anatomy needs to consistently be in the same position as the original plan as well. Consequently, there needs to be some way to track and monitor any potential changes in anatomy throughout the course of

treatment in order to ensure proper dose delivery to the patient and to adapt the proton therapy treatment if necessary.

A review of our institution's numbers for proton therapy patients suggests this need for treatment evaluation. Figure 5 shows the total number of new patients treated and the total number of patients who received some sort of adaptive planning intervention at our institution for select services in the years 2011-2013 (Matt B. Palmer, MBA, CMD, e-mail communication, February 2014). Over these three years, a grand total of 3,033 new patients from these services were treated, of which 199 (7%) of them required an adaptive intervention. In terms of the absolute number of patients, thoracic cancer patients received the most adaptive plans, followed by CNS and pediatric cancer patients, and then head and neck patients. Figure 6 shows a graph of the percentage of the total patients who received an adaptive intervention each year separated by treatment site. Other than gynecological (GYN) patients who had a high percentage due to the small number of cases treated, head and neck and thoracic cancer patients lead with the most percentage of patients within their group requiring adaptive planning. The relative percentage of these patients requiring adaptive planning has been fairly steady over the past three years, suggesting similar needs for adaptive planning within this population of patients.

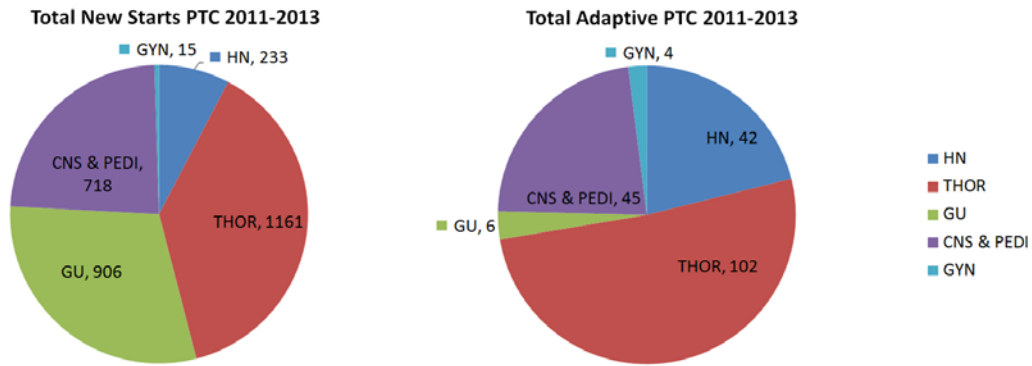


Figure 5: Patient statistics for new start and adaptive cases at the MD Anderson Cancer Center Proton Therapy Center (PTC) for select services in the years 2011-2013. On the left is the total number of new patients treated and on the right is the total number of patients who received some sort of adaptive planning intervention during that time period.

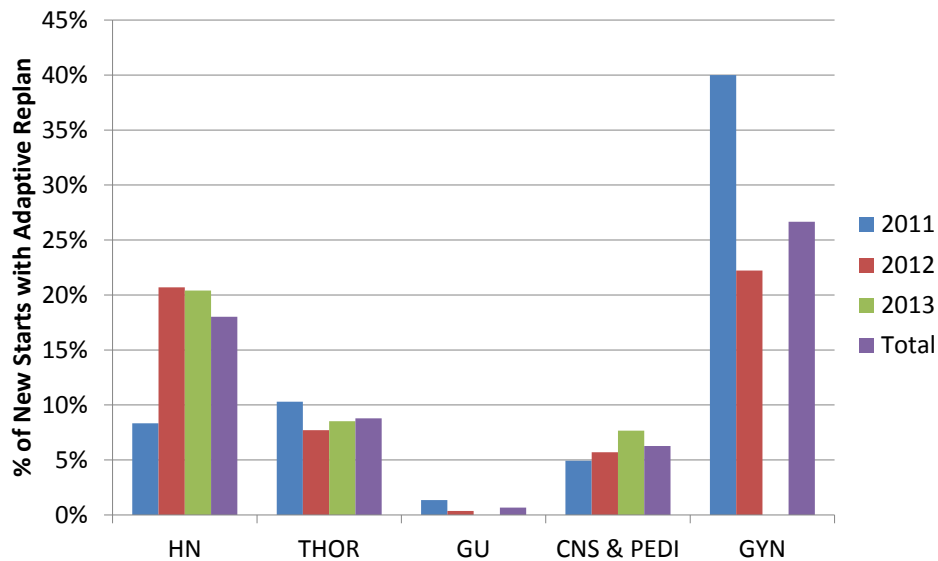


Figure 6: Percentage of the total patients who received an adaptive intervention each year from 2011-2013 separated by treatment site.

### **1.7. Proposed proton dose and range verification methods**

Several methods of proton dose and range verification have been proposed over the past few years using different modalities. One potential method investigated by several groups is the use of positron emission tomography (PET) for imaging activated positron emitting isotopes in tissues.<sup>57-60</sup> Similarly, others have investigated the imaging of prompt gamma ray emissions from similarly activated isotopes in tissues after proton irradiation.<sup>61, 62</sup> Both of these methods have the potential advantage of providing real-time or near real-time verification of dose actually deposited within the patient, but would require the implementation of additional imaging device technologies in the treatment room.

Gensheimer et al. has noticed changes in MRI tissue response after proton radiation exposure that can be used to identify tissues that received dose.<sup>63</sup> However, the extent of these changes seen in MR images will be site dependent and it is difficult to quantify the dose actually delivered to tissues based on MR images alone. Proton “range probes” and proton radiographs or proton CTs have also been proposed to verify in-vivo proton ranges.<sup>64-66</sup> These methods use a high energy proton beam that penetrates through the patient to be detected by a detector. The residual range of the proton beam at the detector can then be compared to a pre-calculated or pre-measured residual range at the time of treatment planning to estimate the range variations. If rotational projection images are acquired, a CT reconstruction can be obtained as well. However, these techniques are still in development and image reconstruction and detection methods are currently being explored.

Another method that can be used to evaluate and monitor proton dose and range variation is with CT imaging. As noted earlier, CT imaging is the foundation for treatment planning which includes dose calculation and evaluation. Additionally, CT-based imaging is



currently used for photon treatment setup for in-room IGRT. Since CT images are currently used for treatment planning in proton therapy, treatment time evaluation with the same modality would allow for an intuitive comparison to the desired doses from the original treatment plan, and would allow for direct replanning on the treatment day CT for adaptive radiation therapy, if necessary.

### **1.8. Proton range calculation from CT imaging**

In order to use CT imaging for proton dose and range verification, we need to understand how to acquire proton range information from the patient images. Proton ranges are commonly described in terms of equivalent ranges in water, often labelled as water-equivalent path length (WEPL) or water-equivalent thickness (WET). This allows for a common comparison of ranges between different types of materials and also allows for an easy way to measure and describe ranges of proton beams through different materials.<sup>67</sup> In order to calculate the WEPL, the linear SPR of the given material to that of water is needed. Information about the SPR for tissues within a patient can be obtained from a CT image by using a CT number-to-SPR calibration curve. An example of the calibration curve used for a clinical CT scanner at the MD Anderson Proton Therapy Center is shown in Figure 7. This calibration curve can be obtained through different means, but the most commonly used technique for radiation therapy planning is the stoichiometric method that was originally proposed by Schneider et al.<sup>68</sup> This method uses both measured Hounsfield units (HU) of tissue substitutes and the chemical composition of tissues in order to predict the HU for human tissues in the images.

With the calibration curve, we can determine the SPR of tissues within each voxel of the CT scan. Therefore, given the path of a proton beam through the CT scan (as can be determined by the beam angle and isocenter of the beam), the WEPL can be calculated by taking the cumulative SPR through the voxels along the path of the proton beam. Therefore, with information obtained from a treatment-time CT image along with the beam parameters that are determined for a patient's treatment, we can calculate the expected penetration depth and position of a proton beam within the patient.

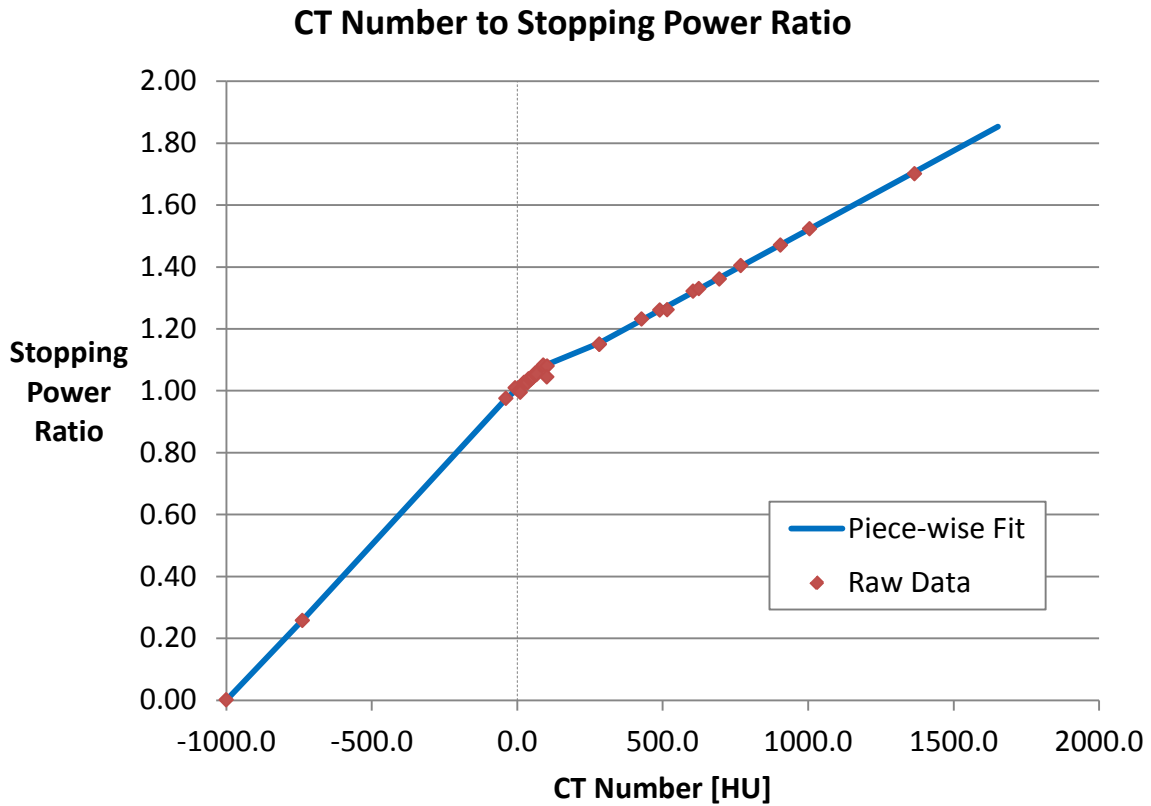


Figure 7: Example of the CT Number-to-SPR calibration curve used for a clinical CT scanner at the MD Anderson Proton Therapy Center

### **1.9. Conceptual shift in utilizing IGRT for protons**

The sensitivity of proton beams to all tissues along the beam path makes it difficult to estimate the impact of visible anatomic changes in a CT image to the dose distribution within the patient. This complicates the idea of image guidance for proton therapy because visible alignment of the target soft tissue or bony anatomy may not be enough to ensure dose coverage.<sup>31, 69-71</sup> This is inherently a big conceptual change compared to current utilization of IGRT techniques in photon therapy.<sup>72</sup> Figure 8 shows the differences between the effects of weekly anatomical change in a lung patient on the dose from a photon intensity-modulated radiation therapy (IMRT) plan and a proton PSPT plan. The doses from each weekly CT scan for this patient, after taking into account patient rigid alignment to bony anatomy, are overlaid on top of the original planning CT. Notice that even though the patient positioning was corrected for using rigid alignment, the doses from the proton plan (particularly in the distal edge of each of the beams) vary considerably whereas the doses from the photon plan remain fairly static. Therefore, the underlying assumption in photon radiotherapy that the target can be shifted as a rigid object in an invariant (or static) dose cloud<sup>73</sup> is not necessarily valid in proton therapy. The proton dose distribution is intrinsically non-static due to the finite range of the proton beam which depends heavily on the density of the material along its beam path. In addition to the anatomical changes, if the patient is rigidly shifted around, the shape of the dose distribution can vary as well depending on the heterogeneities within the path of the beam.

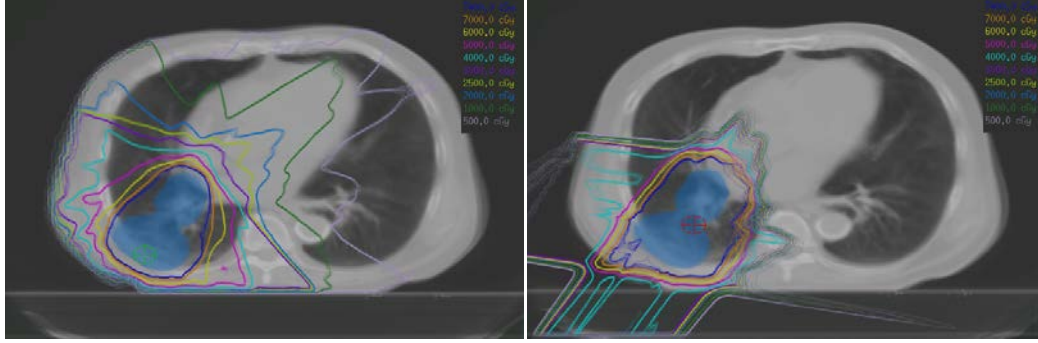


Figure 8: Example of dose variation due to anatomy change between photon and proton beam therapy. Doses due to weekly anatomical motion change overlaid over the original planning CT scan for (left) photon IMRT, and (right) proton PSPT plans. Notice the large amount of dose distribution changes (the blurring of the isodose lines) seen in the distal edges of the proton beam plan compared to the relatively small changes seen in the photon IMRT plan.

In order to fully utilize the daily anatomical information from these volumetric images, we need to take into account the physical dose deposition properties of protons to predict where the dose will go in the patient. Ideally, full dose recalculations with a dose calculation algorithm would be utilized on a daily basis to check the dose distribution on the daily anatomy and to assess different setup positions (i.e. different couch shifts). However, dose calculation engines are currently too slow to use for online dose assessment. Therefore, a quick method of estimating the daily proton range or proton dose distribution is necessary in order to perform online patient verification. If this range or dose information is available, corrections can be performed to adjust for deficiencies in dose delivery.

## **CHAPTER 2: HYPOTHESIS AND SPECIFIC AIMS**

### **2.1. Goals for this project**

The main objective of this work is to investigate the potential use of online 3D volumetric imaging with conventional kilovoltage CT to improve our ability to deliver the correct radiation dose to cancer patients treated with proton therapy. One goal is to transfer the ideology of 3D IGRT from the realm of photons to protons. However, with the unique properties of proton therapy, the ideology of image guidance will need to be modified. As with any image-guidance procedure, this requires the development of a method of detection of anatomy change from imaging information, and a correction intervention strategy. Specifically for this project, this involves the design of a method for treatment day dose verification, and then performing corrective strategies of isocenter shifts or adaptive planning. These objectives will be explored in the three specific aims as described below. All of the techniques developed in this work are aimed to be feasibly used as an online process.

### **2.2. Overall hypothesis**

A radiological pathlength calculation algorithm based on CT imaging can be used for:

- 1) online proton beam treatment day verification and isocenter adjustment, and
  - 2) an online adaptive range adjustment technique based on pathlength correction
- in order to maintain target coverage and reduce normal tissue dose.

### 2.3. Specific Aims

**Specific Aim 1:** To develop an online proton dose verification tool based on daily CT imaging to assess the effect of anatomy change on the proton beam and validate its ability to evaluate target coverage and dose distribution.

**Working Hypothesis:** The online range corrected dose approximation tool can estimate the dose distribution based on the new patient anatomy to an accuracy given by a gamma index  $(3\%/3\text{mm}) \geq 85\%$  when compared to full dose recalculation.

In this aim, we will implement a radiological pathlength calculation algorithm based on CT imaging to map out treatment day range changes and to use this information to create a fast range compensated dose approximation method to estimate the treatment day dose. This technique should be relatively quick and would enable us to perform an online visualization of the impact of daily anatomical changes on proton range and dose. This fast dose approximation will also allow for the use of dose information in the IGRT process and can be used as a tool for quick dose verification in order to determine if adaptive planning is necessary.

**Specific Aim 2:** To devise a novel patient setup correction method for proton therapy based on dosimetric indices and to assess its ability to maintain target coverage and improve normal tissue sparing.

Working Hypothesis: Using the dosimetric alignment method based on the fast range compensated dose approximation technique (from specific aim 1) will result in a statistically significant reduction in normal tissue dose compared to anatomical alignment.

The second aim is to develop an approach to correct for patient anatomy changes by simply performing a rigid couch shift. This is analogous to using the anatomical information in IGRT for target localization and patient setup. However, anatomical alignment is not necessarily the optimal patient position, and range or dose information needs to be taken into account when evaluating patient setup. By developing a methodology for incorporating daily range variations into the online dose verification process, we can use this information to determine the best possible patient setup without modification of beam parameters.

**Specific Aim 3:** To develop an online range compensation beam adjustment technique to correct for range variations due to anatomical changes while preserving target coverage in proton therapy.

Working Hypothesis: The online range-adaptive technique based on pathlength correction can maintain the original target dose coverage (V95%) to within 5% while significantly reducing normal tissue dose compared to non-adaptive treatments for patients with large anatomic change.

The goal of the third aim is to determine if an online range-adaptive or range compensation technique can be used for online adaptive radiation therapy. This range-adaptive technique

will be used to correct for changes in proton range due to anatomy changes and relative shifts in heterogeneities. We propose that, based on the results of the radiological pathlength calculation, proton range perturbations due to anatomy change relative to the nominal plan can be compensated for directly and used to correct the proton beam for day-to-day anatomy changes in order to match the original planned isodose lines without a full reoptimization.



## **CHAPTER 3: SPECIFIC AIM I - DEVELOPMENT OF CT-BASED FAST PROTON RANGE AND DOSE VERIFICATION TOOLS**

(This chapter is based upon *P. C. Park, J. Cheung, X. R. Zhu, N. Sahoo, L. Court and L. Dong, "Fast range-corrected proton dose approximation method using prior dose distribution," Phys. Med. Biol. 57, 3555 (2012)* as published by the author of this dissertation and the right to include this work in the author's own research dissertation is exercised as established under the transfer of copyright agreement with IOP Publishing Ltd.)<sup>74</sup>

### **3.1. Introduction**

#### **3.1.1. Evaluation of setup and anatomical uncertainties for proton therapy**

Understanding and inclusion of various effects of uncertainties on a planned dose distribution are a vital part of the treatment delivery evaluation process. The treatment planning dose distribution is only a snapshot of the dose based on the assumed setting at the time of calculation and is therefore subject to variations under different conditions, including patient setup and anatomical changes. This is particularly true for proton therapy because proton beam ranges depend heavily on the tissue density along its path. Any changes that can influence the given WEPL of the proton beam can potentially result in differences between the delivered and planned dose distributions. This includes anatomical changes over the course of treatment, as well as slight shifts in the patient position or isocenter.

Uncertainties in setup and range can cause differences between the value of WEPL from the treatment plan and actual WEPL at the time of beam delivery.<sup>30, 31, 37, 75</sup> Also, both intra- and inter-fractional anatomical changes have been shown to cause significant changes in the planned dose distribution.<sup>76-78</sup> In addition, trends through the weeks of treatments can

further change the dose distributions compared to the original treatment plan, such as patient weight loss and tumor volume change in response to radiation <sup>79</sup>. For conventional photon therapy such as 3-dimensional conformal radiotherapy or IMRT, geometrically expanded volumes such as PTV or planning organ-at-risk volume (PRV) are routinely used for robust treatment planning and evaluation.<sup>33, 34</sup> A photon treatment plan that is designed to deliver sufficient dose to the PTV can be thought of as a robust plan as long as the CTV resides within the PTV volume. In terms of treatment evaluation, dose coverage to PTV and PRV can be thought of as the worst case scenario for the CTV and organ-at-risk (OAR) volumes, respectively. However, this is based on the assumption that the dose distribution is static and that the calculated dose distribution under the nominal (reference) setting will not change significantly with respect to the changes in patient surface contour, tissue density, and organ motion. In this situation, the photon dose distribution does not need to be re-calculated because it is virtually independent of patient's anatomy. This so called static dose distribution assumption holds true for conventional photon therapy to a certain extent.<sup>73</sup> However, numerous authors have discussed the fallacy of using the static dose distribution assumption in proton therapy primarily due to the fact that proton ranges are sensitive to the change in tissue density or WEPL.<sup>80, 81</sup> This effect can, again, be seen in Figure 8 which shows the photon IMRT dose with minimal blurring while the distal end of the proton dose is blurred noticeably due to changes in patient anatomy.

Ideally, in order to gauge the robustness of a given proton treatment plan under various situations, multiple dose calculations are required in order to simulate different possible changes. Recently, researchers have developed methods which incorporate multiple dose distributions under different setup and range errors to derive dose volume histograms

(DVHs) or its derivatives in order to evaluate treatment robustness.<sup>82-84</sup> Similarly, if the anatomy changes over the course of treatment, the proton dose distribution will need to be recalculated on the new treatment-time image in order to get an accurate assessment of the dose delivered. However, due to the computational cost of calculating proton dose distributions under various circumstances, the clinical feasibility of robust evaluation and optimization are difficult to implement. Additionally, if online dose calculation is needed for patient setup, a full dose recalculation may be too time-intensive if multiple calculations are required for dose reassessment after changing patient position.

### **3.1.2. Using range deviations for dose approximation**

In this aim, we describe a fast range-corrected dose approximation method based on a composite version of the methods described by Unkelbach *et al.*<sup>69</sup> The major difference in our method compared to theirs is that we use the dose distribution from the nominal setting to ‘predict’ the new dose under a small perturbation in WEPL without requiring the detailed knowledge of the individual dose contributions from pre-calculated virtual pencil beams. This is motivated by the heuristic observation that perturbation of the WEPL along the beam path pulls the dose profile proximally or distally from the nominal setting without significantly changing its overall shape. Figure 9 illustrates an example of dose profile variation after a single insertion of a high-density object in the beam path. Therefore, we can estimate the dose delivered by assessing the change in ranges to different locations in the image. One way of visualizing this is by generating a contour map of range-equivalent isodose line compared to a reference image. In essence, this would give an approximation of where the isodose that was intended to cover the target ended up on treatment day anatomy.

This would allow for a very quick estimation of the coverage provided on the treatment day target. An example of this is shown in Figure 10 for a pelvic phantom. Even better, the entire new dose distribution can be estimated by simply shifting the dose profiles based on an “iso-WEPL” along the beam direction. An example of this estimated dose distribution for the same pelvic phantom compared to the treatment planning system dose calculation is shown in Figure 11. This equivalent-WEPL based dose correction strategy can be very quick and can reduce both computational time and computer memory requirements compared to full dose recalculation. We will benchmark the fast range-corrected dose approximation method against the full dose calculation using a commercial treatment planning system that is based on the 3D pencil beam convolution method.<sup>85, 86</sup> Furthermore, we will assess the ability of the dose approximation method to estimate DVH curves.

### **3.2. Methods and Materials**

In principle, the dose to a point can be calculated by summing up all contributions of doses from individual beamlets. Here, we will not pursue the dose calculation of each individual beamlet; rather, we make the assumption that the scattered dose from small changes in the patient’s anatomy will remain constant and the dose effect is only caused by the change in the cumulative WEPL at each voxel along the beam path. This WEPL can be calculated from CT images as was described in Section 1.8. Taking advantage of the full dose calculation at the nominal position, we can derive the new dose distribution by shifting dose along the beam path based on the equivalent WEPL from the original plan. One can think of this as a mapping process where a previously known dose distribution is re-organized to give a new

dose distribution. This requires that a single full dose calculation is performed using the planning CT images under the nominal setting.

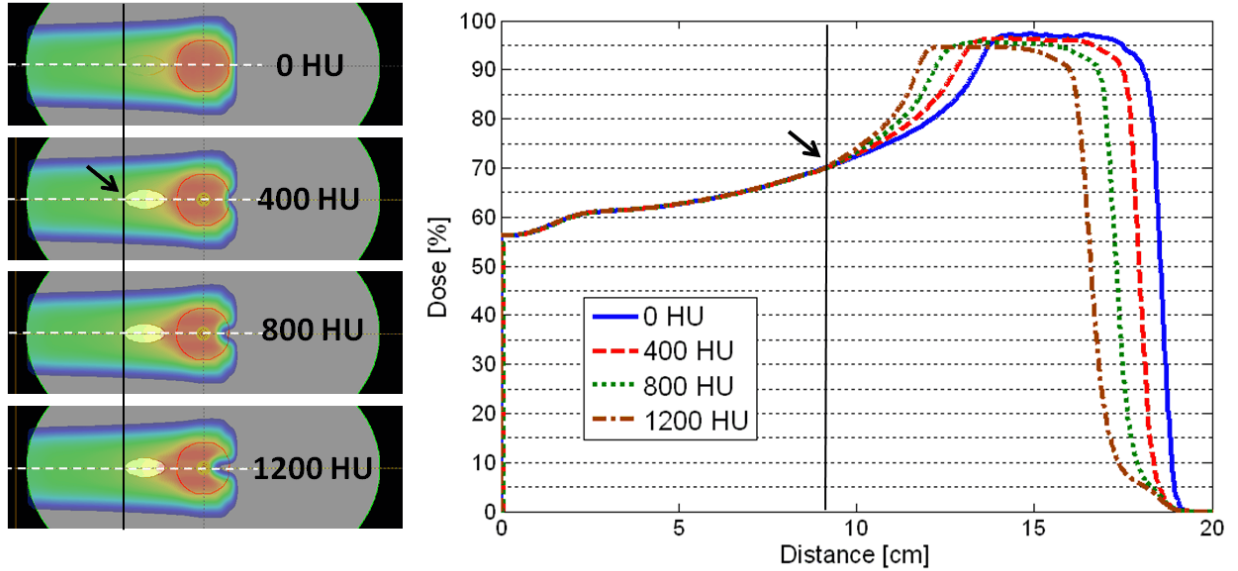


Figure 9: Example of the dose profile variation due to high density material. An oval shaped heterogeneity was inserted in the beam path to simulate anatomical changes. The density of the object varied from 0 HU to 1200 HU in increments of 400 HU. The line dose profiles beyond the start location of heterogeneity (indicated by the arrow) are pulled proximally towards the source as the density of the heterogeneity increases according to the effective change in the WEPL while the rest of the profile proximal to the heterogeneity remains approximately the same.

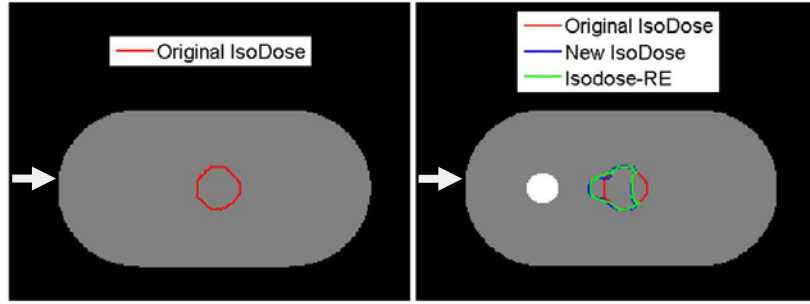


Figure 10: An example of estimating the range variation due to treatment day anatomy change using our radiological pathlength algorithm to calculate a range-equivalent isodose line. A treatment plan was generated for the original anatomy (left) and recalculated on the altered anatomy (right) in which a bone-like object is placed in the beam path. The range perturbation is calculated using the WEPL for the 100% isodose line (isodose-RE) and matches fairly well with the new isodose line from full dose calculation in our treatment planning system.

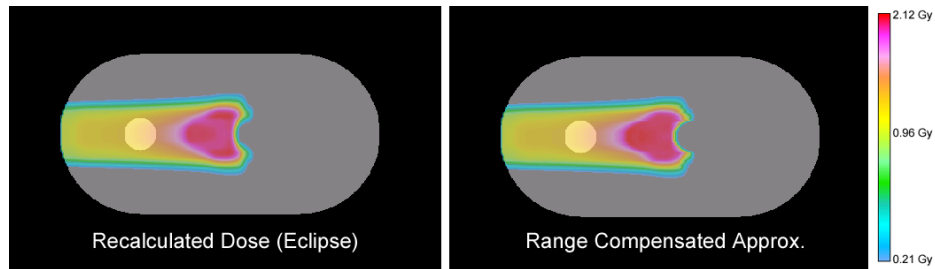


Figure 11: The dose distributions from the full dose recalculation from our treatment planning system (left) versus the range-compensated dose approximation (right) for the pelvic phantom with bone-like material inserted into the path of the beam.

In this study, we used our clinically commissioned proton treatment planning system (Eclipse™ version 8.9, Varian Medical Systems, Inc., Palo Alto, CA, USA). This dose

distribution is referred as the nominal dose distribution ( $D$ ) while the dose under the testing situation is referred as realized dose distribution ( $d$ ).  $D$  will be used as a template when we approximate  $d$  under the influence of both position and anatomical change. For convenience, we used a beam's eye view (BEV) coordinate and the z-axis as the depth along the beam's axis. A point dose at an arbitrary coordinate of  $(x, y, z)$ , with  $(0,0,0)$  being defined at the isocenter, under nominal setting can be written as  $D_{x,y,z}$ . The realized dose to that point can be written as a function of the patient shift error  $(\Delta x, \Delta y, \Delta z)$  and change in physical depth ( $z'$ ), giving  $d_{x,y,z}(\Delta x, \Delta y, \Delta z, z')$ . It should be noted that  $z'$  is a fundamentally different quantity than  $\Delta z$ :  $\Delta z$  is the magnitude of patient position change in physical space whereas  $z'$  is the location in depth under nominal setting which corresponds to the same WEPL for the depth at  $z$  under the realized or testing setting.

For the case of the static dose distribution (i.e. for photon beam), we can immediately approximate the realized dose to a point as follows:

$$d_{x,y,z}(\Delta x, \Delta y, \Delta z) = D_{x+\Delta x, y+\Delta y, z+\Delta z} \quad (\text{Eq. 4})$$

In this formulation, one can see that for static dose distribution, the realized dose can be approximated by simply moving the entire dose cloud to align with the patient anatomy in its new position. To account for the variant dose distribution, we assume that the perturbation in WEPL moves point doses in physical space according to their WEPL values in the original plan.

### 3.2.1. Approximation under setup error or patient shift

If setup error occurs or if a dose calculation is needed after a patient shift, there will be a change in WEPL due to the misaligned tissue density along the plane that is perpendicular to the beam's axis. This will lead to a difference in WEPL between the line segments tracing different locations in space. Therefore, in order to approximate the realized dose at a point, we need to account for the difference in WEPL between the line segments tracing different locations in space by

$$d_{x,y,z}(\Delta x, \Delta y, z') = D_{x+\Delta x, y+\Delta y, z'} \times INV(z, z'), \quad (\text{Eq. 5})$$

where  $z'$  is given by the following line integral relation

$$\int_s^z rsp(x, y, z) dz = \int_s^{z'} rsp(x + \Delta x, y + \Delta y, z) dz \quad (\text{Eq. 6})$$

The function  $rsp(x, y, z)$  is the relative stopping power ratio from the given CT data and  $s$  is the effective source position. Simply put, (Eq. 5) approximates the realized point dose by shifting the ray line geometrically (in the BEV coordinate) while adjusting the longitudinal dose profile given by that shifted ray line according to the effective change WEPL from (Eq. 6). In (Eq. 5),  $INV(z, z') = \left( \frac{z' + VSAD}{z + VSAD} \right)^2$  is the inverse square factor to compensate for the loss in protons in a divergent beam with the effective source-to-axis distance (VSAD). Here, the effect of a patient shift along the direction of the beam axis ( $\Delta z$ ) is ignored (except for the inverse square factor) because it is equivalent to adding an air gap between the source to the patient body surface which adds a negligible change in WEPL.

In general,  $z'$  can only be determined by solving (Eq. 6) iteratively, making it the most time consuming step for this method. The computational time can be decreased by saving the



line integral values at different depth with the corresponding  $D$  values in computer memory and referencing them as a look up table for later use.

### 3.2.2. Approximation under anatomical change

For anatomical deformation without considering the setup error (assuming the images have been registered together), we can approximate the realized dose as

$$d_{x,y,z}(z') = D_{x,y,z'} \times INV(z, z'), \quad (\text{Eq. 7})$$

where  $z'$  is given by the limit of the following integrals

$$\int_s^z rsp(x, y, z) dz = \int_s^{z'} rsp^{New}(x, y, z) dz \quad (\text{Eq. 8})$$

In this case, the realized dose will be a function of the effective change in WEPL caused by the anatomical deformation, which can be tracked using the new images (i.e. treatment-time CT images), which gives the function  $rsp^{New}$ . For the above formula, the location of the line being integrated is identical since no setup error is assumed but  $rsp^{New}(x, y, z)$  is used on the right side of (Eq. 8) to account for the anatomical deformation given by the new images. Finally, the approximation method under setup error and anatomical deformation can be combined to give a general formulation

$$d_{x,y,z}(\Delta x, \Delta y, z') = D_{x+\Delta x, y+\Delta y, z'} \times INV(z, z'), \quad (\text{Eq. 9})$$

where again,  $z'$  is given by the limit of the following integrals

$$\int_s^z rsp(x, y, z) dz = \int_s^{z'} rsp^{New}(x + \Delta x, y + \Delta y, z) dz. \quad (\text{Eq. 10})$$

This range corrected dose approximation method can be summarized as a simple dose mapping algorithm which maps previously calculated dose distributions onto a new one based on the following steps:

**Step 1.** Calculate the WEPL to a point along the beam path under the nominal setting.

**Step 2.** Translate beam's isocenter according to the position change or introduce new CT images.

**Step 3.** Calculate WEPL along the corresponding line segment and locate the physical point along the depth which has the same WEPL as calculated in Step 1.

**Step 4.** Correct for inverse square factor based on the original physical location found in Step 3.

**Step 5.** Repeat steps 1-4 for all points in the image.

### **3.2.3. Validation for patient cases**

In order to validate our dose approximation method, we compared the dose distributions calculated using a static dose approximation, our proposed range-corrected dose approximation, and a full 3D pencil beam convolution method from our clinical treatment planning system (TPS). All dose calculations were performed using a dose grid resolution of  $2 \times 2 \times 2.5 \text{ mm}^3$ . First, a lung cancer patient was selected. The patient received 4-dimensional computed tomography (4DCT) scans for treatment planning and weekly over the course of treatment with a 1mm pixel size and 2.5mm slice thickness over the first 6 weeks (denoted week0 to week6) of treatments. To simplify intra-fractional dose calculation, we used the average image from the 4DCT data sets for each week. Treatment plan under nominal setting and all consequent dose calculations were done on these averaged CT data

sets following the clinical protocol used at our institution.<sup>87</sup> The PTV was generated by a uniform expansion of the CTV with 5mm margins. This margin size was deliberately chosen to push the limit of the plan's robustness to CTV coverage when we simulate position shifts up to 8mm. All the volumes of interest were contoured by a physician on the planning CT and were deformed to weekly CT data sets using an in-house developed deformable image registration software.<sup>88, 89</sup> The nominal dose was calculated using the planning CT data set with no assumed setup error via the spot scanning beam delivery method with single-field optimization.<sup>7</sup> The position shifts were then simulated by shifting the planning CT images along the Anterior-Posterior direction  $\pm 8\text{mm}$  in 2mm intervals. At each interval, doses were calculated using all three different methods: static dose approximation, our proposed range-corrected dose approximation, and a full recalculation with the TPS. For the weekly CT data sets, doses were calculated using all three different methods after manual alignment of beam's isocenter based on the bony anatomy to separate the effect of setup error.

Similarly, we validated the proposed method on a prostate and a head & neck (HN) patient case with inter-fractional anatomic changes to show the applicability of the proposed method to these sites as well. The prostate case was chosen due to a change in the femur position on the day of treatment. The HN case was chosen because of a substantial change in the nasal air cavity in the beam path on week 6 of treatment, which was partially due to a head rotation and tissue/fluid variation in the nasal cavity. We used a  $270^\circ$  beam angle for the prostate case, and a  $0^\circ$  beam angle for the HN case.

The overall accuracy of both approximation methods were quantified through the use of a 3D gamma analysis tool developed in-house.<sup>90</sup> Our gamma analysis was performed using a common 3% dose-difference and 3mm distance-to-distance agreement criteria (3%,

3mm). We also performed the gamma analysis using other criteria, (1%, 3mm) and (3%, 4mm), due to possible interest for different levels of accuracy for different applications. All gamma analyses were performed on the dose distribution greater than 10% of the prescription dose. In order to quantify the accuracy of the cDVHs derived using the range-corrected method, cDVHs were subtracted from the corresponding cDVHs derived using full dose calculation (The difference is denoted as  $\Delta$ cDVH).

### **3.3. Results**

#### **3.3.1. Dose distribution comparison and 3D gamma analysis**

For all cases, the amount of dose variations gradually increased as position shift increased from 0mm to 8mm in both directions (perpendicular to the beam line). For the lung case, the amount of dose variation was gradually increased from week0 to week6 while both prostate and HN cases showed no obvious increment in dose variation over the weeks. Table 2 shows % volume change of the tumor in the entire breathing cycle (i.e. integrated gross tumor volume and clinical target volume (IGTV and ICTV), and GTV-50 and CTV-50, the volumes for the exhale phase of the breathing cycle) for the lung patient over the course of treatment. The largest variation of the planned dose distribution amongst all of the simulations was observed when we recalculated dose using the 6<sup>th</sup> treatment week's CT images for both lung and HN cases and the 1<sup>st</sup> week CT images for the prostate case.

Table 2: The measured volume change of the target volumes of interest observed in the weekly CT images for the lung case in Specific Aim 1. The structures were contoured on the planning CT and deformed to the weekly CT images using in-house deformable image registration software. For the selected patient case, a reduction of 41% of the gross tumor volume (GTV-T50 and IGTV) and 21% of the clinical target volume (CTV-T50 and ICTV) was observed.

Site (week)	Volume [cc] (% Volume change)			
	GTV-T50	CTV-T50	IGTV	ICTV
Lung (week 0)	128 (0%)	323 (0%)	148 (0%)	331 (0%)
Lung (week 1)	110 (−14%)	300 (−7%)	126 (−15%)	307 (−7%)
Lung (week 2)	96 (−25%)	277 (−14%)	110 (−25%)	286 (−14%)
Lung (week 3)	90 (−30%)	275 (−15%)	104 (−29%)	282 (−15%)
Lung (week 4)	82 (−36%)	264 (−18%)	96 (−35%)	272 (−18%)
Lung (week 5)	77 (−40%)	257 (−20%)	90 (−39%)	264 (−20%)
Lung (week 6)	76 (−41%)	254 (−21%)	88 (−40%)	262 (−21%)

Visually noticeable change in dose distribution was observed when position changes and anatomical deformations were introduced. Figure 12 (a) and (b) compares planned dose distribution and the realized dose distribution using full dose calculation. It shows, as a result of weight loss and tumor shrinkage, the proton beam penetrating deeper in to the patient, delivering a significant dose to the contralateral lung. The original spatial dose distribution given by the static approximation (Figure 12 (c)) fails to adjust for such a change and thereby significantly underestimates the dose to contralateral lung. However, the realized dose

distribution computed using the range-corrected method (Figure 12 (d)) is able to estimate the change in depth penetration of the proton beam with a reasonable accuracy.

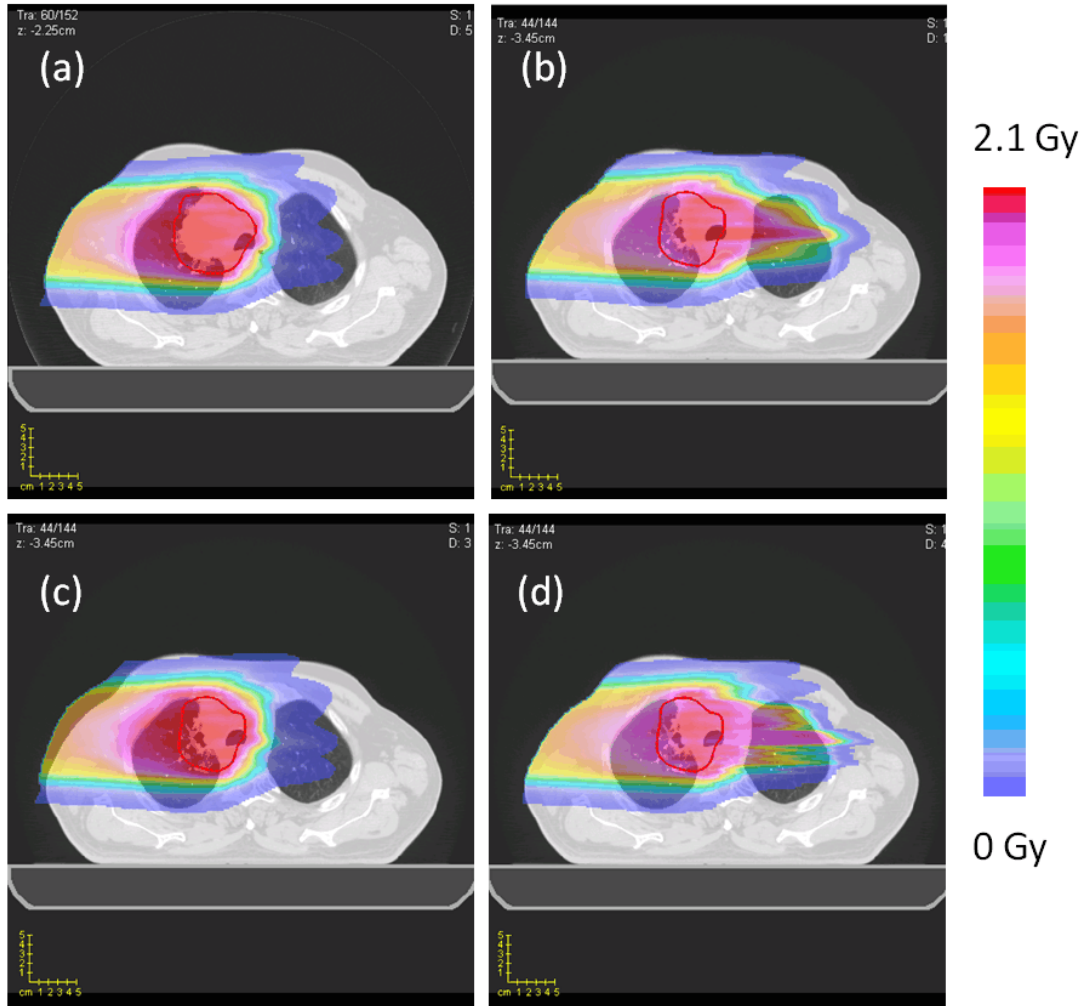


Figure 12: An example of the resultant dose distributions for the lung case for dose approximation. (a) The full dose (TPS) calculation on the lung planning CT (planned dose distribution). (b) The full dose (TPS) calculation on the lung week6 CT (realized dose distribution). (c) The static dose approximation on the lung week6 CT. (d) The range corrected dose approximation on the lung week6 CT.

Percent dose difference map (week6)

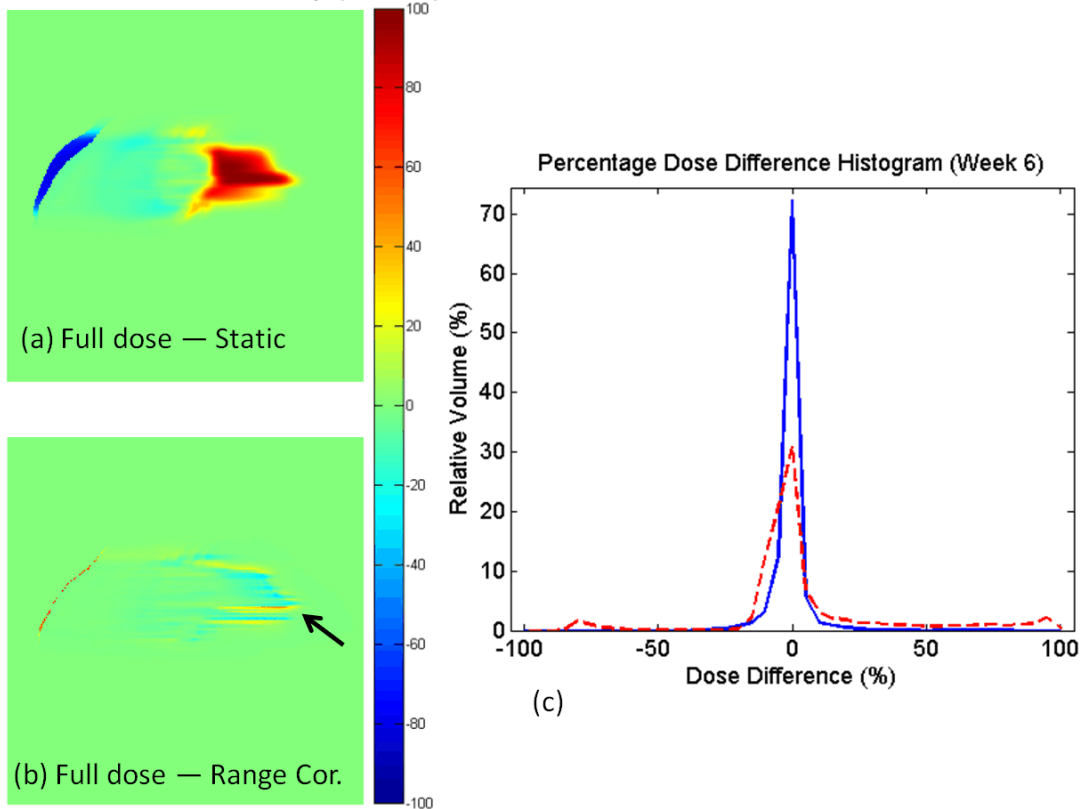


Figure 13: An example of the dose difference between different proton dose calculation methods. The percent dose difference map on the lung week6 CT between dose distribution using full calculation and dose distribution using (a) static dose approximation, (b) range corrected approximation, and (c) the percentage dose difference histograms for the two difference maps. Red dashed line in the histogram is derived from (a) while blue solid line is derived from (b).

Figure 13 shows percentage dose difference maps of the dose distributions between the full dose recalculation and the static dose approximation, and the full dose and the range corrected dose approximation. Note that an over estimation near the patient skin surface and an under estimation in the contralateral lung region was apparent from the static dose

approximation method while a significant improvement was observed when using the range-corrected approximation method.

The results of the gamma analyses are presented in Table 3, Table 4, and Table 5. The lowest passing rate was observed at the limit of our simulation ranges (8mm position changes and lung 6th week). Under the (3%, 3mm) criteria, the range-corrected method achieved a 93% passing rate for an 8mm position change while the static dose approximation method achieved only an 81% passing rate. For the weekly CT simulation, the range-corrected method achieved an 86% passing rate for the 6<sup>th</sup> week CT while the static dose approximation method achieved only 36% passing rate. For the other gamma index criteria, (1%, 3mm) and (3%, 4mm), the general results were similar. They are presented here out of interest for possible other applications in which different passing criteria would be of interest.

For the (3%, 3mm) criteria, the worst passing rate found for the 3D gamma analysis of the prostate case was 89% and 83% for the range corrected and the static approximation methods, respectively. Similarly, the worst passing rate found for the HN case showed 84% and 70% passing rates for range corrected approximation and static approximation methods, respectively. Figure 14 and Figure 15 show the comparisons graphically. The original plan calculated for the anatomy in the treatment planning CT image is shown in the left panel for each case; the dose distributions in the changed anatomy (due to inter-fractional variations) are calculated by the commercial TPS (Eclipse; middle column) and the dose approximation method (right panel), respectively. It can be seen that the range-corrected dose approximation method did a reasonable job overall. Most differences are seen in regions with sharp change in WEPL. In these regions, more accurate modeling of lateral scatter appears to be important.



Table 3: The result of the (3%, 3mm) 3D gamma analysis on both the ranged-corrected approximation and static dose approximation with respect to the full dose (TPS) calculation under position change and weekly CT simulations. For the sake of simplicity, for both prostate and HN cases, only the worst passing rate observed during weekly simulation is shown (week1 for prostate and week6 for HN).

Lung Position change (mm)	3D Gamma (% Passing)		Site (Week)	3D Gamma (% Passing)	
	(3%, 3mm)	(3%, 3mm)		(3%, 3mm)	(3%, 3mm)
	Range corrected	Static		Range corrected	Static
-8	94%	81%	Lung (0)	100%	100%
-6	95%	87%	Lung (1)	89%	75%
-4	97%	93%	Lung (2)	89%	74%
-2	98%	98%	Lung (3)	91%	66%
0	100%	100%	Lung (4)	89%	54%
2	98%	98%	Lung (5)	86%	43%
4	96%	93%	Lung (6)	86%	36%
6	95%	88%	Prostate (1)	89%	83%
8	93%	83%	HN (6)	84%	70%

Table 4: The result of the (1%, 3mm) 3D gamma analysis on both the ranged-corrected approximation and static dose approximation with respect to the full dose (TPS) calculation under position change and weekly CT simulations. For the sake of simplicity, for both prostate and HN cases, only the worst passing rate observed during weekly simulation is shown (week1 for prostate and week6 for HN).

Lung Position change (mm)	3D Gamma (% Passing)		Site (Week)	3D Gamma (% Passing)	
	(1%, 3mm)	(1%, 3mm)		(1%, 3mm)	(1%, 3mm)
	Range corrected	Static		Range corrected	Static
-8	57%	74%	Lung (0)	100%	100%
-6	66%	78%	Lung (1)	64%	44%
-4	77%	83%	Lung (2)	61%	44%
-2	90%	89%	Lung (3)	67%	39%
0	100%	100%	Lung (4)	64%	28%
2	91%	90%	Lung (5)	55%	22%
4	78%	84%	Lung (6)	59%	17%
6	67%	78%	Prostate (1)	58%	49%
8	59%	74%	HN (6)	60%	12%

Table 5: The result of the (3%, 4mm) 3D gamma analysis on both the ranged-corrected approximation and static dose approximation with respect to the full dose (TPS) calculation under position change and weekly CT simulations. For the sake of simplicity, for both prostate and HN cases, only the worst passing rate observed during weekly simulation is shown (week1 for prostate and week6 for HN).

Lung Position change (mm)	3D Gamma (% Passing)		Site (Week)	3D Gamma (% Passing)	
	(3%, 4mm)	(3%, 4mm)		(3%, 4mm)	(3%, 4mm)
	Range corrected	Static		Range corrected	Static
-8	98%	87%	Lung (0)	100%	100%
-6	98%	92%	Lung (1)	94%	82%
-4	99%	96%	Lung (2)	94%	83%
-2	100%	99%	Lung (3)	96%	74%
0	100%	100%	Lung (4)	95%	63%
2	100%	100%	Lung (5)	92%	51%
4	99%	97%	Lung (6)	93%	45%
6	98%	93%	Prostate (1)	94%	89%
8	97%	89%	HN (6)	93%	83%

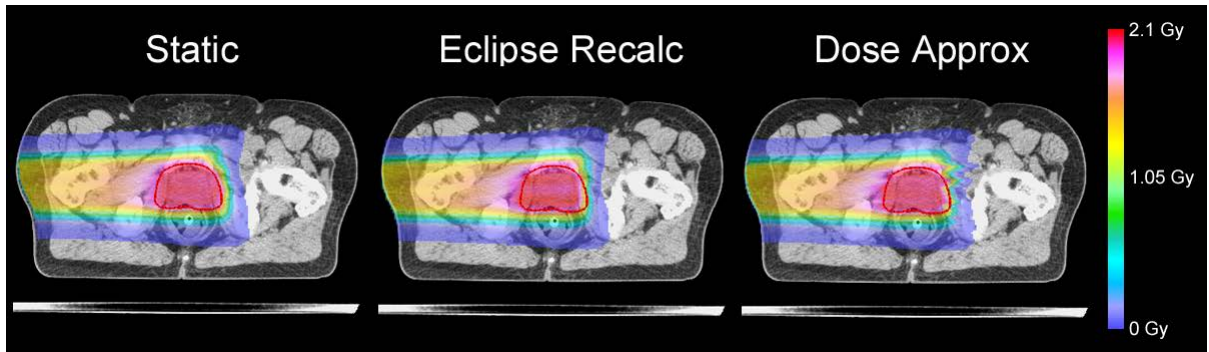


Figure 14: A comparison of the dose calculation results in the presence of inter-fraction anatomical changes for the prostate case. The dose distributions for the changed anatomy calculated by the commercial treatment planning system (Eclipse, Varian Medical Systems) are shown in the middle column, and the dose distributions calculated by the range-corrected dose approximate method are shown to the right, respectively.

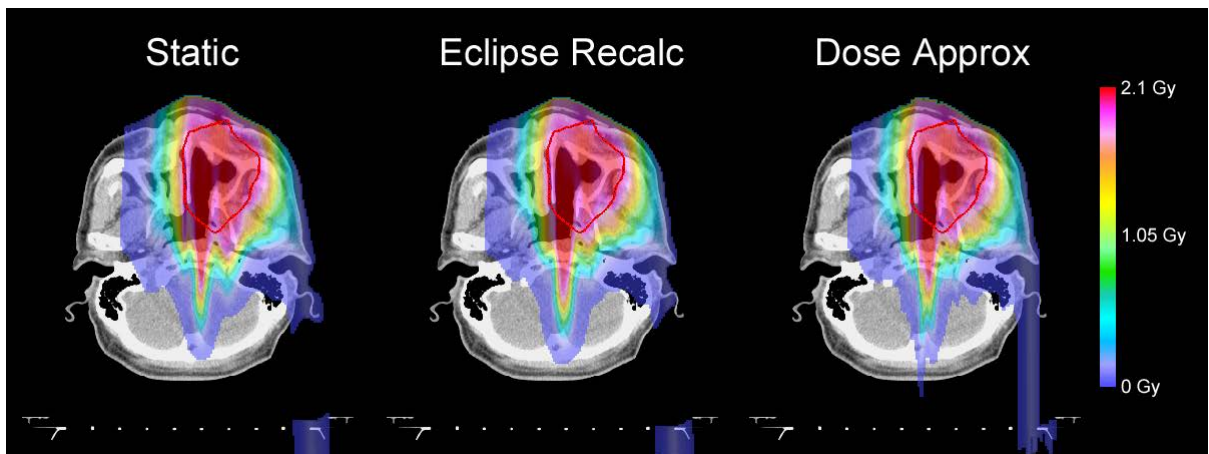


Figure 15: A comparison of the dose calculation results in the presence of inter-fraction anatomical changes for the head-and-neck case. The dose distributions for the changed anatomy calculated by the commercial treatment planning system (Eclipse, Varian Medical Systems) are shown in the middle column, and the dose distributions calculated by the range-corrected dose approximate method are shown to the right, respectively.

### 3.3.2. DVH comparisons

The change in the planned dose distribution due to both setup and anatomical deformation resulted in variation of cDVHs derived from realized dose distributions. Figure 16 compares the DVH-bands (the area enclosed by the envelope of the cDVHs) of various structures using full dose calculation and different dose approximation methods. Figure 17 shows a mesh plot of the differences for visualization of several of the structures that we observed. The overall shape of the DVH-bands derived using range-corrected method closely resembled the DVH-bands derived using the full dose calculation, while the DVH-bands derived using static method mostly under estimated the thickness of the bands for the CTV and other structures (except for the esophagus under setup position change simulation). In the case of weekly simulation, the static dose approximation completely failed to account for the decrease in dose to the target volume and increase in dose to the left lung and esophagus. Table 6 lists the RMS and the maximum difference from the  $\Delta$ cDVH. Overall, the RMS deviation and maximum difference were larger for the CTV and esophagus than for other structures due to their small volume size and their position near the high dose gradient. For the lung case, the largest of the RMS deviation found were within 2% for both the setup and weekly simulation. The largest of the maximum differences were found to be within 4% and 8% for setup and weekly simulation, respectively. The average of the maximum differences over all simulations was found to be 1.5% and 2.6% for setup and weekly simulation, respectively for the lung case.

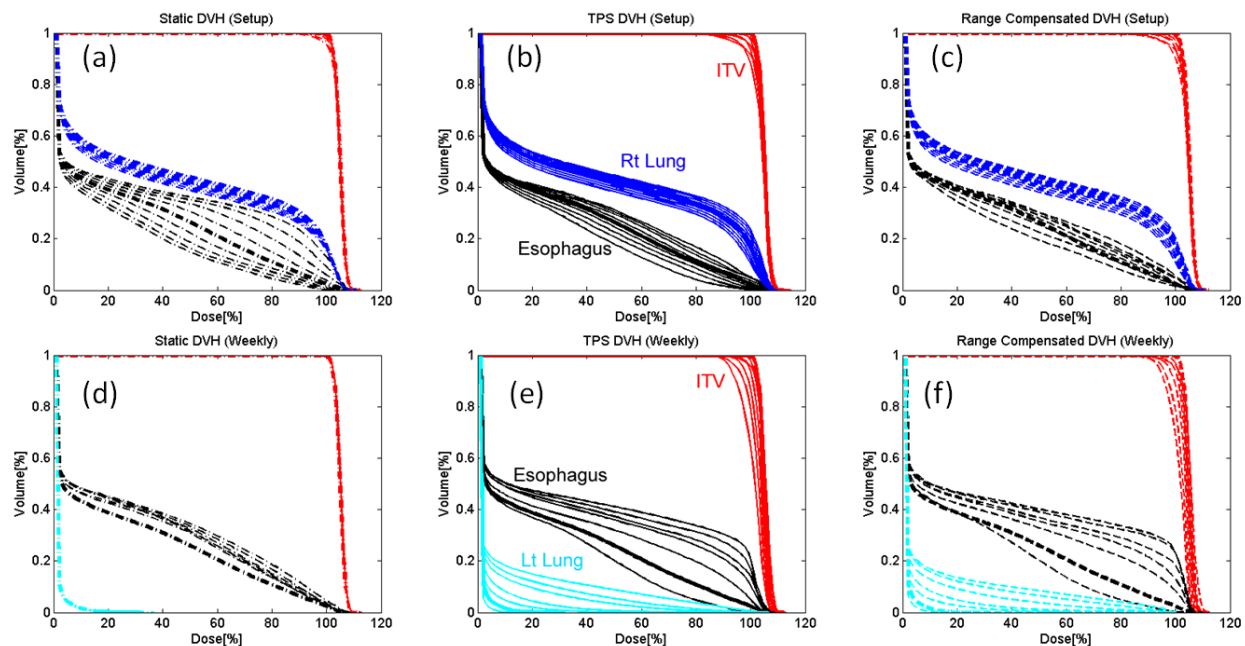


Figure 16: DVH comparisons between different dose calculation methods for a lung patient.

The cDVHs of the ITV (red), involved lung (dark blue), contralateral lung (light blue), and esophagus (black) derived from realized dose distributions under various setup position changes (top row) and weekly imaging (bottom row) using static approximation (a, d), full dose calculation (b, e), and range-corrected approximation methods (c, f). The thicker lines indicate original DVHs derived from the planned dose distribution.

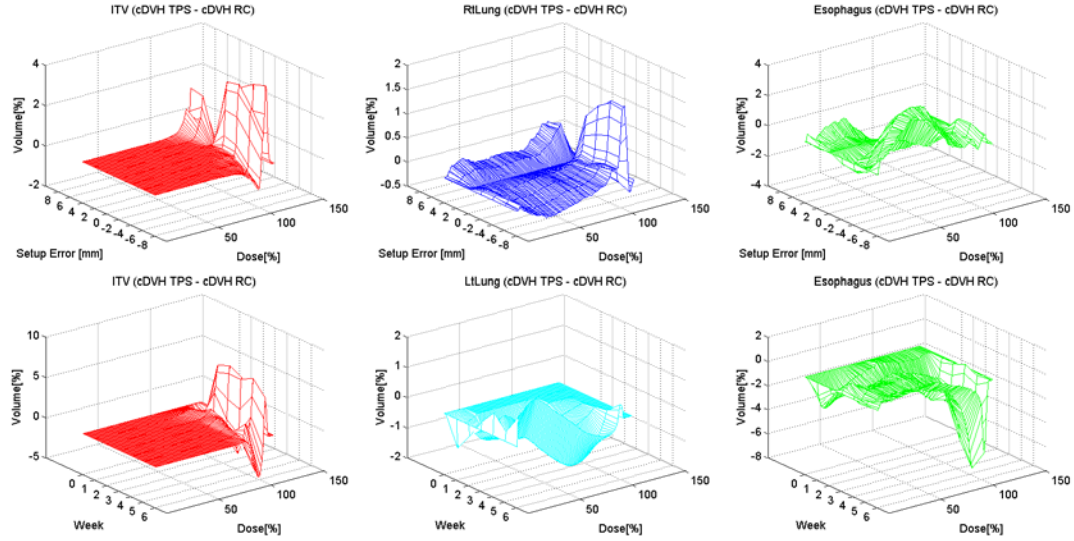


Figure 17: A mesh plot of the differences in DVH between the range-corrected approximation method and the full dose (TPS) calculation. Results are shown for the ITV (red), involved lung (dark blue), contralateral lung (light blue), and esophagus (green). The top row shows the differences for the setup position change cases, and the bottom row shows the differences for the weekly lung cases.

Table 6: The root mean square (RMS) deviations between the cumulative DVHs derived using a full dose (TPS) calculation and range-corrected dose approximation method under various simulations. The first two tables are from setup position changes (in the anterior-posterior direction) and weekly simulations of lung patient. For the sake of simplicity, for both prostate and HN cases, only the worst passing rate observed during weekly simulation is shown (week1 for prostate and week6 for HN).

Lung	CTV		Lung (R)		Esophagus		Lung (L)		Cord	
	$\Delta$ cDVH (% vol)		$\Delta$ cDVH (% vol)		$\Delta$ cDVH (% vol)		$\Delta$ cDVH (% vol)		$\Delta$ cDVH (% vol)	
Setup error (mm)	RMS (%)	Max (%)	RMS (%)	Max (%)	RMS (%)	Max (%)	RMS (%)	Max (%)	RMS (%)	Max (%)
−8	0.4	1.9	0.3	0.6	1.9	3.4	0.4	1.4	1.1	2.5
−6	0.3	1.5	0.3	0.6	1.5	2.3	0.5	1.2	0.9	2.2
−4	0.4	2.2	0.3	0.6	1.1	2.0	0.4	0.9	0.8	1.8
−2	0.4	2.1	0.2	0.7	0.9	1.6	0.3	0.6	0.5	1.3
0	0.0	0.0	0.0	0.0	0.0	0.0	0.0	0.0	0.0	0.0
2	0.6	3.3	0.2	1.0	0.4	0.8	0.3	0.6	0.2	0.5
4	0.7	3.5	0.3	1.4	1.4	2.5	0.4	1.0	0.3	0.4
6	0.6	3.7	0.3	1.6	2.0	3.3	0.5	1.2	0.3	0.6
8	0.7	4.0	0.4	1.6	1.8	3.1	0.6	1.5	0.3	0.7

Site (week)	CTV		Lung (right)		Esophagus		Lung (left)		Cord	
	$\Delta$ cDVH (% vol)		$\Delta$ cDVH (% vol)		$\Delta$ cDVH (% vol)		$\Delta$ cDVH (% vol)		$\Delta$ cDVH (%vol)	
	RMS (%)	Max (%)	RMS (%)	Max (%)	RMS (%)	Max (%)	RMS (%)	Max (%)	RMS (%)	Max (%)
Lung (0)	0.0	0.0	0.0	0.0	0.0	0.0	0.0	0.0	0.0	0.0
Lung (1)	0.5	2.8	0.2	1.2	1.0	2.3	0.4	1.0	1.0	1.6
Lung (2)	1.0	6.1	0.4	1.3	1.6	3.3	0.5	0.7	0.2	0.5
Lung (3)	1.0	6.8	0.6	0.9	0.8	3.0	0.4	0.6	0.3	0.7
Lung (4)	1.0	6.0	0.4	0.6	1.4	5.7	0.4	0.8	0.1	0.3
Lung (5)	1.0	6.6	0.6	1.2	1.9	7.6	0.9	1.4	0.3	0.7
Lung (6)	1.4	5.0	0.6	1.0	1.2	5.9	0.8	1.4	0.4	0.8
Prostate (1)	STV		Bladder		Rectum		Ant rectal wall		Femoral heads	
	1.1	7.2	1.0	1.7	0.6	0.9	0.7	1.8	0.2	0.5
HN (6)	CTV1		Brain stem		Left optic nerve		Right optic nerve		Left parotid	
	0.8	4.8	1.6	6.4	1.6	4.2	2.9	6.2	3.8	7.9



The range-corrected dose approximation method was implemented using MATLAB (MathWorks Inc., Natick, MA) on a computer with an Intel(R) Core™2 Duo CPU of 3.00 GHz clock speed and 3GB of RAM. The typical calculation is less than one second for each beam, which is approximately 50 times faster than the full dose calculation method using the commercial TPS.

### **3.4. Discussion**

The main purpose of the range-corrected dose approximation method is to compute proton dose under various circumstances for evaluating patient setup or for evaluating a given treatment plan's robustness and for potential incorporation into robust optimization techniques. Because such tasks may require hundreds of dose calculations, accuracy of the computed dose may be sacrificed over the computational efficiency. It can be understood that the approximated dose may not reflect the accuracy requirement for the final dose calculation in a clinical plan. Nevertheless, the approximated dose can be used for gauging a plan's sensitivity to setup and range error, for intermediate dose calculations during plan optimization, or for online assessment of major dosimetric impacts. For this reason, it may be sufficient for such important applications.

Our choice to use the 3D gamma analysis was to demonstrate that the approximated dose distribution is spatially comparable to the full dose calculation. The overall accuracy in terms of percentage passing rate presented in Table 3 depends heavily on the choice of passing criteria. In this work, we selected a 3% dose difference and 3mm distance-to-agreement criteria and found that the average passing rate was 93% and 89% for setup errors

and anatomical changes, respectively. The question of what criteria to be used and what the minimum passing rate should be considered acceptable would depend on the nature of applications. In this study, we used CT slice spacing of 2.5mm. When performing ray-tracing in co-planar beam directions, the aliasing effect could affect the accuracy of dose mapping using our method. This is especially true when using a 3-mm distance-to-agreement criterion, which is very close to the CT resolution (2.5 mm) in the slice thickness direction. In the future, we could resample between adjacent CT slices to minimize the aliasing effect.

Aside from the actual dose distribution itself, we also measured the accuracy of cDVHs derived using the approximated dose. This is highly relevant to the application of the proposed method since when evaluating the robustness of a plan or the dose on the day of treatment, it is necessary to summarize the multiple 3D dose distributions into statistical information such as DVH-bands. Previously, Cho et al.<sup>73</sup> discussed the clinical recommendations on accuracy of DVH curves. Based on the assumption that the point dose accuracy of 2-4% is clinically tolerable, the RMS of the difference in relative dose between two cDVH should be less than 1-2%. This RMS criterion measures overall accuracy of the cDVH curve and permits certain dose bins to deviate more than the 2%, while still being clinically acceptable. From our experience, this can happen if the OAR is small or is situated near the beam penumbra and high dose gradient. For the proposed method, Table 6 shows that RMS deviation is well within 2% for all simulations except for the right-optic nerve and left parotid from H&N case.

It should be noted that the lung case chosen in this study was a challenging case for dose calculation. The lateral beam arrangement also maximized the dosimetric effect of anatomical changes. We selected this case to test if our dose approximation method can do

well in the presence of significant anatomical changes. We also challenged the proposed method using a prostate and a HN case. Both cases had a relatively large change in patient's anatomy that would affect the proton beam delivery for these sites. The results were similar to the ones found for the lung case (See Table 3 and Table 6).

In our current implementation, we only used a single CPU for dose calculation, which already can achieve the calculation speed of around one second. Further reduction of computation time can be realized because the proposed method allows for parallel calculation of using independent beamlets or ray-tracing lines. It can be expected that the speed of computation can benefit from the implementation of multi-processor and multi-core CPU methods or even GPU based computation method because our proposed method uses a look-up table approach. Sometimes, additional speed increase is possible if we are only interested in a sub-volume of anatomy. We can selectively choose the dose calculation region of a specific organ to further speed up the DVH calculation if necessary.

One of the limitations of the proposed method is that it does not consider change in scattered dose separately from the primary dose when mapping the pre-calculated nominal dose. The errors resulting from this simplification will be more pronounced for greater displacement of setup error and near regions with a sharp gradient of tissue density change lateral to the beam direction. The pencil-beam based dose calculation algorithm used in Eclipse treatment planning system is also not ideal in modeling the lateral scatter under complex geometries or heterogeneities. A Monte Carlo based dose calculation method would produce more accurate assessment of the proposed method.

### **3.5. Conclusion**

In order to expedite robust plan evaluation, a simple and fast proton dose approximation method was introduced. The proposed method takes advantage of the pre-calculated planned dose distribution when approximating a new dose distribution by correcting the difference in proton range under setup error or anatomical deformation given by the new set of CT images. The accuracy of the range-corrected method was shown to be superior to the static dose approximation method. The main dosimetric differences between the range-corrected method and the clinically used full dose calculation method are in small regions where a shape change in the WEPL exists. These regions are typically narrow and near the edge of a major WEPL change for which the lateral scatter modeling becomes important. In this study the differences between these dose distributions were quantified for selected patient cases using both a 3D gamma analysis and cDVH comparison. Our results show that the static dose approximation is inadequate to approximate dose for proton beam plans while the proposed range-corrected dose approximation method can be used effectively to approximate dose under various setup errors and anatomical deformations. The proposed method could be used for robust evaluation, robust optimization, and online treatment assessment.

## CHAPTER 4: SPECIFIC AIM II - A DOSE-BASED ALIGNMENT PATIENT SETUP TECHNIQUE USING PRE-TREATMENT CT IMAGES

(This chapter is based upon *J. P. Cheung, P. C. Park, L. E. Court, X. R. Zhu, R. J. Kudchadker, S. J. Frank and L. Dong, "A novel dose-based positioning method for CT image-guided proton therapy," Med. Phys. 40, 051714-051719 (2013)* as published by the author of this dissertation and the right to include this work in the author's own research dissertation is exercised as established under the transfer of copyright agreement with AAPM.)<sup>71</sup>

### 4.1. Introduction

Proton therapy has the potential for creating conformal dose distributions and delivering lower doses to normal tissues than traditional photon therapy due to its ability to modulate range.<sup>15, 17</sup> However, this advantage also complicates treatment delivery because changes in patient anatomy affect the proton beam's range within the body.<sup>69, 91</sup> This sensitivity to range uncertainties can cause deviations from the planned dose distribution when significant changes in patient anatomy occur during multi-fractionated radiation therapy.

While image-guidance has allowed for us to position the patient accurately using anatomic landmarks, the resultant dose distribution in the patient is not always apparent and methodologies to obtain this are still being developed.<sup>53, 92</sup> While the static dose cloud approximation is valid for photon beams in most cases, the same is not true for proton beams<sup>73, 74</sup>: as tissue density and thickness change along the proton beam path, so can the resultant dose distribution (potentially to a substantial degree). In theory, a perfect geometry-based target alignment may not guarantee a good dosimetric coverage for the target in proton

therapy because variations of tissue density outside the target may impact the proton dose distribution (depending on the geometry and heterogeneity of the irradiated volume). Current methodologies to mitigate dose variations caused by interfractional patient setup errors include compensator expansion (smearing)<sup>93</sup> and the inclusion of margins.<sup>94</sup> However, these methods are limited to mitigating only rigid shifts of patient and do not address anatomical changes that can result in tissue shrinkage, deformations, misalignment of anatomical structures outside the target, patient weight loss, etc. Therefore, anatomy-based shift will not be ideal to correct all of these daily variations. Adaptive planning may be required to compensate for these changes,<sup>76, 95</sup> but adaptive planning requires more resources, such as segmentation of structures, replanning, quality assurance testing, etc., that may not be practical to apply in every fraction. Different patient setup positions will result in different perturbations to the dose delivered.<sup>70, 96</sup> The magnitude of dose perturbations due to anatomical changes is difficult to assess by looking at anatomy alone, and therefore a timely assessment of the dose distribution for the patient under a given setup condition is desirable. These complexities imply that a dosimetric index to assess target and normal tissue dose under the specific delivery geometry may be necessary for proper treatment-day alignment. In other words, image-guidance in proton therapy may differ from traditional photon therapy in that anatomical alignment based on visual imaging information may not always be adequate, and adjustments may need to be made based on dosimetric assessment due to proton range variations caused by anatomic changes.

We hypothesized that dosimetric based objectives are needed to fully optimize the patient setup position in proton therapy. Instead of replanning, our corrective action uses a simple isocenter shift to correct patient setup, similar to image-guided radiation therapy setup

but using calculated dose information instead of anatomic information. This will make it more practical to apply in routine treatment. Furthermore, by optimizing patient setup using a dose-based alignment method, we can determine whether adaptive planning is necessary to achieve the clinical goal when a simple realignment of the isocenter is inadequate.

## **4.2. Methods and Materials**

### **4.2.1. Patient data set**

We selected 15 lung cancer patients treated at our institution between October 2009 and February 2011 that had clinically approved proton plans with only 2 or 3 coplanar beams for each treatment fraction. This data was chosen in order to simulate the differences between anatomy-based and dose-based alignment. Lung patients were chosen because the proton dose distribution is more sensitive to anatomy change due to large changes in tumor-to-lung boundaries, making them suitable for the purpose of this study. Each passively scattered proton beam was designed to cover the entire planning target volume. Table 7 shows the patients' tumor characteristics for this study. Several of the patients were replanned over the course of treatment to mitigate anatomical changes seen in imaging. While some of the patients received adaptive replans during the course of treatment due to large anatomical changes (as indicated in Table 7), we only used the original treatment plan for our study to observe the impact of these changes to the treatment and assess the ability of our new method to correct for these changes. The patients selected for this study were a subset of protocol patients who were enrolled in a randomized clinical trial to compare proton therapy and photon IMRT for lung cancer.<sup>97</sup> The treatment plans were created with the following parameters: PTV  $D_{99\%} \geq 95\%$  of the prescribed dose; total lung  $V_{20\text{Gy}} \leq 37\%$ ; total mean lung

dose (MLD)  $\leq 22\text{Gy}$ ; maximum spinal cord dose  $\leq 45\text{Gy}$ ; and minimizing dose to the esophagus  $V_{65\text{Gy}}$  and  $V_{45\text{Gy}}$  and heart  $V_{60\text{Gy}}$  and  $V_{30\text{Gy}}$ . The gross tumor volume (GTV) at individual phases from the 4DCT was used to create the internal gross tumor volume (iGTV)<sup>98</sup>, which was expanded by 8mm and manually edited by the treating physician to become internal target volume (ITV). The PTV was created with a 5mm uniform expansion of the ITV. A proximal and distal margin of 3.5% of the total water equivalent path length plus 3mm was added to the ITV along the central beam path to account for range uncertainties, and a lateral expansion of 1.0-1.5cm to the aperture for the ITV in each beam angle was introduced to account for uncertainty in setup position. An expansion of the compensator included to compensate for misregistration of heterogeneities.<sup>93</sup> More details of the treatment planning parameters can be found elsewhere.<sup>87</sup> Figure 18 shows the planned dose distribution on the treatment planning CT scan for patient 1 of this study. Patients were set up with kV orthogonal planar imaging and immobilized using a wing board with vacuum bag and head holder, and knee and foot cradles.<sup>99</sup>



Table 7: Patient and tumor characteristics for Specific Aim 2.

TABLE I. Tumor characteristics.

Patient number	Diagnosis	Tumor location	Beam angles (deg)	Baseline ITV size (cm <sup>3</sup> )	Last ITV size (cm <sup>3</sup> )	ITV volume change (%)	Fraction of last CT	Replanned?
1	NSC NOS	RUL	0/210/295	331.9	262.6	−20.9	35	No
2	Adeno	RUL	205/290	1221.9	999.8	−18.2	35	Yes
3	Squamous	RUL	0/180/245	520.8	426.1	−18.2	34	No
4	Squamous	LUL	120/200/350	865.4	745.1	−13.9	18	Yes
5	Squamous	LUL	35/110/350	131.9	122.9	−6.8	29	No
6	Squamous	RUL	220/250/320	738.6	689.2	−6.7	33	Yes
7	Adeno	RUL	213/240/325	275.5	282.1	+2.4	31	No
8	Squamous	LLL	35/105/170	323.6	313.5	−3.1	35	No
9	Squamous	RUL	160/265/320	470.6	398.7	−15.3	37	Yes
10	Squamous	LUL	35/90/174	531.8	540.6	+1.6	31	No
11	Squamous	RLL	10/255/325	625.3	437.2	−30.1	29	Yes
12	Adeno	RUL	210/290	149.0	133.1	−10.7	34	Yes
13	Squamous	LUL	45/160	1405.2	1304.7	−7.2	29	Yes
14	Squamous	RUL	0/190/345	986.1	843.7	−14.4	37	Yes
15	Adeno	RUL	170/240/330	314.3	308.4	−1.9	32	No

Note: adeno = adenocarcinoma; ITV = internal target volume; LLL = left lower lobe; LUL = left upper lobe; NSC NOS = non-small cell carcinoma, not otherwise specified; RLL = right lower lobe; RUL = right upper lobe; squamous = squamous cell carcinoma. “Replanned” refers to the patient receiving at least one full replan during the course of treatment.

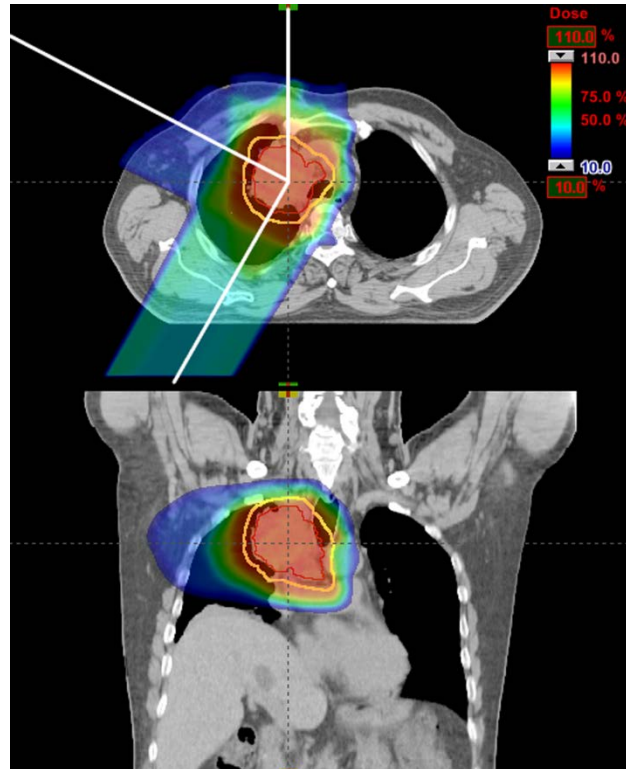


Figure 18: Planned dose distribution and beam angles for patient 1 for Specific Aim 2 study.

Each of these protocol patients had weekly 4DCT for evaluation during the course of treatment. These repeat CT scans were used to simulate treatment-time images for patient alignment. All of these patients were treated in free-breathing condition. We used the time-averaged 4DCT, which was generated by averaging the CT numbers for 10 respiratory phases at each voxel location. To simplify further, we examined the CT image from only the patients' last available weekly CT scans since those scans were expected to have the largest anatomical changes compared with the original treatment planning CT scans. Some of the treatment beams may pass through the CT couch, therefore the CT data representing the imaging couch were replaced with a digital treatment couch using in-house software to properly account for beams that intersected the treatment couch.<sup>100</sup> Contours from the original planning CT image were propagated to the treatment-time image using in-house deformable image registration software<sup>88, 101, 102</sup> to delineate the patient anatomy at the time of treatment for DVH calculations. The algorithm was assessed for use in automatic contour propagation for repeat CT and 4DCT imaging and found that interfraction accuracy of 0.4 mm mean absolute surface-to-surface distance and intrafraction accuracy of >98% volume overlap was achievable when compared to the physician-modified contours.<sup>101</sup>

#### **4.2.2. Anatomy-based alignment**

All weekly images were registered to the planning CT image using bony structures in the vertebrae nearest the target to simulate the image guidance technique used at most proton centers today: kilovoltage orthogonal projection imaging, which can detect bony anatomy sufficiently for alignment purposes. This baseline alignment based on bony anatomy was

used as the reference to compare with the proposed dose-based alignment and will be referred to as anatomy-based alignment through the rest of this manuscript. We also obtained alignment positions for the iGTV to check whether our dose-based alignment ended up clustering close to iGTV alignment. These alignments were performed using in-house image registration software with a region-of-interest based alignment method, which is able to achieve sub-millimeter registration accuracy with disagreements to human adjustments of greater than 3 mm less than 2% of the time.<sup>102, 103</sup>

#### **4.2.3. Dose-based alignment**

For the dose-based alignment, dose metrics need to be extracted from the new treatment day CT image. In order to do this, we need to calculate the dose distributions for a number of couch setup positions with relative patient shifts in the x-, y-, and z- directions from the baseline anatomical alignment. This will allow for the assessment of the impact of the dose delivered for various setup positions in order to find the optimal setup for the patient to achieve the desired target coverage while minimizing dose to normal tissues. Once an optimal shift is established, these coordinate shifts can be applied to the treatment couch to position the patient in the final optimal treatment position.

Again, a full calculation of dose distributions for every possible setup position would require a significant amount of time and/or computational resources that would not be practical for online clinical use. To remedy this problem, we used the fast dose approximation method<sup>74</sup> from Specific Aim 1 to calculate the dose to organs for different patient positions. We showed in the previous section that this calculation method can sufficiently account for changes in tissue density accompanying various setup and anatomical

changes for the purposes of optimization or quick dose assessment. Using this method, we recalculated the dose from each beam for multiple rigid isocenter shifts (no rotations) of up to 8 mm in each direction ( $x$ ,  $y$ , and  $z$ ) in 2 mm increments (based on the dose calculation grid size), resulting in 729 dose calculations per beam angle. The 8 mm search limit was selected because our lateral circular margins for aperture expansion in lung proton therapy are typically 1cm. This allows us to have some room to shift the patient around with the target still confined within the aperture in the high dose region. This search space may need to be defined differently for different applications to suit the treatment plan design.

To further minimize the computation time required, we calculated doses only for the voxels within the volumes of interest, which included the target volume and the ipsilateral lung in this study. DVHs were obtained from each shift, and were used to determine the optimal alignment. We used the target coverage constraint that 99% of the ITV would receive at least 95% of the prescribed dose ( $D_{99\%} \geq 95\%$ ), and optimized the normal tissue dose by minimizing the mean dose to the ipsilateral lung. If the target coverage constraint was not met, the shift that maximized target coverage was defined as the optimal alignment. The optimality of the target coverage and organ-at-risk doses can be visualized in a solution space plot with non-dominated solutions mapped out on a Pareto frontier, which is the set of solutions in which no one parameter can be made better without making the other parameter worse (e.g. lung dose cannot be decreased without reducing target coverage).

Figure 19 shows the general workflow required for dose-based alignment. For this study, the dose-based alignment algorithm was implemented using MATLAB (version 7.12.0 [R2011a]; The MathWorks Inc., Natick, MA) as a plugin to CERR (Computational Environment for Radiotherapy Research, Washington University in St. Louis, St. Louis,

MO)<sup>104</sup> and performed on an Intel Xeon X5680 3.33-GHz central processing unit (Santa Clara, CA). After we obtained the optimal setup position using each dose-based alignment methods, we imported the final isocenter information into the Eclipse proton treatment planning system (Varian Medical Systems, Inc., Palo Alto, CA) for final dose calculations, so we could compare the dose-based alignment with the anatomy-based alignment.

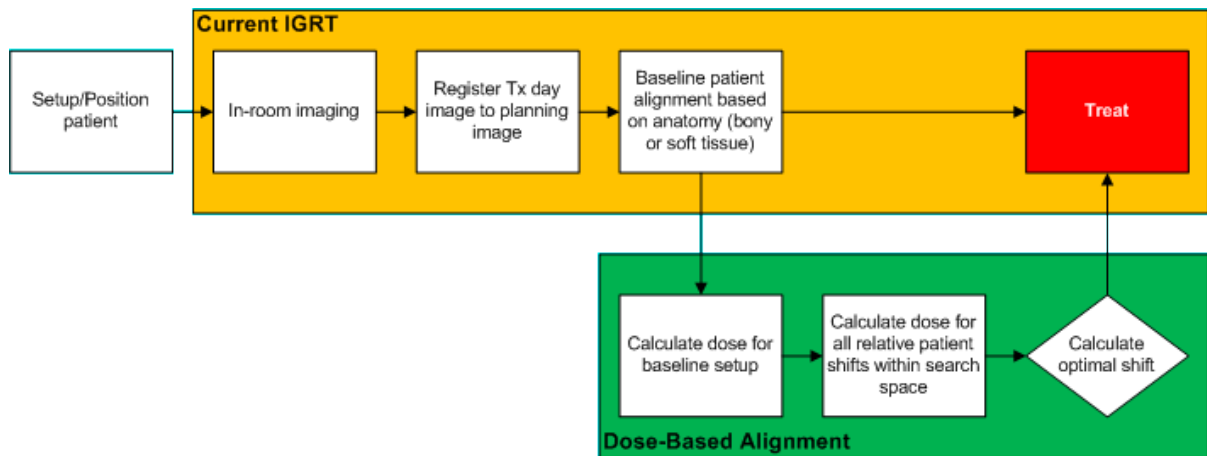


Figure 19: Workflow diagram for the dose-based alignment method compared to the current IGRT workflow.

#### 4.2.4. Statistical analysis

The statistical analysis focused on two sets of comparisons between the optimization methods: coverage of the target, and dose to normal tissue. For the first of these, we used the exact McNemar test to determine whether the methods significantly differed in meeting the target coverage constraint. For the second, we compared the changes in mean dose to the ipsilateral lung using a 2-tailed paired  $t$  test with a 95% confidence interval. We performed our statistical analysis using GraphPad Prism (version 5.00 for Windows; GraphPad

Software, San Diego, CA) and a p-value less than 0.05 was considered statistically significant.

### **4.3. Results**

Seven of the 15 cases did not meet the target coverage constraint of  $D_{99\%} \geq 95\%$  of the prescribed dose to the internal target volume when using the anatomy-based alignment. For five of these patients, the target  $D_{99\%}$  dropped below 90% and two of these dropped below 66%. When applying isocenter corrections using the dose-based alignment shifts, we were able to recover the target dose for all 7 of these patients ( $p=0.0156$ ) and meet the target coverage constraint. Table 8 lists the target (ITV) coverage and mean ipsilateral lung dose statistics for all 15 patients.

The dose-based method resulted in mean ipsilateral lung doses that were lower by an average of 2.74% of the prescribed dose, or 2.03 Gy for a prescribed dose of 74 Gy ( $p = 0.0147$ ). The maximum decrease in mean ipsilateral lung dose was 11.0% of the prescribed dose. If considering only the 8 cases in which the target constraint was met for both the anatomy-based and the dose-based alignment methods, the average decrease in mean ipsilateral lung dose was 4.5% ( $p = 0.0083$ ), with decreases occurring in all but 1 case (patient 5).

Table 8: Target (ITV) coverage requirement and mean ipsilateral lung dose for patients assessed for dose-based alignment.

Patient number	Target (ITV) $D_{99\%}^{*\dagger}$		Mean ipsilateral lung dose (% of prescribed dose)	
	Anatomy-based alignment	Dose-based alignment	Anatomy-based alignment	Dose-based alignment
1	99.4%	96.8%	45.3	38.4
2	95.3%	100.5%	51.5	40.5
3	80.5%*	95.8%	40.3	34.0
4	93.8%*	97.0%	61.8	60.2
5	98.2%	98.9%	21.0	21.7
6	96.9%	96.6%	54.1	52.5
7	100.4%	96.2%	42.9	38.3
8	97.7%	97.2%	53.3	49.0
9	101.1%	98.8%	38.3	35.0
10	87.5%*	96.7%	39.2	42.2
11	80.2%*	95.6%	58.9	61.7
12	94.4%*	96.7%	47.4	46.3
13	65.7%*	95.7%	76.1	73.1
14	57.2%*	95.7%	45.2	46.2
15	100.4%	95.8%	51.0	46.1

\* did not meet target constraint

Figure 20 shows a scatter plot and histogram of the vector magnitude differences of the isocenter shifts comparing the dose-based alignment to bony and internal gross tumor volume (iGTV) anatomy-based alignments, demonstrating that the dose-based alignment was not the same as either bony or iGTV anatomy-based alignments, and that the dose-based shifts did not cluster together toward any other observable anatomy.

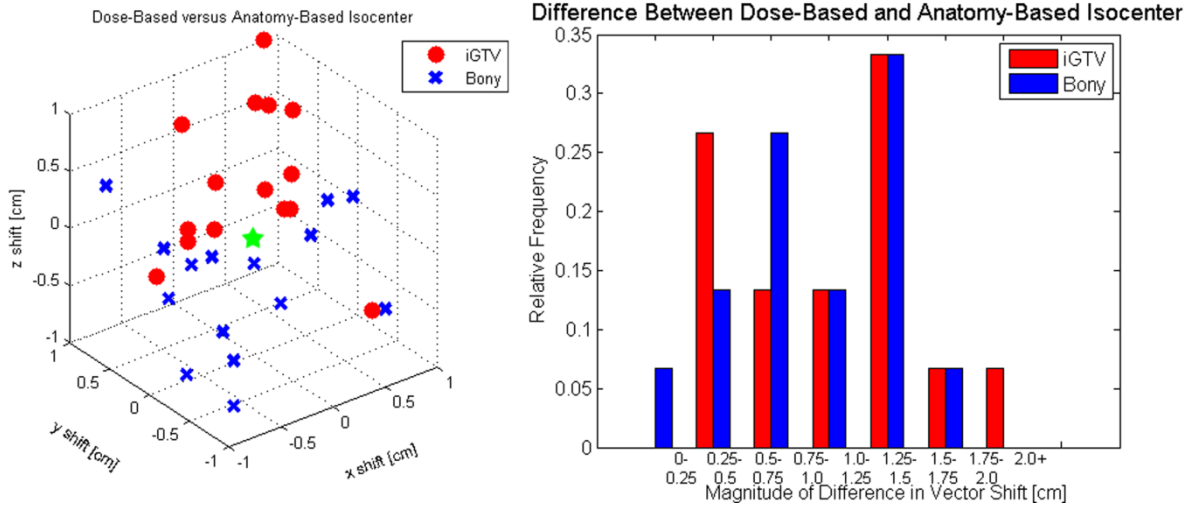


Figure 20: Scatter plot and histogram of vector magnitude differences of the isocenter shifts comparing the dose-based alignments with the bony alignment and iGTV alignment.

Figure 21 shows DVHs for the target and the ipsilateral lung for patient 13, with separate results shown for the anatomy-based alignment and the dose-based alignment methods. In this case, the results of anatomy-based alignment did not meet our target coverage constraint while the results of the dose-based alignment methods met the constraint. In addition, after applying our optimized dose-based alignment shift, we reduced the mean dose to the ipsilateral lung by 2.3 Gy (3% of the prescription dose). Figure 22 shows the optimization tradeoff between target coverage ( $D_{99\%}$ ) and mean ipsilateral lung dose for all dose-based shifts evaluated in the search space. The Pareto frontier, which shows the non-dominating solutions for both the target coverage and normal tissue sparing, is shown as well as the dose-based shifts which satisfy the target coverage constraint and minimized normal tissue dose (green star). The dose distribution images overlaid on the CT for the same patient (patient 13) are shown in Figure 23. When looking at the dose clouds, it is apparent that a



much larger volume in the anatomy-based bony-alignment is underdosed when compared to the dose-based alignment. Interestingly, a lot of the underdosed regions fall near the center of the ITV and not out near the edges, likely due to overshooting of the posterior oblique beam, causing an underdosage in the proximal portion of the resulting spread out Bragg peak. For this patient, the  $D_{99\%}$  improved from 65.7% up to 95.7% using our dose-based alignment.

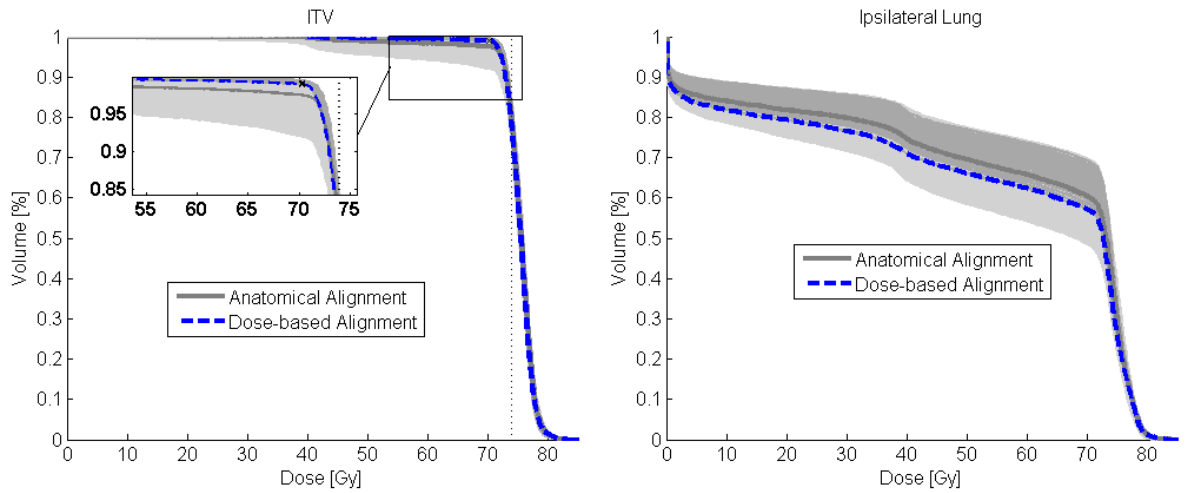


Figure 21: Example DVHs for the dose-based alignment method versus the anatomical alignment method. DVHs are shown for the target (left) and ipsilateral lung (right) for patient 13. The anatomy-based and dose-based alignment DVHs are shown by the gray and blue dashed lines, respectively. The DVH bands show the extent of all of the dose calculations in the search space, with the gray band corresponding to the calculated DVHs that did not meet the target coverage constraint and the red and cyan bands showing the DVHs that did meet the constraint.

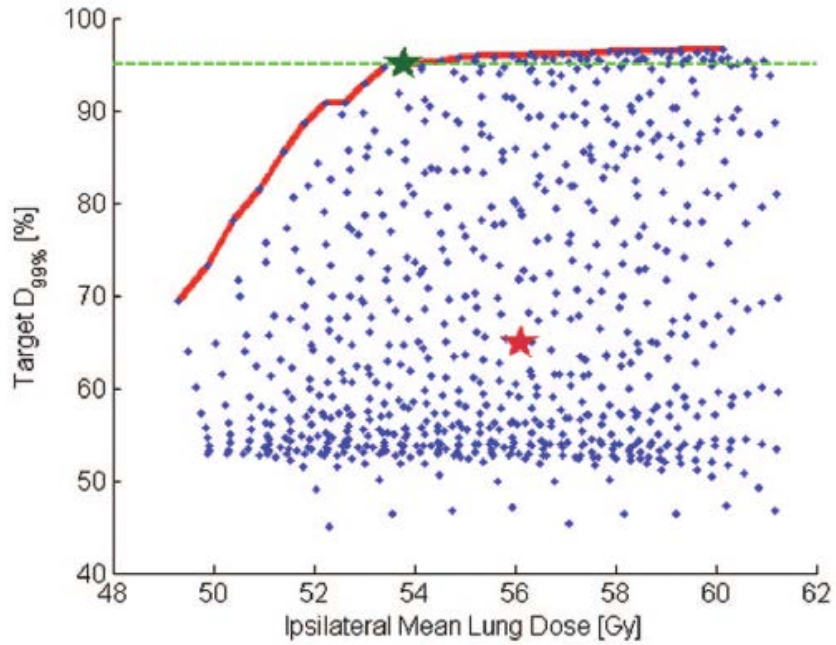


Figure 22: An objective plot of the solution space of mean ipsilateral lung dose versus target  $D_{99\%}$  for the dose-based alignment method. Calculated solutions are shown in the blue dots, with the doses for anatomy-based and optimized single-isocenter dose-based alignments shown in the red and green stars, respectively. The target coverage constraint is shown by the green dashed line (above the line is meeting the constraint), and the Pareto frontier (non-dominated solutions) is shown by the solid red lines.

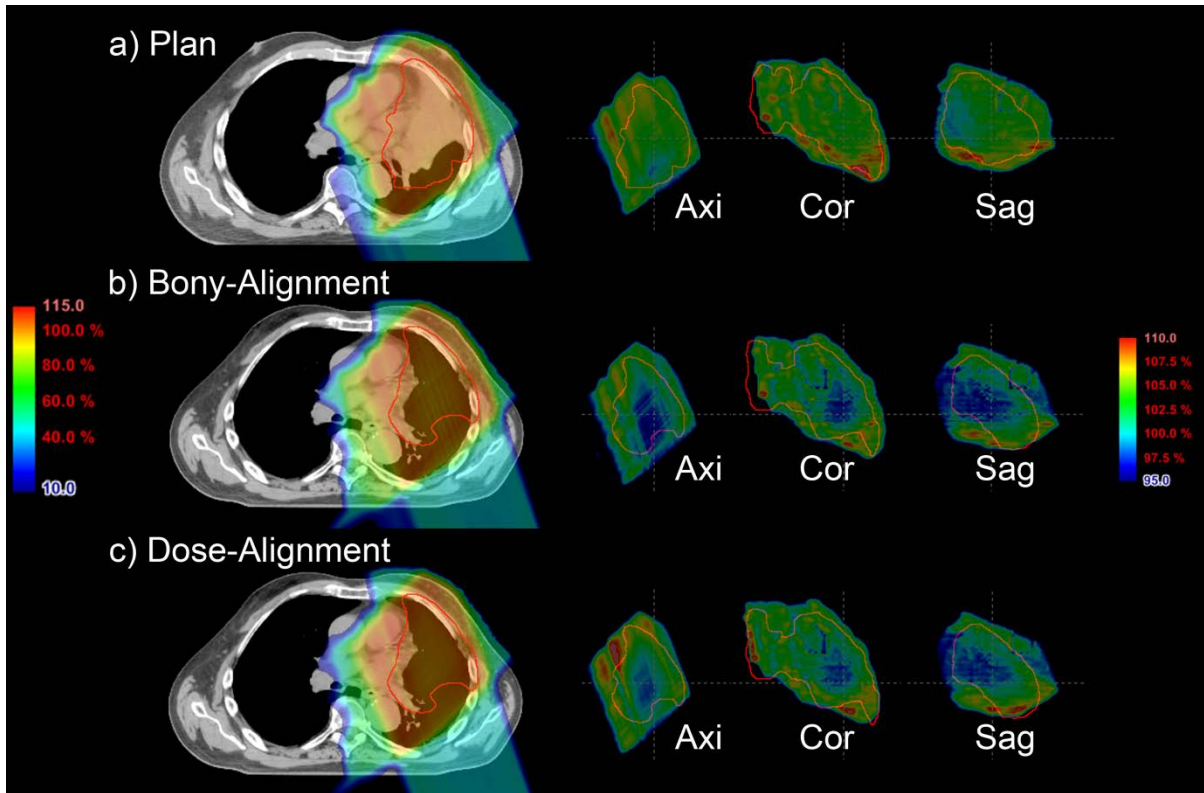


Figure 23: Dose distributions for Patient 13 for the a) plan and the last weekly CT based on b) bony-alignment, and c) dose-alignment. The dose clouds between 95% to 110% prescription dose levels for the bony-alignment and dose-alignment methods are also presented in axial, coronal, sagittal viewing planes to illustrate target coverage and locations of underdosage.

#### 4.4. Discussion

Image-guidance represents the latest development in radiation therapy. Although volumetric (CT-based) image guidance is popular in photon therapy, its deployment and full usage in proton therapy are still in the early stage. Due to the unique characteristics of proton dose distributions, image guidance alone may only solve a part of setup problems. It is important to note that proton compensators are designed with smearing margins in order to be robust to

setup and motion errors, but do not account for anatomical changes during the course of treatment. Therefore, while the patient may be set up correctly based on anatomic landmarks, this may not be the most ideal setup based on the treatment time anatomy. Because proton dose distribution changes with changes in anatomy, the use of dosimetric objectives to set up a patient is perhaps more appropriate for proton therapy. Since our treatment goal is always dosimetric in that we desire the target to receive the treatment prescription, a dose-based assessment is closer to our eventual goal, which makes our dose-based alignment viable in daily management of setup and range uncertainties. The method is based on the imperfect correction by the traditional anatomy/target alignment method. We assume the compensator and aperture will remain the same as in the original plan. Correction to the compensator and aperture will require daily adaptive planning, which is not feasible in current technology or workflow. Our method is an intermediate step towards adaptive radiotherapy. It uses a simple isocenter shift, but the shift is based on dose calculation of the original plan applied to the daily anatomy. Therefore, it may be easier to deploy in clinical practice.

Our analysis is based on CT imaging acquired using the same scanner that is used for CT simulation. Full implementation of this method would require in-room or remote volumetric imaging resources with availability during pre-treatment setup, a robust and accurate deformable image registration tool for propagation of contours, and available software at the treatment workstation for performing the dose-based alignment and subsequent review. During the treatment planning and verification stage, the physician would need to decide on organs-at-risk to monitor for dose-based alignment and action levels could be established to determine when a physician review is necessary or a full adaptive replanning process needs to be triggered. Clinical application of our technique would likely

utilize either a CT-on-rails system, remote patient positioning system<sup>105</sup>, or in-gantry cone-beam CT (CBCT) imaging. If a separate CT scanner is used, effort would need to be made to ensure that the CT calibration curve for conversion from CT number to relative linear stopping power is correct for the verification scanner. A CBCT system can be used if the CT numbers in the CBCT can be accurately corrected to match with the simulation CT or accurately calibrated for conversion to relative linear stopping power for proton dose calculation. A possible method for correcting these images for this purpose is to use deformable image registration to convert the CBCT to a “virtual CT” with CT number corrections, as described by Peroni et al.<sup>106</sup> and others<sup>107</sup>. These corrections would need to be accurate enough to be used in treatment planning to be feasible for use in this application.

As we saw from Table 8, the  $D_{99\%}$  target dose coverage dropped down to as low as 65.7% and 57.2% for two of the patients in our study when using bony anatomy to set up the patient. This is a very large dose decrease to the target resulting from the changes in heterogeneities in the patient which were not accounted for in the planning process. These types of errors could not be directly assessed if no dose information or periodic assessment of anatomy change was included. Fortunately, both of these patients received adaptive replans during the course of treatment due to the establishment of a weekly evaluation of the proton lung protocol patients. However, our results also indicate that a simple isocenter shift based on calculated dose distributions using treatment time CT images could be enough to correct for this drop in target dose coverage. This would allow us to correct it to an acceptable level without full-fledged adaptive replanning which will involve more resources. In addition, the dose-guided alignment could be used to indicate if a full adaptive replan is necessary based

on the dosimetric analysis if the target coverage or normal tissue dose cannot be corrected to an acceptable level.

The accuracy of the algorithms employed for the dose-based alignment method is important to consider when defining action levels for correction or adaptive planning. The fast dose approximation method employed here<sup>74</sup> was shown in the previous chapter to be accurate for DVH calculations with an average and maximum root-mean-square deviation in DVH of 0.50% (average of 0.25% for the ipsilateral lung), which is sufficiently accurate for assessment of MLD. With smaller organs-at-risk that are close to high gradients, this accuracy will decrease, but even for the esophagus which is relatively small and was located right next to the high dose gradient, we found that the average RMS deviation in DVH was only 1.2% (maximum for any one case was 3.4% for shifts of up to 8mm).

Our study and technique is only focused on correcting for interfractional anatomic changes, and currently does not address intrafractional changes due to patient movement or physiologic motion such as patient breathing. Any compensation for motion management is considered to have been accounted for in the treatment planning process. Additionally, while we examined lung patients for our study, this technique is not limited to lung treatments and could be applied to any anatomical site.

It is important to note that anatomy-based alignment may be sufficient in cases where anatomical changes are minimal. However, we have also shown that for cases in which the target coverage is acceptable even with anatomy-based alignment, dose-based alignment reduced dose to the normal tissue of the ipsilateral lung except in 1 case. This patient had the smallest tumor and the treatment therefore was the most sensitive to small differences in dose, especially near high-gradient regions. However, the resultant root mean square (and

maximum) difference in DVH between the dose-based and anatomy-based alignment methods for this case was 1.0% (2.1%), which is within the uncertainty of the fast dose approximation method<sup>74</sup> and perhaps could be due to the search resolution used in this study (2 mm). While the average decrease in mean ipsilateral lung dose of 2.74% (~2 Gy) for all patients is seemingly small, this change is an appreciable dose reduction in the case of the ipsilateral lung due to its large absolute volume. The recent QUANTEC review for dose effects in the lung found that there was no suggested absolute safe MLD below which there is no pneumonitis, and reduction of risk for radiation pneumonitis is suggested to decrease by about 8% for a 2 Gy reduction based on a logistic regression fitted to multi-institutional data.<sup>108</sup>

For this study, we evaluated only the dose to the target and one organ-at-risk (ipsilateral lung) to show that the methodology works. In general, any number of organs-at-risk can and should be incorporated into the objective function, and the optimal dose to normal tissues will be a tradeoff, in which case the optimal dose to normal tissues will necessarily require prioritizing/balancing the doses to each organ-at-risk. There are many ways to implement multicriteria optimization. In optimizing multiple criteria for dose-based alignment, a dose-volume-based single objective function similar to that implemented in treatment planning can be used. For each case, the user can select the objectives to reflect the best clinical scenario. For example, the dose to the spinal cord is generally an important objective that needs to be monitored. For patient 7, we noticed that the maximum dose to the spinal cord dose was above 45 Gy for both the anatomic and dose-based alignment setup positions. By adding equally weighted constraints to minimize the maximum dose to the spinal cord maximum dose and the mean dose to the esophagus, we were able to reduce the

maximum dose to the spinal cord by 18 Gy to below 45 Gy and mean dose to the esophagus by 7 Gy but raising the mean dose to the ipsilateral lung by 6 Gy. Depending on whether this increase dose to the lung is acceptable or not, decisions need to be made to reweight the optimization parameters to achieve the best clinical solution for the specific needs of the patient. The ultimate choice of the specific organs and weights to be included in the objective function should be left to the physician and depend on patient-specific acceptable target and normal tissue dose compromises. Depending on the optimization parameters selected, the dose-based alignment may potentially be the same as the anatomy-based alignment; however, unless dose-based evaluation is performed, there is no way to validate if the anatomy-based alignment is indeed the best solution. We developed a graphical user interface to allow users to input specific DVH parameters to optimize the patient alignment and assess the cost-benefit for competing objectives (Figure 24).

Currently, we are using an exhaustive approach with discrete intervals since it allows us to demonstrate the concept because our current resources are powerful enough that we can calculate doses in about 7–15 min depending on the number of beams in the plan and the volume of the organs of interest. Ideally, total time for setup and imaging evaluation should take about 5-10 minutes or less. A refined optimization algorithm for determining search directions might improve the calculation speed. Computing time could also be greatly reduced by incorporating parallel computing, as discussed in the previous chapter. We could also take advantage of the fact that shifting the patient in a direction parallel to the beam axis (*i.e.* changing the air gap) does not change the proton dose distribution by much, thereby further reducing size of the search space.



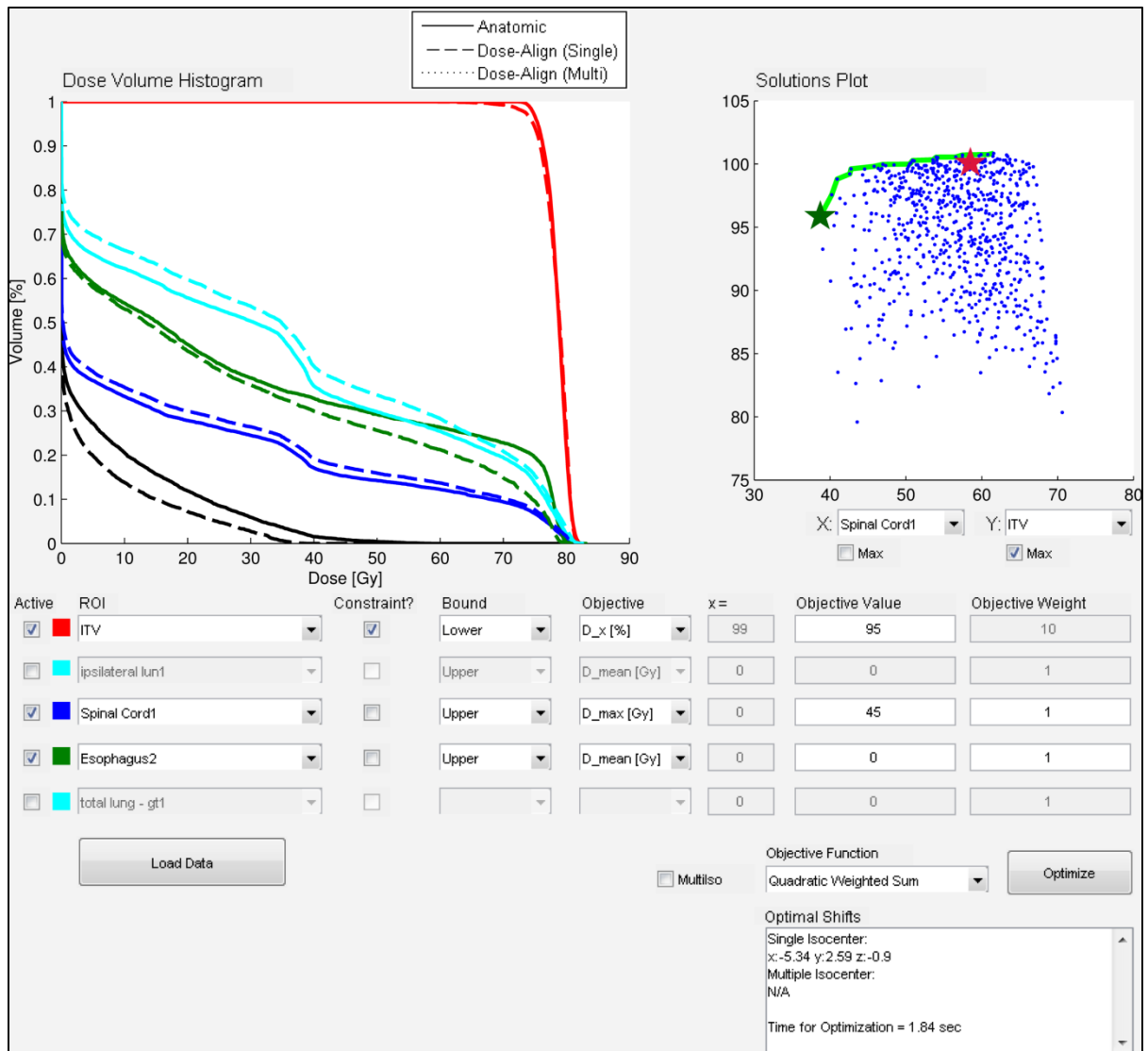


Figure 24: A graphical user interface for dose-based alignment with inputs for DVH-based objectives.

Since anatomy change can affect the proton range from each individual beam differently, a beam-specific isocenter shift may potentially further improve the dose delivered to the patient. Additionally, individual field alignments may be applicable for multi-room facilities where prolonged waiting times between beams may be routinely observed. Ideally,

this beam-specific isocenter shift would take into account the total dose from every beam in our optimization process. However, the search space is unacceptably large for a brute force search. For example, calculating the optimal shift for linked beams for a 3-beam plan would require  $729^3$  or 387,420,498 combinations of beams. Even with all of the possible doses precalculated for each beam separately, calculating the objective function for all combinations of beams using our current methodology would take too long to be feasible for real-time application. We performed an initial study looking at performing a multiple isocenter shift using independent beam-specific dose optimization. We did this by looking at each beam separately and finding the isocenter shift that optimizes the dose to the target and the ipsilateral lung with the same parameters as our single isocenter dose-based optimization weighted by the relative beam-weighting in the treatment plan. It is important to point out that this multiple isocenter shift method makes sense only for proton delivery techniques in which each field is separately optimized to deliver uniform dose to fully cover the target. After this independent optimization, we looked at the resultant total dose delivered for each beam with the obtained isocenter shifts. In this study, we did not demonstrate the significant advantage of using the beam-specific isocenter shift method over the single-isocenter shift method. The mean ipsilateral lung doses for the single- and multiple-isocenter shifts did not significantly differ ( $p = 0.9464$ ). The multiple-isocenter dose-based method resulted in mean (max) ipsilateral lung doses that were lower by an average of 2.77% (11.0%) of the prescribed dose ( $p = 0.0086$ ) compared to 2.74% (11.3%) of the prescribed dose for single-isocenter ( $p = 0.0147$ ). While these doses are not significantly different, we can see that there is potential advantage to performing multiple-isocenter beam shifts to better optimize the dose that is delivered to the patient.

#### **4.5. Conclusion**

We showed that because proton dose distribution changes with changes in anatomy in the beam path, a pure geometry-based target alignment is potentially insufficient for patient setup in proton therapy. On the other hand, we demonstrated that a dose-based patient setup was an effective image guidance approach for proton therapy. This particular approach improved target coverage and/or reduced dose to nearby normal tissue compared with the traditional anatomy-based image guidance approach based on our analysis of the dose to the ipsilateral lung. We proposed a unique approach to use a dose-based objective function to guide patient setup (i.e. isocenter adjustment), which bridges the gap between traditional image guided setup and the more complex adaptive radiotherapy. We showed that 7 of 15 plans did not meet the target coverage constraint when we used anatomy-based alignment. After we applied dose-based isocenter alignment, all met the target coverage constraint. The proposed dose-based alignment approach will also be useful as a trigger for adaptive radiotherapy when the dose-based simple isocenter shift method becomes inadequate to correct for more complicated dosimetric deviations in the treatment plan.

## **CHAPTER 5: SPECIFIC AIM III - A FAST ONLINE RANGE-ADAPTIVE TECHNIQUE TO CORRECT FOR RANGE VARIATIONS BASED ON CT IMAGING**

### **5.1. Introduction**

The potential for proton therapy to deliver improved dose distributions is well documented in both planning studies and clinical outcome studies.<sup>15, 17, 109</sup> However, a frequent concern with proton and other particle therapy techniques is their sensitivity to range variations due to anatomical changes over the course of treatment.<sup>31, 79, 94, 110-112</sup> As discussed earlier, it is also well-known that patient anatomy does not remain constant over the entire course of treatment, with changes stemming from patient weight loss, tumor shrinkage, radiation-induced swelling, and inconsistent patient setup, to list a few common examples.<sup>36-39</sup> Because of the finite range of protons within the patient, any of these changes can potentially affect the delivered dose to the patient, compromising the treatment by causing overdosing of normal tissues or underdosing of the target. Therefore, adaptive strategies are commonly used to correct these problems.<sup>95, 113, 114</sup> Koay et al.<sup>95</sup> found that as many as 20% of patients in the proton therapy arm of a trial of radiation therapies for non-small-cell lung cancer (NSCLC) required adaptive intervention at some point during the course of their treatment. Additionally, they found that most of their adaptive corrections required only aperture, compensator, or beam energy adjustments and did not require changes in beam angles or number of beams.

However, an issue with adaptive replanning is that it requires a large amount of resources and can take several days to implement. This can lead to a strain on resources

within the department and forces patients and radiation oncologists to choose between using an inadequate treatment plan or interrupting treatment while replanning is done. Therefore, a method for quick adaptive replanning would be immensely beneficial. Implementation of such a method would require a quick turnaround time for the entire process: treatment assessment, reimaging for treatment planning, treatment planning itself, data transfer to the delivery system, and all quality assurance measures to ensure safe delivery of the treatment. In SSPT,<sup>8, 25, 115</sup> the proton beams are delivered using electronically controlled scanning magnets, beam energy, and beam intensity so no special patient-specific hardware is required to be manufactured. Therefore, with SSPT we have the potential for adapting plans on the fly by programmatically adjusting the beam energy and by adjusting the lateral scanning position by changing the magnetic steering.

To begin to assess this potential, we explored a potential range-adaptive method for quick adaptive planning based solely on the use of the original treatment plan and a new treatment-time CT image of the patient. The objective of this method is to make minimal modifications to the original treatment plan to simplify the adaptive process and reduce the amount of quality assurance needed for a safety check. In addition, the use of CT imaging allows for possible implementation into the process of image-guided patient setup and evaluation. Here we report our findings on the successes and limitations of this range adaptive method for single-field optimized (SFO) SSPT.

## **5.2. Methods and Materials**

### **5.2.1. Patient data set**

Fourteen patients with NSCLC who were previously treated with passive scattering proton therapy were selected for this study. These patients were a subset of patients who were enrolled in a randomized clinical trial to compare proton therapy and photon intensity-modulated radiation therapy for lung cancer (NIH P01 CA021239-29A1). All of the patients selected for the present study had received at least one adaptive intervention during the course of treatment to mitigate potential dose delivery deviations caused by large changes in their anatomy. In addition, these patients all had undergone weekly 4DCT imaging during the course of treatment to monitor for such changes. The patients were treated in free breathing conditions and were set up daily using orthogonal x-ray imaging. We elected to select lung patients for this study in order to take advantage of their large anatomical changes during the course of treatment. Again, no special motion management was used in our adaptive planning. Table 9 shows some treatment and tumor characteristics of the patients we studied in this aim.

### **5.2.2. Treatment Planning**

For the patients selected, we generated SFO SSPT plans using our clinically commissioned treatment planning system, Eclipse™ (version 8.9.08a, Varian Medical Systems, Inc., Palo Alto, CA). All contours (including the target volumes and normal tissue structures), beam angles, and beam weights were selected to be the same as those in the clinically approved passive scattering proton therapy treatment plans used for our patients.

Table 9: Tumor and treatment characteristics for Specific Aim 3 study.

Patient	Diagnosis	Tumor Location	Beam Angles	Initial ITV Size (cm <sup>3</sup> )	Repeat-CT ITV Size (cm <sup>3</sup> )	Volume Change (%)	iGTV Size (cm <sup>3</sup> )	Repeat-CT iGTV Size (cm <sup>3</sup> )	Volume Change (%)	Fraction at which CT was repeated
1	Adeno	RUL	205/290	1221.9	999.8	-18.2	723.4	517.2	-28.5	35
2	SCC	LUL	120/200/350	865.4	745.1	-13.9	410.0	278.1	-32.2	18
3	SCC	RUL	220/250/320	738.6	689.2	-6.7	381.9	331.7	-13.1	33
4	SCC	RUL	160/265/320	470.6	398.7	-15.3	185.6	124.4	-33.0	37
5	SCC	RLL	10/255/325	625.3	437.2	-30.1	305.5	187.4	-38.7	29
6	Adeno	RUL	210/290	149.0	133.1	-10.7	30.9	24.2	-21.6	34
7	SCC	LUL	45/160	1405.2	1304.7	-7.2	721.6	575.4	-20.3	29
8	SCC	LLL	165/90	818.4	687.1	-16.0	457.0	307.4	-32.7	34
9	SCC	LLL	35/105/170	323.6	313.5	-3.1	101.8	92.2	-9.4	35
10	SCC	RUL	210/260/325	603.0	507.8	-15.8	267.2	169.3	-36.6	29
11	Adeno	LLL	200/90/150	260.6	255.5	-2.0	100.3	93.1	-7.1	32
12	SCC	RUL	340/25/260	804.4	669.1	-16.8	391.7	264.7	-32.4	34
13	SCC	LUL	205/275/345	147.9	114.6	-22.5	384.0	338.7	-11.8	27
14	LCLC	LLL	180/95/140	335.5	363.6	8.4	49.1	50.6	3.1	32

Abbreviations: Adeno = adenocarcinoma; SCC = squamous cell carcinoma; LCLC = large cell lung carcinoma; RUL = right upper lobe; LUL = left upper lobe; RLL = right lower lobe; LLL = left lower lobe

The treatment plans were created to meet clinical DVH based guidelines at our institution (same as in Specific Aim II): PTV  $D_{99\%} \geq 95\%$  of the prescribed dose; total lung volume receiving a dose of at least 20 Gy ( $V_{20Gy} \leq 37\%$ ); total mean lung dose (MLD)  $\leq 22$  Gy; maximum spinal cord dose ( $D_{max}$ )  $\leq 45$  Gy; and minimizing the esophageal  $V_{65Gy}$  and  $V_{55Gy}$  and heart  $V_{60Gy}$  and  $V_{40Gy}$ . The prescription dose for all patients was 74 Gy to the target in 37 fractions. For the target volumes, the GTVs at all phases from the 4DCT were combined to create the internal gross tumor volume (iGTV). The ITV was generated by uniformly expanding the iGTV by 8 mm, followed by manual editing by the physician. The

PTV was then generated by applying a 5 mm uniform expansion of the ITV, with some edits to avoid non-involved bone and superficial structures.

For treatment planning optimization, we optimized to the PTV as the target, but for evaluation we looked at the ITV. Note that we did not include additional margins for range uncertainty in our planning or evaluations<sup>33, 94, 116</sup> because the purpose of this work was to determine whether we can adjust beam parameters to match the original coverage to the target after correcting for anatomy change. Therefore, we wished to isolate the effect of anatomy change from treatment planning range uncertainties in this study. We did, however, include a 1.0 cm margin based on the plan spot spacing to allow for the placement of a single shell of spots outside of the target. This was done to allow freedom for the optimizer to deliver uniform dose to the target. The average 4DCT image was used for plan optimization and dose calculation.

### **5.2.3. Treatment-time image pre-processing**

The average 4DCT from the last available weekly scan was used for evaluation of delivered dose using the non-adaptive and adaptive plans. Deformable image registration was performed using in-house software<sup>88, 89, 101, 102</sup> in order to transfer the original contours of the treatment target and normal tissues to the new treatment-day anatomy for assessment. Again, image processing was also performed in order to digitally replace the couch on the CT scan with the treatment couch, since the two differ.<sup>100</sup>

In order to recreate the patient's treatment position, we performed image registration to obtain the isocenter for the treatment-time CT. The alignment target was to the iGTV soft tissue.



#### **5.2.4. Range calculation in CT imaging**

As described in Section 1.8, the proton range to any point in a patient can be calculated by integrating the relative stopping power of all tissues along the beam path in a CT image. Information regarding the relative stopping power of tissues within the patient can be estimated from CT imaging through previously measured calibration curves.<sup>68</sup> Therefore, the proton radiological range, or WEPL, to any voxel in the CT image can be calculated by integrating the relative stopping power ratios along the line segment from the beam source to the voxel of interest in the image.

#### **5.2.5. Adaptive algorithm**

With information about the new target anatomy on the treatment-time CT image, we can calculate the new ranges for the proton beamlets that are needed in order to cover the new target anatomy. If the new anatomy requires a smaller range than the original plan, then the energies of the proton beamlets can be decreased in order to avoid unnecessarily overdosing normal tissues distal to the target. Similarly, if a larger range is needed, then the energies of the proton beamlets can be increased to ensure that the target is adequately covered. Our current implementation of such changes are similar to those described by Zhang et al.,<sup>117</sup> but with additional correction factors to account for target morphology changes and proton beam changes. Before range adaptation of the spot positions were performed on the new anatomy, we calculated the difference between the range to the distal edge of the target on the planning CT image and the actual range of the distal proton spots in the plan to obtain the excess spot position range that was needed for each beamlet in the optimized proton plan to deliver a

uniform dose to the target. This excess range distal to the target was added to the corresponding beamlets in the range-adapted plans in order to cover the distal edge of the target. The range-adaptive adjustments were then performed on a ray-by-ray basis (i.e. spots with the same X and Y positions in the two-dimensional spot grid but with different energies) uniformly in order to match the range to the distal edge of the new target. The spots were then matched to available discrete energies from our synchrotron-based clinical proton beam. Thereafter, any spots that ended up lying outside of the target proximally were removed. If more spots were required to cover the proximal side of the target (e.g. the target volume increased or the upstream density decreased), then additional spots were added to accommodate the disparity. This process is similar to adjusting the beam parameters on a daily basis to optimize a 2.5D modulation field as described by Lomax.<sup>118</sup> An example of this step in the process is shown on a pelvic phantom in Figure 25. We devised the original plan to deliver a uniform dose to a circular target at the center of the phantom. After introducing a bone-like material in the path of the beam, the delivered proton spots are pulled back proximally due to the increased density of the material along the beam path. Therefore, we can dial up the energies of the proton spots to account for this necessary change in range and obtain a spot placement close to that of the original plan on the new anatomy.

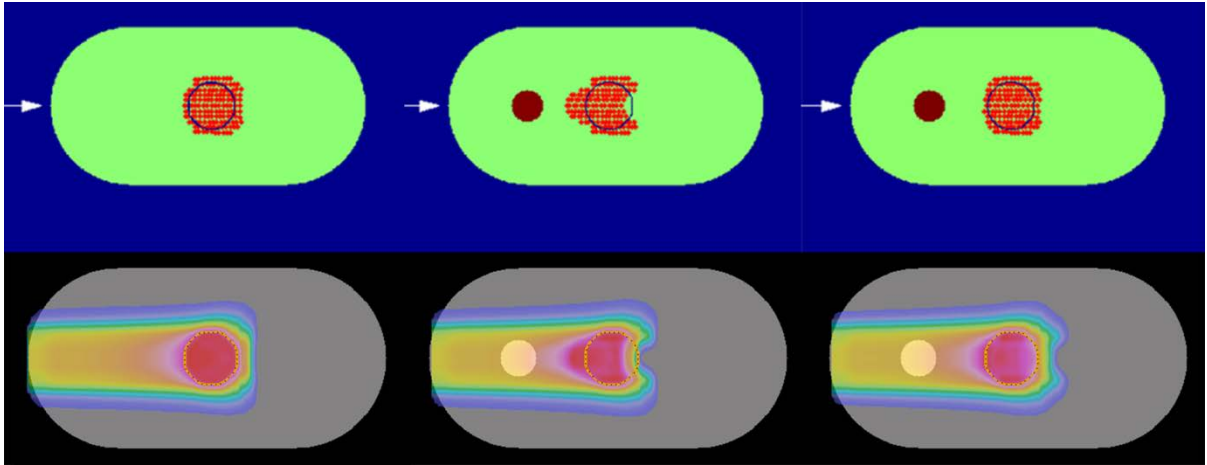


Figure 25: An example of the range-adaptation on a pelvic phantom. On the top row are the spot positions that are needed to deliver a uniform dose to the circular target at the center of the phantom. On the bottom row are the resultant dose distributions. The first column shows the original plan with no range perturbations. The second column shows what happens to the original plan when a bone-like material is introduced in the path of the beam. The third column shows the resulting spot position and dose when the ranges of the spots are adjusted to compensate for the change in anatomy.

As shown in Figure 26, a change in the energy of the beam with a fixed spot weight, or monitor unit (MU), will result in a difference in dose that is delivered both at the peak dose depth and at locations proximal to the peak dose because of changes in the energy straggling and lateral scattering of the beam. Therefore, if we change the energy of an individual spot, the MU for that spot will need to change as well in order to compensate for the difference in dose delivered. In addition, any change in the MU for a given spot will affect the dose that is delivered proximal to the spot, and therefore the MU for all spots proximal to the adjusted spot will also need adjustment. Different methods for correcting the

MU based on integral depth dose (IDD) and central axis depth dose (CAX) were explored in order to directly correct for this effect after applying our range correction. The relative doses for all energies less than each available clinical energy were included in a lookup table to obtain adjustment factors needed (Figure 26). Therefore, the cumulative adjustment needed for any proton spot along a ray could be calculated as needed.

The lateral coverage of the proton beam also had to be considered as we adapted the original plans to match the patients' new anatomy. As shown in Figure 27, proton beam optimizers tend to favor increasing the spot weights to the peripheral spots in a proton plan in order to achieve a uniform dose distribution and increase the sharpness of the penumbra. Therefore peripheral spots cannot simply be removed if the target anatomy shrinks in the lateral direction, or the target coverage will deteriorate. Similarly, if the target size grows in the lateral direction, adding spots outside the peripheral spots will adversely increase dose to the normal tissue outside of the target.

We selected correction factors to increase or decrease the peripheral spots depending on changes in the target's lateral size. The correction factor lookup table was generated based on a phantom study in which we delivered a SFO SSPT plan to a cylindrical target uniform water phantom. In this phantom study (Figure 28), we changed the target's lateral size in increments of 1 mm to  $\pm 10$  mm to assess how target coverage responded to adjustments in the peripheral spot weights, which we changed in increments of 1% to  $\pm 30\%$ . Correction factors for lateral changes were determined based on preserving target  $V_{99\%} \geq 95\%$ , while ensuring hot spots were kept to a minimum (target  $V_{110\%} < 5\%$ ) (Figure 29). Figure 30 shows the correction factors that were determined from the phantom study.

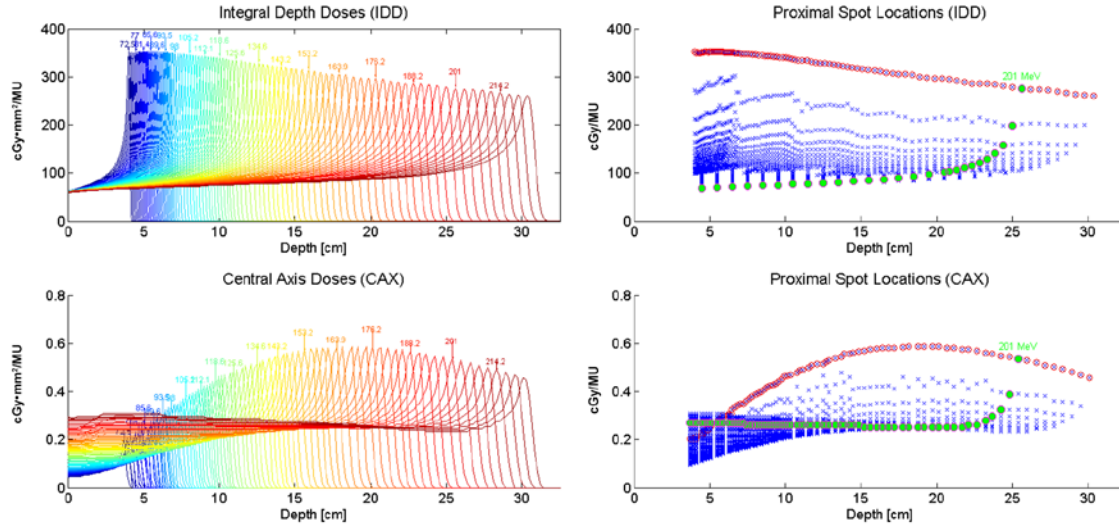


Figure 26: Depth dose curves of all of the clinically available energies at our proton therapy center and the relative doses for all spots proximal to the given energies. (Left panels) Integral depth dose (IDD) and central axis depth dose (CAX) curves for all 94 available clinical beam energies of our proton therapy system based on treatment planning system calculations for individual spot doses of different energies with a fixed monitor unit (MU). Note that for different energies, the deposited dose changes when delivering the same MU and that any change to spot weights for those with higher energies will affect the dose delivered along the entire path of the beam. (Right panels) Lookup table generation for relative spot positions and intensity corrections for different energies for the IDD and CAX methods based on relative locations of proximal spots. The spot correction locations needed for beam energies of 201 MeV are highlighted in green.

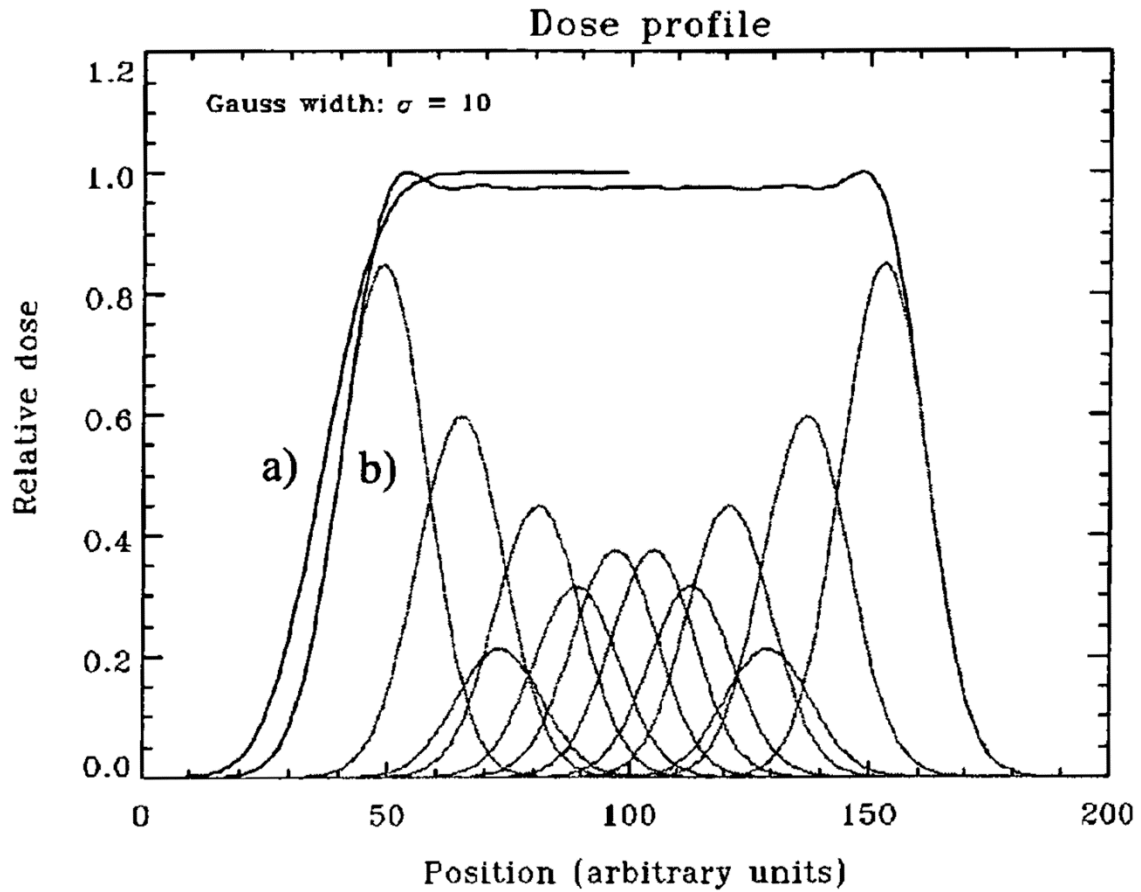


Figure 27: A graph showing the difference in the proton beam penumbra for a spot scanning system between (a) a uniform proton fluence and (b) an “edge-enhanced” proton fluence. The “edge-enhanced” proton fluence as represented by the summation of the individual proton spot profiles with the protons on the periphery given more weight as shown in the figure.

Reprinted from E. Pedroni, United States Patent No. 7560715 (July 14, 2009 2009).

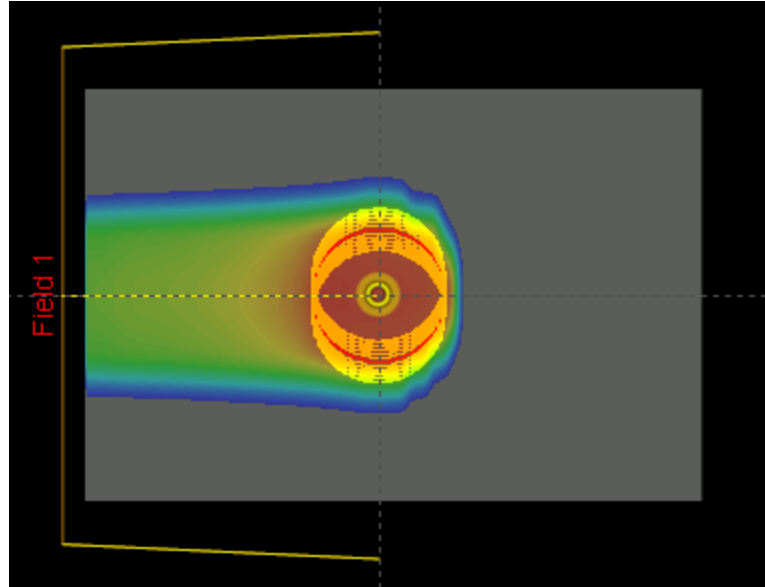


Figure 28: Image of the phantom and contours that were used for generation of the lateral size corrections lookup table. The red contour shows the original target and the yellow contours show the target with increasing and decreasing lateral margins.

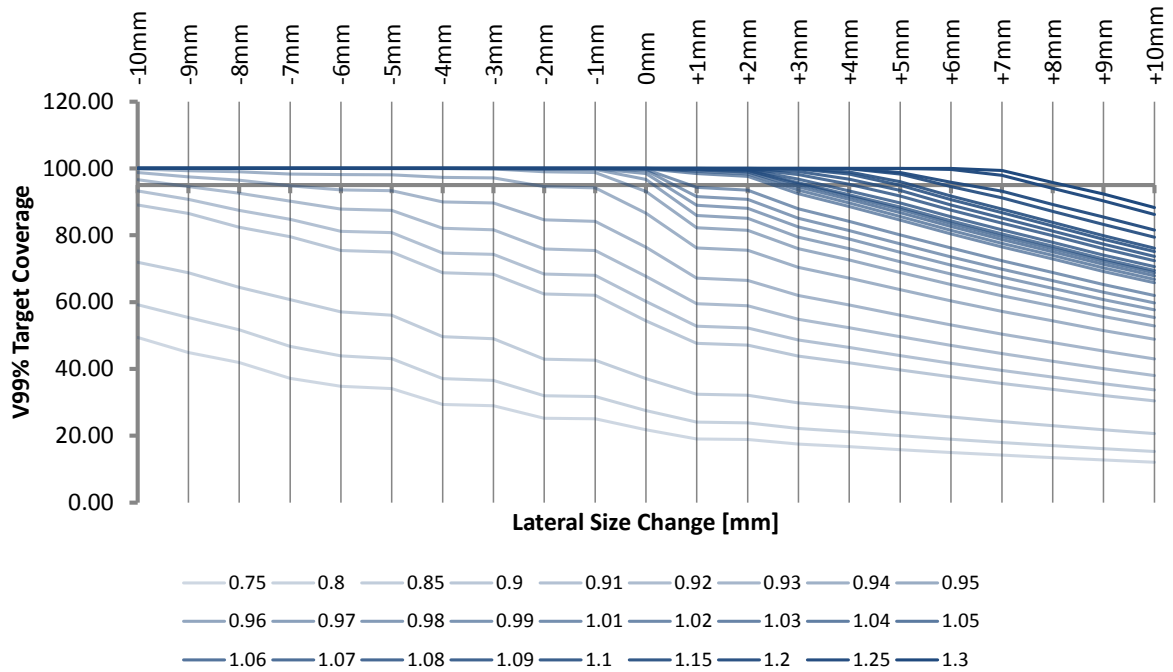


Figure 29: Generation of lookup table for lateral size corrections. Each curve shows the target coverage ( $V_{99\%}$ ) for different lateral size changes of the target volume. Scalar adjustment factors between 0.75 and 1.3 in increments of 0.01 were applied to the peripheral spot weights to compensate for lateral size changes.

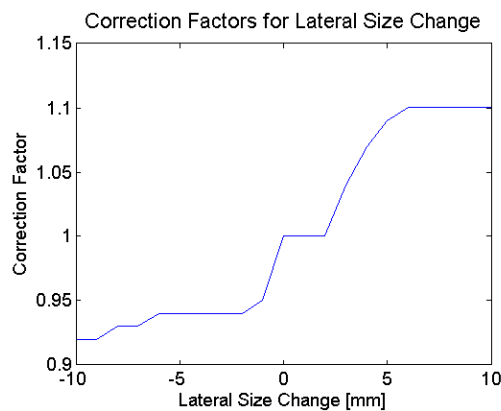


Figure 30: The resultant correction factors for lateral size changes based on target coverage (target  $V_{99\%} \geq 95\%$ ) and target hot spot (target  $V_{110\%} < 5\%$ ) criteria.



The plan parameters, including beam configurations, spot positions, and spot energies, from the original treatment plan were registered to the treatment-time image to obtain the verification (non-adaptive) dose distribution. This verification plan, along with the original plan parameters, was exported to be modified based on our range-adaptive algorithm. The plan parameters and the treatment-time CT were read into Matlab (The MathWorks Inc., Natick, MA) using the CERR<sup>104</sup> file format structure, and the plan was adapted with the various techniques for energy correction and with and without lateral corrections as described earlier. We looked at adaptations with:

- 1) range adaptation only (Range Adapt),
- 2) range adaptation with lateral corrections only (Adapt w/ Lat Corr),
- 3) range adaptation with CAX-based energy corrections only (Adapt w/ CAX Corr),
- 4) range adaptation with both lateral and CAX-based energy corrections (Adapt w/ Lat Corr and CAX Corr),
- 5) range adaptation with IDD-based energy corrections only (Adapt w/ IDD Corr),
- and
- 6) range adaptation with both lateral and IDD-based energy corrections (Adapt w/ Lat Corr and IDD Corr).

#### **5.2.6. Adaptive Plan Evaluation**

The resultant adaptive plans were evaluated against the non-adaptive verification plans. We looked at various DVH parameters for the target and normal tissues, including the ITV coverage ( $V_{95\%}$ ), ITV hot spots ( $V_{110\%}$ ), spinal cord maximum dose ( $D_{\max}$ ), total and

contralateral lung dose ( $V_{20\text{Gy}}$ ), heart dose ( $V_{40\text{Gy}}$ ), and esophagus dose ( $V_{55\text{Gy}}$ ). Differences between these values in the adaptive and non-adaptive plans were then subjected to statistical analysis.

We compared the various adaptive techniques to each other by using a repeated-measures analysis of variance of the differences in DVH parameters between each of the adaptive and non-adaptive plans. To determine whether there was a statistically significant improvement for each of the adaptive plans compared to the non-adaptive plans, we performed a 2-tailed paired  $t$  test with a 95% confidence interval. We performed our statistical analysis using GraphPad Prism (version 5.00 for Windows; GraphPad Software, San Diego, CA), and a p-value less than 0.025 and 0.010 was considered statistically significant for the target and normal tissues, respectively, based on a Bonferonni correction to correct for the multiple comparisons we are making in this analysis.

### **5.3. Results**

On average, all of the adaptive plans reduced the dose to normal tissues when compared to the non-adaptive plans. However, improvements in the target coverage varied greatly and, in general, resulted in hot spots that were not exhibited in the non-adaptive plans.

Figure 31 shows columnar scatter plots of the differences in normal tissue DVH statistics between the non-adaptive and each adaptive plan and the means and standard deviations in those statistics for the 14 patients. The paired mean differences for these comparisons along with the p-values for the paired  $t$  tests are shown in Table 10. The paired mean differences showed a decrease in the normal tissue dose for the population for all of the adaptive techniques used. This difference was statistically significant for all of the adaptive

techniques without lateral correction for the spinal cord  $D_{\max}$  and total lung  $V_{20\text{Gy}}$ , and for all of the adaptive techniques for the contralateral lung  $V_{20\text{Gy}}$ . They were not statistically significant for the heart  $V_{40\text{Gy}}$  and were mixed for the esophagus  $V_{55\text{Gy}}$ . For all patients except one (patient 5), there was an improvement in normal tissue dose sparing for a majority of the organs evaluated. Patient 5 had an increase in normal tissue dose for all organs. However, this patient also had the largest change in tumor size and the largest improvement in target coverage. The repeated-measures analysis of variance indicated that there were statistically significant differences between the different adaptive techniques for the total lung doses, but not for the other normal tissues evaluated.

Figure 32 shows columnar scatter plots of the absolute values of and differences between the adaptive and non-adaptive plans for the ITV target coverage ( $V_{95\%}$ ) and hot spots ( $V_{110\%}$ ) for all the patients, along with means and standard deviations. On average, all adaptive methods except for that with both lateral and IDD energy corrections showed a reduction in target coverage. Furthermore, in almost all cases, the adaptive techniques resulted in an increase in hot spots compared to the non-adaptive plans, with many showing substantial increases of over 10% in  $V_{110\%}$ ; the mean increase in target hot spots for all the plans was statistically significant. The repeated-measures analysis of variance indicated that there were statistically significant differences in the population means between the different techniques for both target coverage and target hot spots. The addition of lateral corrections to all techniques resulted in improved target coverage but worse hot spots. The CAX corrections were best at reducing hot spots but also resulted in reductions in target coverage. The IDD corrections tended on the whole to increase the dose to the target, resulting in better target coverage but worse hot spots.

Table 10: Target and normal tissue DVH metric comparisons for all of the adaptive techniques relative to the non-adaptive plans

Analysis	Target Coverage (V <sub>95%</sub> ) [%]		Target Hot Spots (V <sub>100%</sub> ) [%]		Spinal Cord Max Dose (D <sub>max</sub> ) [Gy]		Contralateral Lung (V <sub>200%</sub> ) [%]		Total Lung (V <sub>200%</sub> ) [%]		Heart (V <sub>400%</sub> ) [%]		Esophagus (V <sub>550%</sub> ) [%]	
	Paired mean difference	p-value	Paired mean difference	p-value	Paired mean difference	p-value	Paired mean difference	p-value	Paired mean difference	p-value	Paired mean difference	p-value	Paired mean difference	p-value
Range Adapt	-1.7	0.029	13.7	*0.001	-7.8	*0.008	-3.2	*0.007	-2.3	*0.010	-1.2	0.082	-3.7	*0.010
Adapt w/ Lat Corr	-0.2	0.880	19.9	*0.001	-6.5	0.041	-3.0	*0.008	-1.9	0.048	-1.6	0.088	-2.2	0.260
Adapt w/ CAX Corr	-6.2	*0.002	5.5	*0.008	-8.3	*0.006	-3.2	*0.007	-2.6	*0.007	-1.3	0.078	-4.3	*0.008
Adapt w/ Lat and CAX Corr	-4.9	*0.008	8.1	*0.003	-6.9	0.030	-3.2	*0.006	-2.3	0.019	-1.2	0.135	-3.6	0.027
Adapt w/ IDD Corr	-0.4	0.700	25.9	*0.001	-7.5	*0.012	-3.1	*0.007	-2.2	0.015	-1.8	0.052	-2.9	0.068
Adapt w/ Lat and IDD Corr	0.4	0.740	31.5	*0.001	-6.1	0.049	-3.0	*0.007	-1.8	0.051	-0.7	0.510	-1.9	0.310
Average	-2.2		17.4		-7.2		-3.1		-2.2		-1.3		-3.1	
Repeated-measures ANOVA														
	p-value		p-value		p-value		p-value		p-value		p-value		p-value	
	*0.001		*0.001		0.043		0.091		*0.001		0.582		0.058	

\*p-value < 0.025 for target anatomy

\*p-value < 0.010 for normal tissue anatomy

Figure 31: Columnar scatter plots of the normal tissue DVH metric differences between the adaptive and non-adaptive plans for all 14 patients and for each of the six adaptive correction methods.

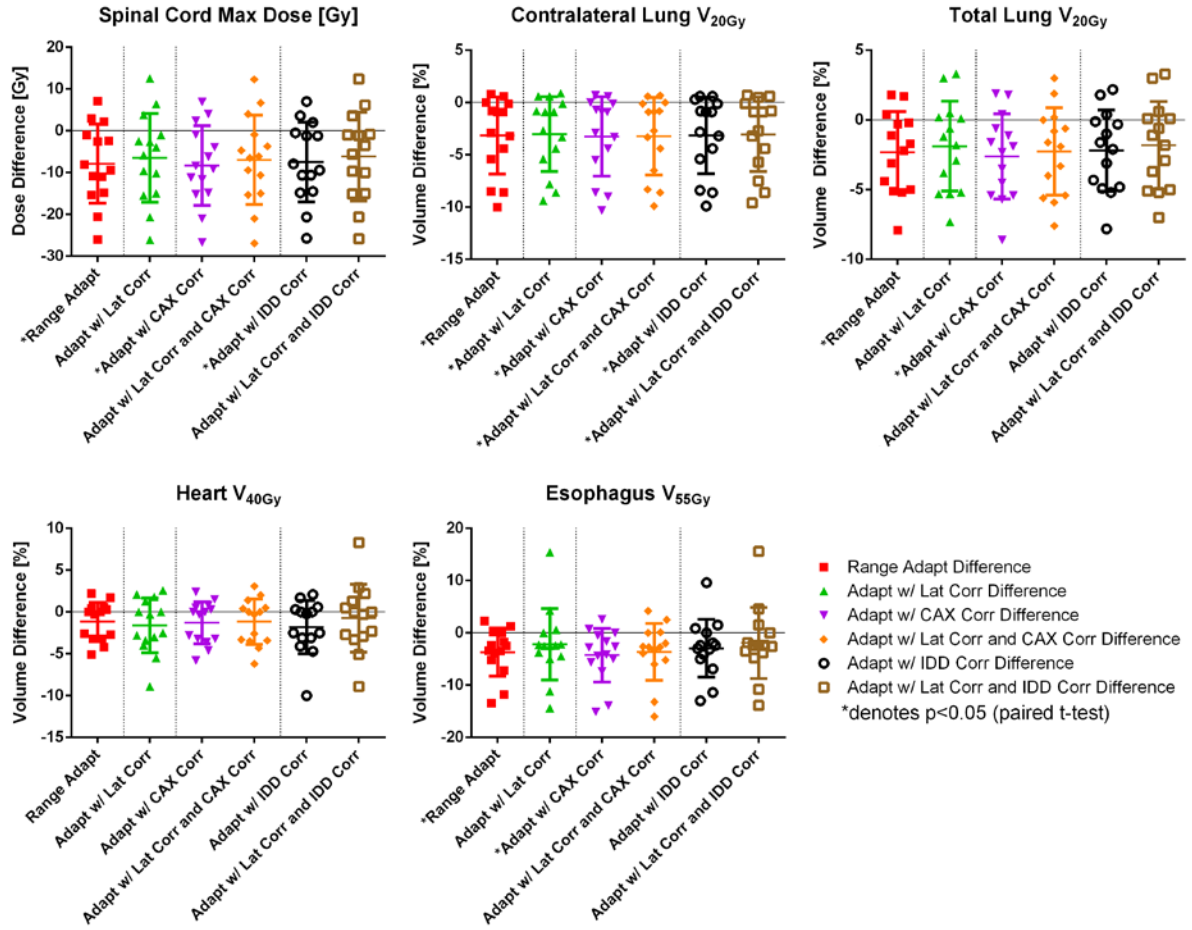
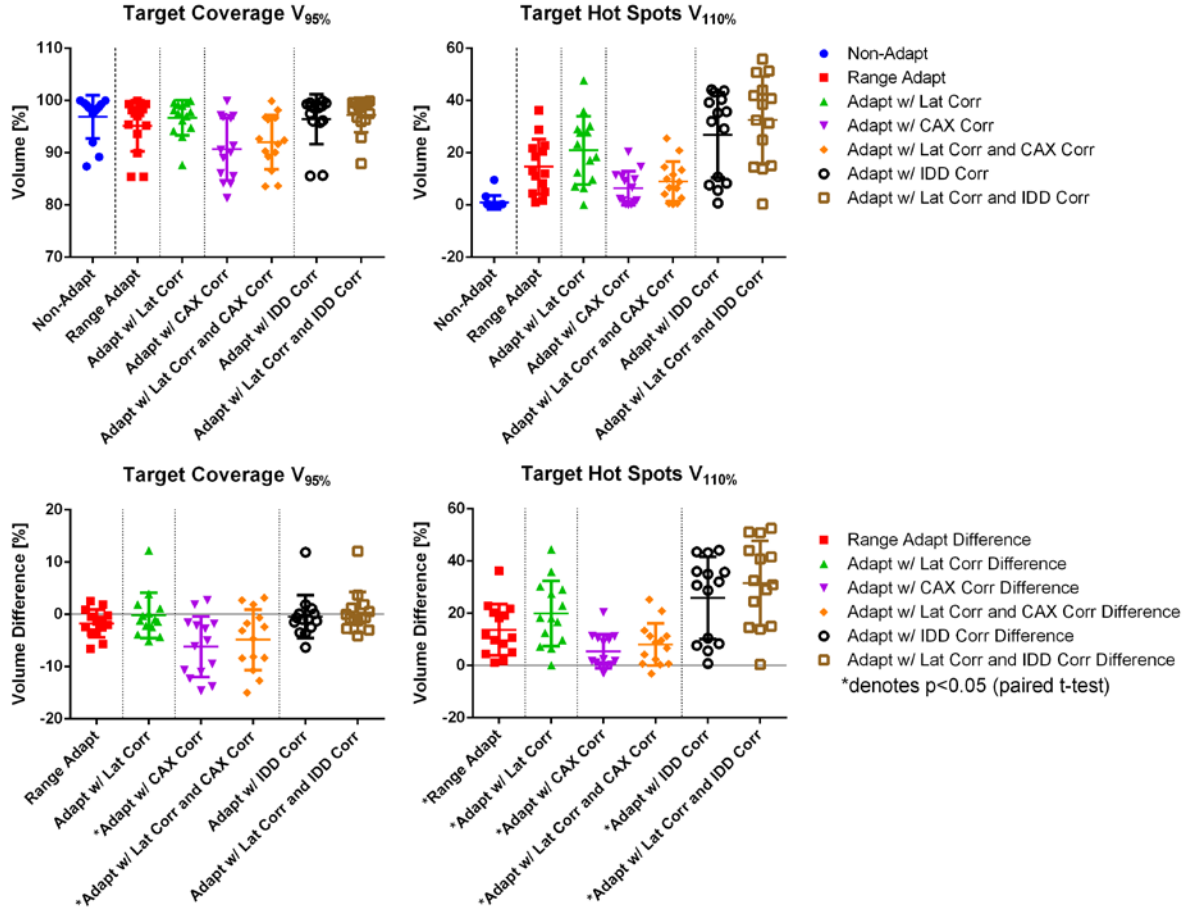


Figure 32: Columnar scatter plots for the ITV DVH metrics (top) and DVH metric differences between the adaptive and non-adaptive plans (bottom) for all 14 patients and for each of the six different adaptive correction methods.



## 5.4. Discussion

Taken together, our data show that adaptive planning by making direct adjustments to the original treatment beams for SFO SSPT is difficult to achieve without creating undesirable dosimetric effects that may compromise outcomes. However, our adaptive techniques all performed well in reducing the normal tissue dose. Since they all rely principally on adjusting the range of the delivered proton spots to match the ranges calculated on the new

target anatomy, normal tissues that lie distal to the target anatomy stand to benefit most. Such benefits are apparent when looking at the spinal cord and contralateral lung doses. Both of these structures saw relatively large decreases in dose after applying our adaptive techniques since the clinical beam angles tended to avoid going through these structures to treat the target; as is common, though, the plans often necessitated aiming at least one beam toward or near these structures in order to viably treat the target. In the case of lung cancers, the tumor response typically results in shrinkage of the soft tissue target, exposing more lung tissue in the path of the beam and resulting in an overshooting into the normal tissue distal to the target. The range adaptive techniques described here allow for these problems to be mitigated.

While the esophagus and heart saw noticeable decreases in dose when adaptive replanning was done, the differences between the adaptive and non-adaptive plans were generally not statistically significant, likely because of the locations of these structures. That is, the esophagus and heart tended to be close to the target for most of our cases and therefore already contained areas receiving high dose. This was especially apparent for the heart, as the heart  $V_{40\text{Gy}}$  varied considerably between the different adaptive techniques.

While these adaptive techniques showed some success with normal tissue sparing in our cases, the resultant dose to the new target anatomy varied and resulted in increased heterogeneity and reduced target coverage. Efforts to correct these problems by making fundamental adjustments to the proton spot intensities based on calculated depth dose curves and lateral size changes were unsuccessful in correcting these issues. The main objective of this work was to come up with an adaptive methodology that could potentially be applied as an online process, with minimal modifications to the original optimized plan. However, our

results show that changes in patient anatomy for cases that require adaptive intervention are substantial enough that the original optimized conditions break down and that a clinically acceptable plan cannot be recovered with the simple modifications proposed here. We believe some sort of dose-based reoptimization of the plan is likely needed to acquire an acceptable adaptive plan; future work in adaptive planning therefore should be focused on fast reoptimization techniques.

In response to the results, we wished to see if there was any way to predict whether a given patient would be a good candidate for applying this adaptive technique. To do this, we evaluated whether there was any correlation between the magnitude of anatomy change to the change in target coverage and target hot spots for the different adaptive techniques. For the magnitude of anatomy change we evaluated both the iGTV volume change and the difference in weighted average of the maximum WEPL range for the adaptive plans compared to the non-adapted plans. Unfortunately, we found no statistically significant correlations between these variables when evaluating target coverage. The degree of target hot spots showed moderate statistically significant correlation to iGTV volume change for both of the IDD correction methods (R-square of 0.6253 and 0.5420 for the Adapt w/ IDD Corr and Adapt w/ Lat Corr and IDD Corr methods, respectively) and weak correlation to the average maximum WEPL difference for the Adapt w/ IDD Corr method (R-square of 0.2723). However, due to the lack of correlation for the target coverage criteria, this correlation is not clinically meaningful.

We chose again to examine only lung cancer patients for this study because the impacts of anatomical change in proton therapy are potentially the greatest in these cases due to the low-density tissues involved and the typically large tumor responses. Therefore, these



cases stand to gain the most benefit from adaptive planning in proton therapy. Additionally, this allowed us to include a wide range of tumor size changes in our study to test our adaptive techniques. In prostate treatments, anatomical changes have been shown to have minimal effects if appropriate measures were taken to ensure proper planning and accurate patient setup , and so our findings are not particularly applicable in that setting.<sup>110, 111, 119, 120</sup>

Conversely, while such variations have demonstrated large effects in head and neck proton therapy,<sup>121</sup> the use of SFO SSPT for those cancers is limited due to the close proximity of critical normal tissue structures and the complex target structures in most of these cases, and multi-field optimized or full intensity-modulated proton therapy is a more promising method. Thus, while the adaptive technique described here can be in general applied to any treatment site with SFO SSPT planning, specific advantages and disadvantages need to be assessed, especially with the problems seen with target coverage and hot spots.

While in-room volumetric imaging is not currently available in most proton facilities, CT scanners in proton therapy vaults have been planned for many future centers. Integrated x-ray or possibly proton cone-beam CT scanners can potentially be used as well.<sup>122</sup> While accurate dose calculations in proton therapy have not been sufficiently demonstrated using cone-beam CT imaging,<sup>123-125</sup> work on CT number correction has shown promise for potential future use in proton therapy. Therefore, in-room volumetric imaging for proton therapy and their effective use for proton image-guidance and adaptive therapy is likely to be of forthcoming clinical importance.

## **5.5. Conclusion**

Since proton beams are very sensitive to anatomical changes in the target and along the beam path, online adaptive therapy may be essential to ensure acceptable delivery of the proton therapy. This work is important because it identifies key successes and limitations of applying various simple adaptive methodologies to correct for interfractional anatomic changes in spot scanning proton therapy. We determined that normal tissue doses can be minimized with these methods but that the dose to the target is not adequately corrected for and that large changes will likely require some form of reoptimization for adaptive planning.

## **CHAPTER 6: DISCUSSION AND CONCLUSION OF DISSERTATION**

### **6.1. Testing of hypotheses**

At the beginning of the dissertation, we hypothesized that we could use information from CT imaging to verify and assess the dose delivered on the day of treatment, and to make corrections as necessary to patient setup and to adapt the treatment in order to maintain target coverage and reduce normal tissue dose. To test this hypothesis, we devised the three specific aims presented in the preceding chapters.

#### **6.1.1. Overall hypothesis**

The overall hypothesis was that a radiological pathlength calculation algorithm based on CT imaging could be used for online proton beam treatment day verification and isocenter adjustment, and online adaptive range adjustment technique based on pathlength correction in order to maintain target coverage and reduce normal tissue dose. We were able to develop and test the techniques proposed at the beginning of this dissertation and demonstrate their relative successes and limitations.

#### **6.1.2. Specific Aim I**

The goal of this aim was to develop an online proton dose verification tool based on daily CT imaging to assess the effect of anatomy change on the proton beam and validate its ability to evaluate target coverage and dose distribution. The working hypothesis was that the online range corrected dose approximation tool could estimate the dose distribution based on the new patient anatomy to an accuracy given by a gamma index  $(3\%/3\text{mm}) > 85\%$  when

compared to full dose recalculation. We were able to successfully develop a proton dose verification tool that can feasibly be used as an online process utilizing treatment-time CT imaging. We demonstrated that a range-corrected proton dose approximation method can be used to estimate the delivered dose to a patient to better than 93% and 84% for setup position changes and severe anatomy changes, respectively, when looking at the 3D gamma analysis passing rate with a 3% dose difference and 3 mm distance-to-agreement criteria. Moreover, the DVHs agreed very well with treatment planning system calculations with an average of RMS (maximum deviation) of 0.5% (1.5%) for setup position changes and 0.6% (2.7%) for weekly anatomic change. The goal of meeting an 85% passing rate for the 3D gamma analysis was met for all of the cases evaluated in this study except for the worst case head and neck instance, in which we saw a Gamma Index passing rate of 84%. Therefore, while our results strictly require us to reject the hypothesis, the method presented is still useful as a tool for dose assessment. The cases tested in this study were intentionally extreme examples of anatomical changes that have been seen at our institution. In addition, the beam angles that were selected for this evaluation were chosen to exaggerate the effect of the anatomical changes on the proton beam. The dose approximation did well under these circumstances and can be very useful tool to catch major errors in dose delivery. Moreover, when looking at the DVH, our technique shows good agreement to full dose calculation. Therefore, use of this technique with either dose distribution maps or DVH-based metrics can potentially be an indicator for compromised treatments, informing further decisions for possible corrective action. Additionally, the results looking at the accuracy of the dose approximation algorithm on setup variations showed very good agreement, making it useful for applications for robust analysis, or dose-based patient setup evaluation as is used in Specific Aim II.

### **6.1.3. Specific Aim II**

The goal of this aim was to devise a novel patient setup correction method for proton therapy based on dosimetric indices and to assess its ability to maintain target coverage and improve normal tissue sparing. The working hypothesis was that this dosimetric alignment method based would result in a statistically significant reduction in normal tissue dose compared to anatomical alignment. Here, we used the tools developed in Specific Aim I to calculate the dose for numerous patient setup positions within a defined search space to obtain the optimal patient setup position. This is a basic adaptive correction principle that is commonly used in the clinic with IGRT patient localization, but current practice is limited to looking at anatomy-based alignment only. By using dose information for patient setup, we are not only able to obtain the best setup position for the patient, but we can also use this to inform us of the need for a more comprehensive adaptive correction if the treatment is compromised for all possible isocenter shifts.

Testing this technique on our cohort of patients, we found that we were able to recover our target coverage to meet clinical constraints in all of the cases where the anatomy-based alignment did not. In addition, we were able to statistically significantly improve the normal tissue sparing in cases where both anatomy-based and dose-based alignment methods met the target constraint. We demonstrated its use in lung patients, but the application can easily be extended to any treatment site. As discussed, clinical implementation will require decisions to be made regarding trade-offs of optimizing to different normal tissues. This decision can be site or patient specific. If clinical requirements are not met by this process then other adaptive strategies such as that tested in Specific Aim III can be considered.

#### **6.1.4. Specific Aim III**

The goal of this aim was to develop an online range compensation beam adjustment technique to correct for range variations due to anatomical changes while preserving target coverage in SFO spot scanning proton therapy. The working hypothesis was that this online range-adaptive technique based on pathlength correction could maintain the original target dose coverage (V95%) to within 5% while significantly reducing normal tissue dose compared to non-adaptive treatments. We developed an adaptive technique that takes advantage of the ability to adjust the proton beam on the fly for a spot scanning system. The corrections included in the process are meant to be applicable without any need for iterative dose-based reoptimization. It is important to note here that the dose approximation algorithm from Specific Aim I would not be applicable to estimate the dose after applying this adaptive strategy since the beam parameters are different from the original planned parameters. Therefore, the assumptions of our dose approximation algorithm break down and the dose cannot be estimated by the remapping process.

We found that our adaptive techniques were able to reduce the dose to normal tissues but were unsuccessful at preserving target coverage and uniformity. While the results for Specific Aim III were negative, we were able to demonstrate relative success in reducing normal tissue dose. The problem with making such proposed changes to the proton beams is that the original optimization conditions are disrupted and direct changes to accommodate changes in the proton delivery are not enough. Furthermore, we were unable to determine a

priori which patients may benefit from such an adaptive technique based on anatomical changes.

Future studies looking at further exploring other correction factors for adaptive planning may allow for improvements to target uniformity. For example, one factor that was not taken into account in this study was the change in spot size due to energy changes. In order to preserve the original optimization conditions, we elected to maintain the same spot spacing as was needed in the original treatment plan. However, the spot spacing may necessarily be changed as well in order to address the differences in energies for spot delivery. Exploration of such modifications may allow for a more homogenous dose to be delivered to the target. A different approach may be to utilize the updated dose information after performing our initial adaptive adjustments to determine additional modifications that can be made to manage target coverage and perhaps even further reduce normal tissue dose. This approach moves toward performing a full reoptimization of the plan but can possibly be performed using just a few iterations with the initial adaptive adjustments serving as a starting point. If this approach is utilized, the time savings and the quality of the adaptive plan compared to a full-fledged adaptive replan would need to be assessed to determine clinical applicability. We hope that the adaptive techniques assessed in our study will be informative of future efforts to implement quick adaptive planning for proton therapy.

## **6.2. Future work**

There is much work that needs to be done in order to implement the work presented in this publication in the clinic. While the analysis may be specific to our clinic and mostly tested on lung patients, the methods as presented are general processes that are non-specific with

regards to institutional clinical guidelines, treatment site, and vendor, and can be widely implemented to specific clinical needs. However, all of the work presented here is developmental and full application of them will require streamlining the processes and implementation into a clinically viable workflow. This requires many steps, including system integration, workflow process, clinical training, and validation for the specific clinical applications of interest. The quality assurance that is needed for such techniques was not a focus of the project and is left as an open question. Quality assurance needs will be very specific to the application and the specific system in place at an institution and careful consideration is needed in implementing any aspects of these processes.

An additional issue that needs to be considered is the utilization of other developed processes that are needed within this adaptive procedure. Our studies examined the use of repeat CT imaging for patients. Therefore, in order to implement these processes, the ability to image the patient in the treatment room is necessary. On top of this, automatic segmentation is needed in order to streamline the process and reduce the time needed for data preparation. Solutions for data management and system integration of these components will be an essential part of implementing these processes.

Due to the complexity of proton therapy and the dynamic nature of patient anatomy and physiology, verification of proper dose delivery is an important endeavor. An individual patient's response to treatment will be unique and difficult to predict. Additionally, the increasing value and trend toward personalized medicine is indicative of the desire for adaptive radiation therapy. We hope that the methods and results presented in this work will be of benefit toward this goal to deliver the best care to radiation therapy patients.



## BIBLIOGRAPHY

1. W. K. Röntgen, "On a new kind of rays," *Nature* **53**, 274-277 (1896).
2. ASTRO, "Fast facts about radiation therapy," <https://www.astro.org/News-and-Media/Media-Resources/FAQs/Fast-Facts-About-Radiation-Therapy/Index.aspx>
3. American Cancer Society, "Cancer Facts & Figures 2012," (American Cancer Society, Atlanta, 2012).
4. L. B. Marks, R. K. Ten Haken and M. K. Martel, "Guest editor's introduction to QUANTEC: a users guide," *Int. J. Radiat. Oncol. Biol. Phys.* **76**, S1-S2 (2010).
5. R. R. Wilson, "Radiological use of fast protons," *Radiology* **47**, 487-491 (1946).
6. W. P. Levin, H. Kooy, J. S. Loeffler and T. F. DeLaney, "Proton beam therapy," *Br. J. Cancer* **93**, 849-854 (2005).
7. A. Smith, M. Gillin, M. Bues, X. R. Zhu, K. Suzuki, R. Mohan, S. Woo, A. Lee, R. Komaki, J. Cox, K. Hiramoto, H. Akiyama, T. Ishida, T. Sasaki and K. Matsuda, "The M. D. Anderson proton therapy system," *Med. Phys.* **36**, 4068-4083 (2009).
8. M. T. Gillin, N. Sahoo, M. Bues, G. Ciangaru, G. Sawakuchi, F. Poenisch, B. Arjomandy, C. Martin, U. Titt, K. Suzuki, A. R. Smith and X. R. Zhu, "Commissioning of the discrete spot scanning proton beam delivery system at the University of Texas M.D. Anderson Cancer Center, Proton Therapy Center, Houston," *Med. Phys.* **37**, 154-163 (2009).
9. E. Pedroni, R. Bacher, H. Blattmann, T. Bohringer, A. Coray, A. Lomax, S. Lin, G. Munkel, S. Scheib, U. Schneider and A. Tourovsky, "The 200-MeV proton therapy project at the Paul Scherrer Institute: Conceptual design and practical realization," *Med. Phys.* **22**, 37-53 (1995).

10. J. M. Slater, J. O. Archambeau, D. W. Miller, M. I. Notarus, W. Preston and J. D. Slater, "The proton treatment center at Loma Linda University Medical Center: Rationale for and description of its development," *International Journal of Radiation Oncology Biology Physics* **22**, 383-389 (1992).
11. J. M. Slater, D. W. Miller and J. O. Archambeau, "Development of a hospital-based proton beam treatment center," *International Journal of Radiation Oncology Biology Physics* **14**, 761-775 (1988).
12. "Proton Therapy Co-Operative Group," PTCOG, <http://ptcog.web.psi.ch/>
13. M. Steneker, A. Lomax and U. Schneider, "Intensity modulated photon and proton therapy for the treatment of head and neck tumors," *Radiother. Oncol.* **80**, 263-267 (2006).
14. T. A. van de Water, A. J. Lomax, H. P. Bijl, M. E. de Jong, C. Schilstra, E. B. Hug and J. A. Langendijk, "Potential benefits of scanned intensity-modulated proton therapy versus advanced photon therapy with regard to sparing of the salivary glands in oropharyngeal cancer," *Int. J. Radiat. Oncol. Biol. Phys.* **79**, 1216-1224 (2011).
15. J. Y. Chang, X. Zhang, X. Wang, Y. Kang, B. Riley, S. Bilton, R. Mohan, R. Komaki and J. D. Cox, "Significant reduction of normal tissue dose by proton radiotherapy compared with three-dimensional conformal or intensity-modulated radiation therapy in Stage I or Stage III non-small-cell lung cancer," *Int. J. Radiat. Oncol. Biol. Phys.* **65**, 1087-1096 (2006).
16. B. S. Chera, C. Vargas, C. G. Morris, D. Louis, S. Flampouri, D. Yeung, S. Duvvuri, Z. Li and N. P. Mendenhall, "Dosimetric study of pelvic proton radiotherapy for high-risk prostate cancer," *Int. J. Radiat. Oncol. Biol. Phys.* **75**, 994-1002 (2009).

17. A. J. Lomax, T. Bortfeld, G. Goitein, J. Debus, C. Dykstra, P. A. Tercier, P. A. Coucke and R. O. Mirimanoff, "A treatment planning inter-comparison of proton and intensity modulated photon radiotherapy," *Radiother. Oncol.* **51**, 257-271 (1999).
18. C. B. Simone II, D. Ly, T. D. Dan, J. Ondos, H. Ning, A. Belard, J. O'Connell, R. W. Miller and N. L. Simone, "Comparison of intensity-modulated radiotherapy, adaptive radiotherapy, proton radiotherapy, and adaptive proton radiotherapy for treatment of locally advanced head and neck cancer," *Radiother. Oncol.* (2011).
19. D. Weber, H. Wang, L. Cozzi, G. Dipasquale, H. Khan, O. Ratib, M. Rouzaud, H. Vees, H. Zaidi and R. Miralbell, "RapidArc, intensity modulated photon and proton techniques for recurrent prostate cancer in previously irradiated patients: a treatment planning comparison study," *Radiat. Oncol.* **4**, 34 (2009).
20. L. Widesott, A. Pierelli, C. Fiorino, A. J. Lomax, M. Amichetti, C. Cozzarini, M. Soukup, R. Schneider, E. Hug, N. Di Muzio, R. Calandrino and M. Schwarz, "Helical tomotherapy vs. intensity-modulated proton therapy for whole pelvis irradiation in high-risk prostate cancer patients: dosimetric, normal tissue complication probability, and generalized equivalent uniform dose analysis," *Int. J. Radiat. Oncol. Biol. Phys.* **80**, 1589-1600 (2011).
21. X. Zhang, Y. Li, X. Pan, L. Xiaoqiang, R. Mohan, R. Komaki, J. D. Cox and J. Y. Chang, "Intensity-modulated proton therapy reduces the dose to normal tissue compared with intensity-modulated radiation therapy or passive scattering proton therapy and enables individualized radical radiotherapy for extensive stage IIIB non-small-cell lung cancer: A virtual clinical study," *Int. J. Radiat. Oncol. Biol. Phys.* **77**, 357-366 (2010).

22. M. J. Berger, J. S. Coursey, M. A. Zucker and J. Chang, "ESTAR, PSTAR, and ASTAR: Computer programs for calculating stopping-power and range tables for electrons, protons, and helium ions (version 1.2.3)," National Institute of Standards and Technology, <http://physics.nist.gov/Star>
23. B. Gottschalk, "On the scattering power of radiotherapy protons," *Med. Phys.* **37**, 352-367 (2010).
24. D. E. Bonnett, "Current developments in proton therapy: A review," *Phys. Med. Biol.* **38**, 1371-1392 (1993).
25. T. Kanai, K. Kawachi, Y. Kumamoto, H. Ogawa, T. Yamada, H. Matsuzawa and T. Inada, "Spot scanning system for proton radiotherapy," *Med. Phys.* **7**, 365-369 (1980).
26. P. Giraud, S. Elles, S. Helfre, Y. De Rycke, V. Servois, M.-F. Carette, C. Alzieu, P.-Y. Bondiau, B. Dubray, E. Touboul, M. Housset, J.-C. Rosenwald and J.-M. Cosset, "Conformal radiotherapy for lung cancer: different delineation of the gross tumor volume (GTV) by radiologists and radiation oncologists," *Radiother. Oncol.* **62**, 27-36 (2002).
27. J. C. O'Daniel, D. I. Rosenthal, A. S. Garden, J. L. Barker, A. Ahamad, K. K. Ang, J. A. Asper, A. I. Blanco, R. de Crevoisier, F. C. Holsinger, C. B. Patel, D. L. Schwartz, H. Wang and L. Dong, "The effect of dental artifacts, contrast media, and experience on interobserver contouring variations in head and neck anatomy," *Am. J. Clin. Oncol.* **30**, 191-198 (2007).
28. M. van Herk, "Errors and margins in radiotherapy," *Semin. Radiat. Oncol.* **14**, 52-64 (2004).

29. M. Engelsman, M. Schwarz and L. Dong, "Physics controversies in proton therapy," *Semin. Radiat. Oncol.* **23**, 88-96 (2013).
30. A. J. Lomax, "Intensity modulated proton therapy and its sensitivity to treatment uncertainties 1: the potential effects of calculational uncertainties," *Phys. Med. Biol.* **53**, 1027 (2008).
31. A. J. Lomax, "Intensity modulated proton therapy and its sensitivity to treatment uncertainties 2: the potential effects of inter-fraction and inter-field motions," *Phys. Med. Biol.* **53**, 1043 (2008).
32. M. Yang, X. R. Zhu, P. C. Park, U. Titt, R. Mohan, G. Virshup, J. E. Clayton and L. Dong, "Comprehensive analysis of proton range uncertainties related to patient stopping-power-ratio estimation using the stoichiometric calibration," *Phys. Med. Biol.* **57**, 4095 (2012).
33. *Prescribing, recording, and reporting proton-beam therapy*. Report No. 78. International Commission on Radiation Units and Measurements, 2007.
34. *Prescribing, recording, and reporting photon beam therapy*. Report No. 50. International Commission on Radiation Units and Measurements, 1993.
35. L. J. Verhey, M. Goitein, P. McNulty, J. E. Munzenrider and H. D. Suit, "Precise positioning of patients for radiation therapy," *Int. J. Radiat. Oncol. Biol. Phys.* **8**, 289-294 (1982).
36. K. M. Langen and D. T. L. Jones, "Organ motion and its management," *Int. J. Radiat. Oncol. Biol. Phys.* **50**, 265-278 (2001).
37. J. L. Barker, A. S. Garden, K. K. Ang, J. C. O'Daniel, H. Wang, L. E. Court, W. H. Morrison, D. I. Rosenthal, K. S. C. Chao, S. L. Tucker, R. Mohan and L. Dong,

- "Quantification of volumetric and geometric changes occurring during fractionated radiotherapy for head-and-neck cancer using an integrated CT/linear accelerator system," *Int. J. Radiat. Oncol. Biol. Phys.* **59**, 960-970 (2004).
38. K. R. Britton, G. Starkschall, H. Liu, J. Y. Chang, S. Bilton, M. Ezhil, S. John-Baptiste, M. Kantor, J. D. Cox, R. Komaki and R. Mohan, "Consequences of anatomic changes and respiratory motion on radiation dose distributions in conformal radiotherapy for locally advanced non-small cell lung cancer," *Int. J. Radiat. Oncol. Biol. Phys.* **73**, 94-102 (2009).
  39. J.-J. Sonke, J. Lebesque and M. van Herk, "Variability of four-dimensional computed tomography patient models," *Int. J. Radiat. Oncol. Biol. Phys.* **70**, 590-598 (2008).
  40. J.-J. Sonke and J. Belderbos, "Adaptive radiotherapy for lung cancer," *Semin. Radiat. Oncol.* **20**, 94-106 (2010).
  41. L. Xing, B. Thorndyke, E. Schreibmann, Y. Yang, T.-F. Li, G.-Y. Kim, G. Luxton and A. Koong, "Overview of image-guided radiation therapy," *Med. Dosim.* **31**, 91-112 (2006).
  42. C. Amies, A. Bani-Hashemi, J.-C. Celi, G. Grousset, F. Ghelmansarai, D. Hristov, D. Lane, M. Mitschke, A. Singh, H. Shukla, J. Stein and M. Wofford, "A multi-platform approach to image guided radiation therapy (IGRT)," *Med. Dosim.* **31**, 12-19 (2006).
  43. L. Xing, J. Siebers and P. Keall, "Computational challenges for image-guided radiation therapy: framework and current research," *Semin. Radiat. Oncol.* **17**, 245-257 (2007).
  44. M. Van Herk, "Different styles of image-guided radiotherapy," *Semin. Radiat. Oncol.* **17**, 258-267 (2007).

45. L. A. Dawson and M. B. Sharpe, "Image-guided radiotherapy: rationale, benefits, and limitations," *The Lancet Oncology* **7**, 848-858 (2006).
46. M. Ghilezan, D. Yan, J. Liang, D. Jaffray, J. Wong and A. Martinez, "Online image-guided intensity-modulated radiotherapy for prostate cancer: How much improvement can we expect? A theoretical assessment of clinical benefits and potential dose escalation by improving precision and accuracy of radiation delivery," *Int. J. Radiat. Oncol. Biol. Phys.* **60**, 1602-1610 (2004).
47. L. K. Schubert, D. C. Westerly, W. A. Tome, M. P. Mehta, E. T. Soisson, T. R. Mackie, M. A. Ritter, D. Khuntia, P. M. Harari and B. R. Paliwal, "A comprehensive assessment by tumor site of patient setup using daily MVCT imaging from more than 3,800 helical tomotherapy treatments," *Int. J. Radiat. Oncol. Biol. Phys.* **73**, 1260-1269 (2009).
48. L. Wang, S. Feigenberg, L. Chen, K. Pasklev and C. C. M. Ma, "Benefit of three-dimensional image-guided stereotactic localization in the hypofractionated treatment of lung cancer," *Int. J. Radiat. Oncol. Biol. Phys.* **66**, 738-747 (2006).
49. D. Yan, F. Vicini, J. Wong and A. Martinez, "Adaptive radiation therapy," *Phys. Med. Biol.* **42**, 123 (1997).
50. M. Guckenberger, J. Wilbert, A. Richter, K. Baier and M. Flentje, "Potential of adaptive radiotherapy to escalate the radiation dose in combined radiochemotherapy for locally advanced non-small cell lung cancer," *Int. J. Radiat. Oncol. Biol. Phys.* **79**, 901-908 (2011).
51. D. L. Schwartz and L. Dong, "Adaptive radiation therapy for head and neck cancer- can an old goal evolve into a new standard?," *Journal of Oncology* (2011).

52. D. Yan, "Adaptive radiotherapy: merging principle into clinical practice," *Semin. Radiat. Oncol.* **20**, 79-83 (2010).
53. J. Cheung, J.-F. Aubry, S. S. Yom, A. R. Gottschalk, J. C. Celi and J. Pouliot, "Dose recalculation and the dose-guided radiation therapy (DGRT) process using megavoltage cone-beam CT," *Int. J. Radiat. Oncol. Biol. Phys.* **74**, 583-592 (2009).
54. F. Albertini, M. Casiraghi, S. Lorentini, B. Rombi and A. Lomax, "Experimental verification of IMPT treatment plans in an anthropomorphic phantom in the presence of delivery uncertainties," *Phys. Med. Biol.* **56**, 4415 (2011).
55. D. Pflugfelder, J. J. Wilkens and U. Oelfke, "Worst case optimization: A method to account for uncertainties in the optimization of intensity modulated proton therapy," *Phys. Med. Biol.* **53**, 1689-1700 (2008).
56. J. Unkelbach, T. C. Chan and T. Bortfeld, "Accounting for range uncertainties in the optimization of intensity modulated proton therapy," *Phys. Med. Biol.* **52**, 2755 (2007).
57. S. Vynckie, "Is it possible to verify directly a proton-treatment plan using positron emission tomography?," *Radiother. Oncol.* **26**, 275-277 (1993).
58. A. Knopf, K. Parodi, H. Paganetti, E. Cascio, A. Bonab and T. Bortfeld, "Quantitative assessment of the physical potential of proton beam range verification with PET/CT," *Phys. Med. Biol.* **53**, 4137-4151 (2008).
59. T. Nishio, A. Miyatake, T. Ogino, K. Nakagawa, N. Saijo and H. Esumi, "The development and clinical use of a beam ON-LINE PET system mounted on a rotating gantry port in proton therapy," *Int. J. Radiat. Oncol. Biol. Phys.* **76**, 277-286 (2010).



60. K. Parodi, H. Paganetti, H. A. Shih, S. Michaud, J. S. Loeffler, T. F. DeLaney, N. J. Liebsch, J. E. Munzenrider, A. J. Fischman, A. Knopf and T. Bortfeld, "Patient study of in vivo verification of beam delivery and range, using positron emission tomography and computed tomography imaging after proton therapy," *International Journal of Radiation Oncology Biology Physics* **68**, 920-934 (2007).
61. J. C. Polf, S. Peterson, G. Ciangaru, M. Gillin and S. Beddar, "Prompt gamma-ray emission from biological tissues during proton irradiation: a preliminary study," *Phys. Med. Biol.* **54**, 731 (2009).
62. J. C. Polf, S. Peterson, M. McCleskey, B. T. Roeder, A. Spiridon, S. Beddar and L. Trache, "Measurement and calculation of characteristic prompt gamma ray spectra emitted during proton irradiation," *Phys. Med. Biol.* **54**, N519 (2009).
63. M. F. Gensheimer, T. I. Yock, N. J. Liebsch, G. C. Sharp, H. Paganetti, N. Madan, P. E. Grant and T. Bortfeld, "In vivo proton beam range verification using spine MRI changes," *Int. J. Radiat. Oncol. Biol. Phys.* **78**, 268-275 (2010).
64. M. Mumot, C. Algranati, M. Hartmann, J. M. Schippers, E. B. Hug and A. Lomax, "Proton range verification using a range probe: definition of concept and initial analysis," *Phys. Med. Biol.* **55**, 4771 (2010).
65. U. Schneider, J. Besserer, P. Pemler, M. Dellert, M. Moosburger, E. Pedroni and B. Kaser-Hotz, "First proton radiography of an animal patient," *Med. Phys.* **31**, 1046-1051 (2004).
66. U. Schneider and E. Pedroni, "Proton radiography as a tool for quality control in proton therapy," *Med. Phys.* **22**, 353-363 (1995).

67. R. Zhang and W. D. Newhauser, "Calculation of water equivalent thickness of materials of arbitrary density, elemental composition and thickness in proton beam irradiation," *Phys. Med. Biol.* **54**, 1383-1395 (2009).
68. U. Schneider, E. Pedroni and A. Lomax, "The calibration of CT Hounsfield units for radiotherapy treatment planning," *Phys. Med. Biol.* **41**, 111 (1996).
69. J. Unkelbach, T. Bortfeld, B. C. Martin and M. Soukup, "Reducing the sensitivity of IMPT treatment plans to setup errors and range uncertainties via probabilistic treatment planning," *Med. Phys.* **36**, 149-163 (2009).
70. J. Cheung, P. C. Park, X. R. Zhu, L. E. Court, S. Frank, R. J. Kudchadker and L. Dong, "Comparison of dosimetric benefit of online dose-guided alignment versus anatomy-guided alignment for proton therapy," *Med. Phys.* **38**, 3854 (2011).
71. J. P. Cheung, P. C. Park, L. E. Court, X. R. Zhu, R. J. Kudchadker, S. J. Frank and L. Dong, "A novel dose-based positioning method for CT image-guided proton therapy," *Med. Phys.* **40**, 051714-051719 (2013).
72. S. Mori, S. Zenklusen and A.-C. Knopf, "Current status and future prospects of multi-dimensional image-guided particle therapy," *Radiological Physics and Technology* **6**, 249-272 (2013).
73. B. Cho, M. van Herk, B. Mijnheer and H. Bartelink, "The effect of set-up uncertainties, contour changes, and tissue inhomogeneities on target dose-volume histograms," *Med. Phys.* **29**, 2305 (2002).
74. P. C. Park, J. Cheung, X. R. Zhu, N. Sahoo, L. Court and L. Dong, "Fast range-corrected proton dose approximation method using prior dose distribution," *Phys. Med. Biol.* **57**, 3555 (2012).

75. S. J. Frank, R. J. Kudchadker, D. A. Kuban, R. D. Crevoisier, A. K. Lee, R. M. Cheung, S. Choi, S. L. Tucker and L. Dong, "A volumetric trend analysis of the prostate and seminal vesicles during a course of intensity-modulated radiation therapy," *Am. J. Clin. Oncol.* **33** (2010).
76. Z. Hui, X. Zhang, G. Starkschall, Y. Li, R. Mohan, R. Komaki, J. D. Cox and J. Y. Chang, "Effects of interfractional motion and anatomic changes on proton therapy dose distribution in lung cancer," *Int. J. Radiat. Oncol. Biol. Phys.* **72**, 1385-1395 (2008).
77. M. Yoon, D. Kim, D. H. Shin, S. Y. Park, S. B. Lee, D. Y. Kim, J. Y. Kim, H. R. Pyo and K. H. Cho, "Inter- and intrafractional movement-induced dose reduction of prostate target volume in proton beam treatment," *Int. J. Radiat. Oncol. Biol. Phys.* **71**, 1091-1102 (2008).
78. J. C. O'Daniel, A. S. Garden, D. L. Schwartz, H. Wang, K. K. Ang, A. Ahamad, D. I. Rosenthal, W. H. Morrison, J. A. Asper, L. Zhang, S.-M. Tung, R. Mohan and L. Dong, "Parotid gland dose in intensity-modulated radiotherapy for head and neck cancer: is what you plan what you get?," *Int. J. Radiat. Oncol. Biol. Phys.* **69**, 1290-1296 (2007).
79. A. Trofimov, P. L. Nguyen, J. A. Efstathiou, Y. Wang, H.-M. Lu, M. Engelsman, S. Merrick, C.-W. Cheng, J. R. Wong and A. L. Zietman, "Interfractional variations in the setup of pelvic bony anatomy and soft tissue, and their implications on the delivery of proton therapy for localized prostate cancer," *Int. J. Radiat. Oncol. Biol. Phys.* **80**, 928-937 (2011).

80. M. F. Moyers, D. W. Miller, D. A. Bush and J. D. Slater, "Methodologies and tools for proton beam design for lung tumors," *Int. J. Radiat. Oncol. Biol. Phys.* **49**, 1429-1438 (2001).
81. M. Engelsman and H. M. Kooy, "Target volume dose considerations in proton beam treatment planning for lung tumors," *Med. Phys.* **32**, 3549-3557 (2005).
82. A. Trofimov, J. Unkelbach, T. F. DeLaney and T. Bortfeld, "Visualization of a variety of possible dosimetric outcomes in radiation therapy using dose-volume histogram bands," *Practical Radiation Oncology* **2**, 164-171 (2012).
83. F. Albertini, E. B. Hug and A. Lomax, "Is it necessary to plan with safety margins for actively scanned proton therapy?," *Phys. Med. Biol.* **56**, 4399 (2011).
84. A. J. Lomax, E. Pedroni, H. Rutz and G. Goitein, "The clinical potential of intensity modulated proton therapy," *Zeitschrift fur medizinische Physik* **14**, 147-152 (2004).
85. L. Hong, M. Goitein, M. Bucciolini, R. Comiskey, B. Gottschalk, S. Rosenthal, C. Serago and M. Urie, "A pencil beam algorithm for proton dose calculations," *Phys. Med. Biol.* **41**, 1305 (1996).
86. B. Schaffner, E. Pedroni and A. Lomax, "Dose calculation models for proton treatment planning using a dynamic beam delivery system: an attempt to include density heterogeneity effects in the analytical dose calculation," *Phys. Med. Biol.* **44**, 27 (1999).
87. Y. Kang, X. Zhang, J. Y. Chang, H. Wang, X. Wei, Z. Liao, R. Komaki, J. D. Cox, P. A. Balter, H. Liu, X. R. Zhu, R. Mohan and L. Dong, "4D proton treatment planning strategy for mobile lung tumors," *Int. J. Radiat. Oncol. Biol. Phys.* **67**, 906-914 (2007).

88. H. Wang, L. Dong, J. C. O'Daniel, R. Mohan, A. S. Garden, K. K. Ang, D. A. Kuban, M. Bonnen, J. Y. Chang and R. Cheung, "Validation of an accelerated 'demons' algorithm for deformable image registration in radiation therapy," *Phys. Med. Biol.* **50**, 2887 (2005).
89. H. Wang, L. Dong, M. F. Lii, A. L. Lee, R. de Crevoisier, R. Mohan, J. D. Cox, D. A. Kuban and R. Cheung, "Implementation and validation of a three-dimensional deformable registration algorithm for targeted prostate cancer radiotherapy," *Int. J. Radiat. Oncol. Biol. Phys.* **61**, 725-735 (2005).
90. M. Wendling, L. J. Zijp, L. N. McDermott, E. J. Smit, J.-J. Sonke, B. J. Mijnheer and M. van Herk, "A fast algorithm for gamma evaluation in 3D," *Med. Phys.* **34**, 1647-1654 (2007).
91. S. Mori and G. T. Y. Chen, "Quantification and visualization of charged particle range variations," *Int. J. Radiat. Oncol. Biol. Phys.* **72**, 268-277 (2008).
92. D. C. van Rooijen, N. van Wieringen, G. Stippel, J. Crezee, C. C. E. Koning and A. Bel, "Dose-guided radiotherapy: potential benefit of online dose recalculation for stereotactic lung irradiation in patients with non-small-cell lung cancer," *Int. J. Radiat. Oncol. Biol. Phys.* **83**, e557-e562 (2012).
93. M. Urie, M. Goitein and M. Wagner, "Compensating for heterogeneities in proton radiation therapy," *Phys. Med. Biol.* **29**, 553 (1984).
94. P. C. Park, X. R. Zhu, A. K. Lee, N. Sahoo, A. D. Melancon, L. Zhang and L. Dong, "A beam-specific planning target volume (PTV) design for proton therapy to account for setup and range uncertainties," *Int. J. Radiat. Oncol. Biol. Phys.* **82**, 329-336 (2011).

95. E. J. Koay, D. Lege, R. Mohan, R. Komaki, J. D. Cox and J. Y. Chang,  
"Adaptive/Nonadaptive proton radiation planning and outcomes in a phase II trial for  
locally advanced non-small cell lung cancer," *Int. J. Radiat. Oncol. Biol. Phys.* **84**,  
1093-1100 (2012).
96. C. Cheng, I. J. Das and P. A. S. Johnstone, "Isocenter shift in image-guided proton  
therapy (IGPT) of prostate irradiation," *Int. J. Radiat. Oncol. Biol. Phys.* **75**, S697-  
S697 (2009).
97. R. Mohan, X. Zhang, J. Matney, J. Bluett, L. Dong, P. Balter, M. Engelsman, N.  
Choi, R. Komaki and Z. Liao, "IMRT vs. passively scattered proton therapy (PSPT)  
for locally advanced non-small cell lung cancer (LA NSCLC) randomized trial - is  
there equipoise?," *Int. J. Radiat. Oncol. Biol. Phys.* **78**, S201-S202 (2010).
98. M. Ezhil, S. Vedam, P. Balter, B. Choi, D. Mirkovic, G. Starkschall and J. Chang,  
"Determination of patient-specific internal gross tumor volumes for lung cancer using  
four-dimensional computed tomography," *Radiat. Oncol.* **4**, 4 (2009).
99. L. Dong, J. P. Cheung and X. R. Zhu, "Image-guided proton and carbon ion therapy,"  
in *Proton and Carbon Ion Therapy*, (CRC Press, 2012), pp. 127-149.
100. L. Dong, Y. Zhang, X. R. Zhu, N. Sahoo, R. Wu, P. Balter, R. Mohan and M. Gillin,  
"A digital couch solution for treatment planning beams through the treatment couch,"  
presented at the PTCOG 46, Zibo, China, 2007.
101. H. Wang, A. S. Garden, L. Zhang, X. Wei, A. Ahamad, D. A. Kuban, R. Komaki, J.  
O'Daniel, Y. Zhang, R. Mohan and L. Dong, "Performance evaluation of automatic  
anatomy segmentation algorithm on repeat or four-dimensional computed

- tomography images using deformable image registration method," *Int. J. Radiat. Oncol. Biol. Phys.* **72**, 210-219 (2008).
102. L. Zhang, L. Dong, H. Wang, M. Gillin and R. Mohan, "Validation of CT-assisted targeting (CAT) software for soft tissue and bony target localization," *Med. Phys.* **32**, 2106 (2005).
  103. L. Court and L. Dong, "Automatic registration of the prostate for computed-tomography-guided radiotherapy," *Med. Phys.* **30**, 2750 (2003).
  104. J. O. Deasy, A. I. Blanco and V. H. Clark, "CERR: A computational environment for radiotherapy research," *Med. Phys.* **30**, 979-985 (2003).
  105. A. Bolsi, A. J. Lomax, E. Pedroni, G. Goitein and E. Hug, "Experiences at the Paul Scherrer Institute with a remote patient positioning procedure for high-throughput proton radiation therapy," *Int. J. Radiat. Oncol. Biol. Phys.* **71**, 1581-1590 (2008).
  106. M. Peroni, D. Ciardo, M. F. Spadea, M. Riboldi, S. Comi, D. Alterio, G. Baroni and R. Orecchia, "Automatic segmentation and online virtual CT in head-and-neck adaptive radiation therapy," *Int. J. Radiat. Oncol. Biol. Phys.* **84**, e427-e433 (2012).
  107. X. Zhen, X. Gu, H. Yan, L. Zhou, X. Jia and S. B. Jiang, "CT to cone-beam CT deformable registration with simultaneous intensity correction," *Phys. Med. Biol.* **57**, 6807 (2012).
  108. L. B. Marks, S. M. Bentzen, J. O. Deasy, F.-M. Kong, J. D. Bradley, I. S. Vogelius, I. El Naqa, J. L. Hubbs, J. V. Lebesque, R. D. Timmerman, M. K. Martel and A. Jackson, "Radiation dose-volume effects in the lung," *Int. J. Radiat. Oncol. Biol. Phys.* **76**, S70-S76 (2010).

109. L. Widesott, M. Amichetti and M. Schwarz, "Proton therapy in lung cancer: Clinical outcomes and technical issues. A systematic review," *Radiother. Oncol.* **86**, 154-164 (2008).
110. M. Soukup, M. Sohn, D. Yan, J. Liang and M. Alber, "Study of robustness of IMPT and IMRT for prostate cancer against organ movement," *Int. J. Radiat. Oncol. Biol. Phys.* **75**, 941-949 (2009).
111. Y. Wang, J. A. Efstathiou, G. C. Sharp, H. Lu, I. Frank Ciernik and A. V. Trofimov, "Evaluation of the dosimetric impact of interfractional anatomical variations on prostate proton therapy using daily in-room CT images," *Med. Phys.* **38**, 4623 (2011).
112. X. Zhang, L. Dong, A. K. Lee, J. D. Cox, D. A. Kuban, R. X. Zhu, X. Wang, Y. Li, W. D. Newhauser, M. Gillin and R. Mohan, "Effect of anatomic motion on proton therapy dose distributions in prostate cancer treatment," *Int. J. Radiat. Oncol. Biol. Phys.* **67**, 620-629 (2007).
113. J. Y. Chang, R. Komaki, H. Y. Wen, B. De Gracia, J. B. Bluett, M. F. McAleer, S. G. Swisher, M. Gillin, R. Mohan and J. D. Cox, "Toxicity and patterns of failure of adaptive/ablative proton therapy for early-stage, medically inoperable non small cell lung cancer," *Int. J. Radiat. Oncol. Biol. Phys.* **80**, 1350-1357 (2011).
114. D. R. Gomez and J. Y. Chang, "Adaptive radiation for lung cancer," *J Oncol* **2011** (2011).
115. A. J. Lomax, T. Bohringer, A. Bolsi, D. Coray, F. Emert, G. Goitein, M. Jermann, S. Lin, E. Pedroni, H. Rutz, O. Stadelmann, B. Timmermann, J. Verwey and D. C. Weber, "Treatment planning and verification of proton therapy using spot scanning: Initial experiences," *Med. Phys.* **31**, 3150-3157 (2004).



116. S. J. Thomas, "Margins for treatment planning of proton therapy," *Phys. Med. Biol.* **51**, 1491-1501 (2006).
117. M. Zhang, D. C. Westerly and T. R. Mackie, "Introducing an on-line adaptive procedure for prostate image guided intensity modulate proton therapy," *Phys. Med. Biol.* **56**, 4947 (2011).
118. A. J. Lomax, "Intensity modulation methods for proton radiotherapy," *Phys. Med. Biol.* **44**, 185 (1999).
119. J. Meyer, J. Bluett, R. Amos, L. Levy, S. Choi, Q.-N. Nguyen, X. R. Zhu, M. Gillin and A. Lee, "Spot scanning proton beam therapy for prostate cancer: treatment planning technique and analysis of consequences of rotational and translational alignment errors," *Int. J. Radiat. Oncol. Biol. Phys.* **78**, 428-434 (2010).
120. S. V. Sejpal, R. A. Amos, J. B. Bluett, L. B. Levy, R. J. Kudchadker, J. Johnson, S. Choi and A. K. Lee, "Dosimetric changes resulting from patient rotational setup errors in proton therapy prostate plans," *Int. J. Radiat. Oncol. Biol. Phys.* **75**, 40-48 (2009).
121. A. C. Kraan, S. van de Water, D. N. Teguh, A. Al-Mamgani, T. Madden, H. M. Kooy, B. J. M. Heijmen and M. S. Hoogeman, "Dose uncertainties in IMPT for oropharyngeal cancer in the presence of anatomical, range, and setup errors," *Int. J. Radiat. Oncol. Biol. Phys.* **87**, 888-896 (2013).
122. P. Zygmanski, K. P. Gall, M. S. Z. Rabin and S. J. Rosenthal, "The measurement of proton stopping power using proton-cone-beam computed tomography," *Phys. Med. Biol.* **45**, 511 (2000).

123. G. G. Poludniowski, P. M. Evans and S. Webb, "Cone beam computed tomography number errors and consequences for radiotherapy planning: an investigation of correction methods," *Int. J. Radiat. Oncol. Biol. Phys.* **84**, e109-e114 (2012).
124. I. Fotina, J. Hopfgartner, M. Stock, T. Steininger, C. Lütgendorf-Caucig and D. Georg, "Feasibility of CBCT-based dose calculation: Comparative analysis of HU adjustment techniques," *Radiother. Oncol.* **104**, 249-256 (2012).
125. M. van Zijtveld, M. Dirkx and B. Heijmen, "Correction of conebeam CT values using a planning CT for derivation of the “dose of the day”," *Radiother. Oncol.* **85**, 195-200 (2007).

## VITA

Joey Cheung was born on March 7, 1986 and raised in the San Francisco Bay Area. He is the first of two sons to Peter Cheung and May Shaw. After graduating as the salutatorian of his high school class at San Leandro High School, he attended the University of California, Berkeley and graduated in 2008 with a double major in Physics and Astrophysics. During the summer before his last year of undergraduate study, he worked with Dr. Jean Pouliot at the University of California, San Francisco (UCSF) in the Department of Radiation Oncology as an AAPM summer undergraduate fellow. After graduation, he continued working at UCSF as a research assistant for a year. In December of 2008, he happily married his long-time girlfriend, Robin Luo. Joey started his doctoral study in Medical Physics at the University of Texas Health Science Center in Houston Graduate School of Biomedical Sciences in the fall of 2009. There, he joined Dr. Lei Dong's group and continued his PhD work under the mentorship of Dr. Laurence Court. His research interests include image-guided radiation therapy, adaptive radiation therapy, and clinical workflow management. In his spare time, he enjoys road biking, running, hiking, playing tennis, reading, and going on long walks with his dog, Tinker.

Permanent Address:

1143 Sandelin Ave

San Leandro, CA 94577